SPECTROSCOPIC AND ELECTROCHEMICAL INVESTIGATION OF PHENYL, PHENOXY, AND HYDROXYPHENYL-TERMINATED ALKANETHIOL MONOLAYERS

by

Francisco T. Cavadas

A Dissertation Submitted to the Faculty of the Virginia Polytechnic Institute and State University in Partial Fulfillment of the Requirements for the Degree of

Doctor of Philosophy

in

Chemistry

Mark R. Anderson, Chairman

Paul A. Deck, Co-Chairman

Brian E. Hanson

Paul R. Carlier

John R. Morris

June 6th, 2003

Department of Chemistry
Virginia Tech
Blacksburg, Virginia

Keywords: Self-assembled monolayers, RAIRS, Reductive Desorption, Synthesis, Alkanethiols, Monolayers

ABSTRACT

Francisco T. Cavadas

SPECTROSCOPIC AND ELECTROCHEMICAL INVESTIGATION OF PHENYL, PHENOXY, AND HYDROXYPHENYL-TERMINATED ALKANETHIOL MONOLAYERS

4-(12-mercaptododecyloxy)phenol (**1**), 3-(12-mercaptododecyloxy)phenol (**2**), 4-(12-mercaptododecyl)phenol (**3**), 4-(12-mercapto-dodecyl)phenol (**4**), 12-phenyldodecyl-mercaptan (**5**), 12-phenylundecyoxymercaptan (**6**), 4-(6-mercapto-hexyl)phenol (**7**), and 4-(12-mercaptododecyloxy)phenol (**8**) were synthesized. The thiol products were characterized by NMR, HRMS, and elemental analysis. Self-assembled monolayers (SAMs) on gold substrates were prepared from thiols **1**-**8**, and the resulting monolayer surfaces were analyzed using Reflectance Absorbance Infrared Spectroscopy (RAIRS), contact angle goniometry, ellipsometry, reductive desorption cyclic voltametry, and impedance spectroscopy.

Several aromatic C-C vibrational frequencies in the RAIRS spectra, for SAMs of **1**-**8**, reveal a dependence of peak intensity on substitution regiochemistry of the aromatic ring. This result suggests that the orientation of the aromatic ring changes with substitution. Peak intensity, and peak widths of alkyl C-H vibrational features in the RAIRS spectra also reveal a dependence of the environment of the alkyl chain on structure of thiols **1**-**8**. Meta-substitution seems to significantly alter the projection of the terminal –OH group relative to para-substitution.

Contact angles were obtained for each SAM surface using water, glycerol, and ethylene glycol. From the contact angle data, Zisman and Fowkes analyses were performed in order to determine surface free energy values and also to determine the dispersive contribution to the surface energy. The energy values obtained from the Zisman plots as well as the dispersive contributions obtained from the Fowkes plots suggest a dependence of surface energy on substitution regiochemistry of the aromatic ring. The results are consistent with the interpretation of the RAIRS spectra as they relate to the effect substitution regiochemistry has on SAM structure and interfacial properties.

The results of the reductive desorption measurements performed on each monolayer surface, indicate that changes in substitution regiochemistry do not seem to affect the surface coverage of SAMs **1**-**8**. Desorption potentials however, are affected by the structure of the thiols composing the SAM, which suggests that the lateral stability resulting from interactions of the terminal groups and alkyl chains, is different for each monolayer surface. Specifically SAMs of 12-phenyldodecylmercaptan (**5**) and SAMs of 4-(12-mercaptododecyloxy)phenol (**1**) seem to be more stable due to interactions of the terminal aromatic ring in SAMs of (**5**) and due to an increase in van der Waals interactions in SAMs of (**1**).

Film thicknesses, as determined by ellipsometry, also suggest that meta-substitution of the aromatic ring results in lower thicknesses for SAMs of (**4**), which is consistent with the interpretation of the structural changes resulting from

meta-substitution, suggested by the interpretation of the RAIRS spectrum of SAMs of (**4**). Thickness measurements also indicate that most of the functionalized SAMs (**1**-**4**, **7**, **8**) react with OTS, which suggests the terminal –OH group is not shielded at the interface and is available for reaction. Following reaction with OTS the RAIRS spectra of the reacted surfaces reveal structural changes to the underlying SAM.

Impedance spectroscopic measurements performed on SAMs of **1**-**8** reveal what seems to be a correlation between the orientation of the aromatic ring and the resistance properties of the SAM. It appears meta-substitution of the ring lowers the monolayers ability to resist electron transfer.

These data suggest that meta-substitution of the aromatic ring has a significant impact upon the structure of the resulting monolayer relative to monolayers composed of para-substituted molecules. The data also suggests that there is a correlation between molecular structure and interfacial properties particularly as it relates to surface energy and reactivity. Small atomic changes in the molecules composing the SAM result in measurable differences in macroscopic properties of the interface. It is important to recognize the need for understanding structure-property relationships in self-assembled monolayers particularly if logical design of surfaces is to be achieved and applied towards solving problems associated with corrosion and adhesion of metal surfaces.

Acknowledgements

First of all I would like to thank my wife for all of her love, support, extreme patience, and dedication. I dedicate this thesis to you. I would also like to thank my parents and my brother for all their love, and support. They have allowed me to pursue my interests and have always provided for my every need.

I would especially like to thank Dr. Leo A. Bares who has been my mentor for so many years and to whom I owe so much.

I would also like to thank Dr. Gordon Yee for all the helpful discussions throughout the last year, for all of the helpful advice, and for his extreme generosity.

I would also like to thank my advisors Dr. Mark Anderson and Dr. Paul Deck for their guidance and instruction throughout these last 5 years.

Finally I would like to thank the members of both of my research groups: Matt Thornberry, Eric Hawrelak, Owen Lofthus, Xu Cheng, Alice Harper, Stephanie Hooper, Rich Baltzersen and Huimin Kang for your helpful discussions, assistance in lab, and for putting up with me all this time.

Table of Contents

List of Figures

List of Tables

Chapter 1 Literature Review

1.1 Introduction to Self-Assembled Monolayers (SAMs)

During the past 15 years significant effort has been devoted to the study of self-assembled monolayers and their applications in chemistry and materials science.[1-3] Due to their often dense and stable structure, SAMs have been investigated for use in chemical[4,5] and biosensor technology,[6-8] corrosion prevention,[9-14] lubrication,[15] adhesion,[16-18] nonlinear optimal films,[19-22] electronics,[23] and other areas. The breadth of potential applications has directed academic research toward understanding the fundamental relationships between structure and interfacial monolayer properties. Research in the electronics and polymer industries have emphasized the use of SAMs in thin film technologies.[24-30] The ability to tailor the functionality of the constituent molecules makes SAMs ideal for the investigation of fundamental principles governing intermolecular forces (van der Waals interactions, hydrogen bonding, π-π interactions), molecular substrate interactions, and molecule-solvent interactions that affect interfacial properties such as wetting,[31-34] ordering,[35,36] growth,[37-39] adhesion,[40-42] lubrication,[36,43] and corrosion.[10,14,44]

The ultimate goal of most SAM research is to understand the structure-property relationships and, more importantly, to determine which structural factors enable rational but wide-ranging control over the properties of the resulting SAM. The next few sections summarize recent research in the area of self-assembled monolayers. Synthetic efforts to introduce various functional groups into self-assembled monolayers are also reviewed.

1.2 Self-Assembled Monolayers- a Review

Self-assembled monolayers (SAMs) are ordered molecular assemblies formed by the spontaneous adsorption of an active surfactant on a solid support.[3] SAMs are described as being highly ordered and uniformly oriented. They are typically composed of alkyl

chains, which can incorporate various functionalities at the chain termini, allowing access to many chemically tailored surfaces.[3]

1.2.1 Methods for Preparing Monolayers. SAMs are prepared by two primary methods. In the Langmuir-Blodgett (LB) approach, an amphiphilic molecule is first spread at an air-water interface. This deposited layer must be mechanically compressed to obtain a densely packed arrangement in which the amphiphiles are approximately normal to the surface. Subsequent dipping of a substrate into the water transfers a layer of the amphiphilic molecule onto the substrate surface.[39]

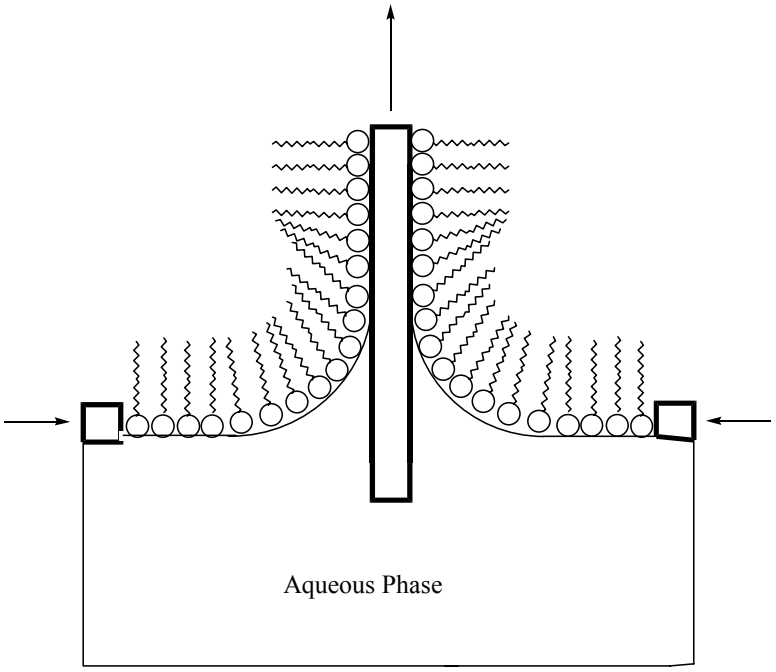

Figure 1. Langmuir-Blodgett monolayer preparation method

The Langmuir-Blodgett method is particularly useful when creating multilayers. However the LB method suffers several drawbacks. First, LB films are not covalently bonded to the surface and are therefore not robust.[45] Temperature changes can often lead to reorganization of the molecular components of the monolayer or deterioration of the film altogether.[46] Second, structural changes in the monolayer can occur upon transfer to a substrate. Uneven or incomplete distribution of the monolayer on the substrate can

occur upon transfer. Third, one is restricted to compounds that form LB films on water, so solubility of the molecular components is a major limiting factor.[39]

In the second approach, monolayers are formed by deposition of the surfactant onto a solid substrate directly from solution. The SAM forms because of strong substrate-head group interactions (e.g. RS-Au) and strong Van der Waals and dipole-dipole interactions amoung hydrophilic (e.g. n-alkyl) groups. The resulting layers are thermodynamically stable and mechanically robust. SAMs are stable enough that reactions can be performed on the formed monolayer to investigate structure and reactivity.[39]

1.3 Properties of Alkane Thiol Self-Assembled Monolayers on Gold

Self-assembly of surfactant molecules on metal surfaces was reported by Zisman[47] in 1946. Zisman discovered that eicosyl alcohol ($C_{20}H_{41}OH$) in hexadecane formed hydrophilic surfaces on platinum, nickel, copper, gold and a series of other metal substrates. Nuzzo and Allara[48] showed more recently that di-*n*-alkyl disulfides self-assembled on gold surfaces. This discovery prompted significant research in the area of SAMs. Most of the initial investigations on self-assembled monolayers focus on the adsorption of linear alkanethiols onto gold surfaces as shown in Figure 2. The number of methylene units in the chain is designated by n and can vary in number from 2-20 and where X can be one of several functional groups that do not disrupt chain packing and are chemically compatible with the thiol moiety.[39]

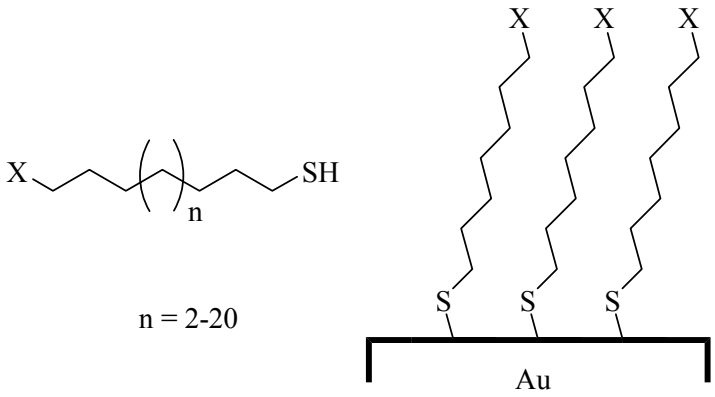

Figure 2. Linear alkane thiol and thiolate SAM

Following extensive characterization, by a range of techniques such as optical ellipsometry[49] contact angle goniometry,[31,50,51] reflection adsorption infrared spectroscopy[48] and electrochemistry[49], the picture which emerges is a monolayer film of densely packed hydrocarbon chains in an all anti-conformation bound to the gold surface by the sulfur atom.[39] The alkyl chains are tilted ~30° relative to the surface normal. According to diffraction studies[35,46]the sulfur atoms form a $\left(\sqrt{3} \times \sqrt{3}\right)$ R 30° overlayer on the Au (111) lattice (Figure 3).

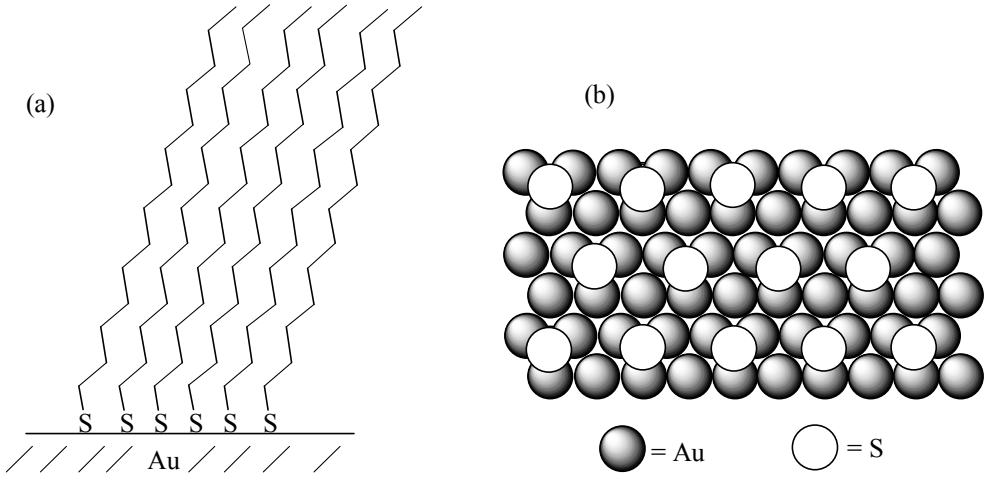

Figure 3. (a) Side view of alkanethiolates on gold. (b) Top view of an epitaxial hexagonal coverage scheme for alkanethiolates on gold

Another important structural characteristic of SAMs is the arrangement of the alkyl chains within the monolayer. The alkyl chains are almost exclusively anti extended with the axis of the chain tilted at ~30°.[49] Computer simulations[52] suggest that the outermost ends of the the chains have greater mobility than inner portions of the chain which suggests the possibility of occasional gauche defects at the chain termini (Figure 4).

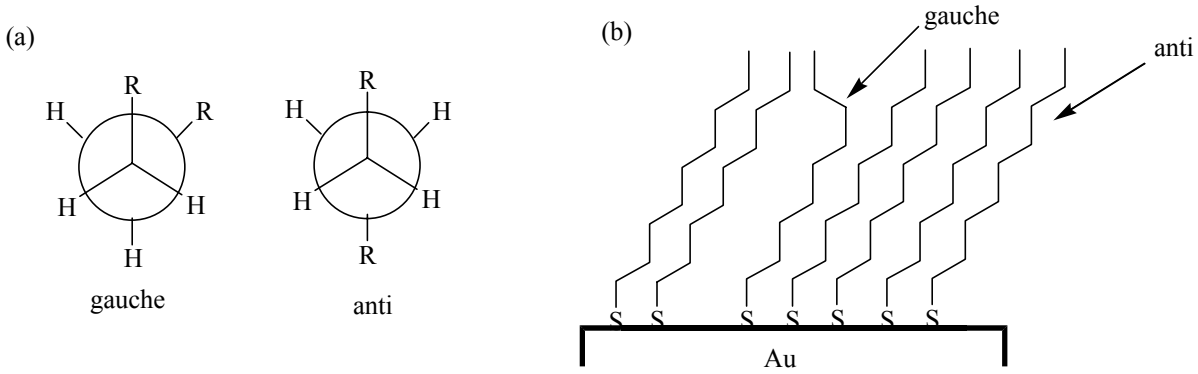

Figure 4. (a) Conformational minima for n-alkanes. (b) Orientation of alkyl chains in SAMs

The nature of the bonding has been established by XPS, infrared spectroscopy, and electrochemistry.[3] The alkanethiol reaction with the gold substrate can be described as an oxidative addition of the S-H bond to gold followed by reductive elimination of hydrogen:

$$R{-}S{-}H \quad + \quad Au^{o} \longrightarrow \quad R{-}S^{-}Au^{+} \; + \; 1/2\, H_2$$

The combination of hydrogen atoms yields H_2, which is an exothermic process. The bonding of the thiolate group to the gold surface is strong and the homolytic RS-Au bond strength is ~ 40 kcal/mol.[3]

1.3.1 Chain Length Effect on Monolayer Structure. Further investigations demonstrate that alkyl chain length affects terminal group orientation, packing density, and coverage.[49,53] Porter *et al.*[49] report that, for methyl terminated alkanethiols with $n \leq 9$, the monolayer is much less densely packed, leading to lower film thicknesses. Measured film thicknesses reveal that chains with $n \leq 9$ the measured thickness is 40% less than that predicted by theoretical closest packing. The theoretical model assumes a length of 1.3 Å per CH_2 unit and a 30^{o} tilt angle for an all anti alkyl chain. The deviation of the experimental data from the model indicates that either the chains are not fully extended, are more tilted, are not in an all anti arrangement, or that the chains are not as densely packed leading to a lower refractive index. A combination of effects may account for the observed film thicknesses. For chains with $n \geq 11$ the monolayer adopts a more densely

packed crystalline structure (~10% more) than predicted by theory, indicating that the chain tilt angle may be less than 30^{o}. Infrared spectroscopic data reveal low band intensities for CH_2 vibrational modes (2800-2950 cm^{-1}) for short chains. Average values for short chain symmetric and asymmetric CH_2 stretching modes are 4-6 cm^{-1} higher than the corresponding values observed for longer chain SAMs. Comparison of infrared spectra of crystals and liquids of each compound to the infrared spectra of each compound adsorbed to gold reveals that short chain SAMS are more liquid-like and longer chain SAMs are more crystalline. Electrochemical data indicate that short chain SAMs are more permeable to Cl^- and ClO_4^- ions than their longer chain counterparts, indicating a less densely packed surface structure.[49]

For monolayers composed of alkanethiols of varying chain length ("mixed monolayers"), chain length has a significant effect on the wetting properties of the resulting film. Bain *et al*.[37,45,54] demonstrate that disorder in mixed monolayers can be controlled by mixing two alkanethiols of different chain length in different relative concentrations in the adsorbing solution. Dodecanthiol ($CH_3(CH_2)_{11}SH$) and docosanethiol $CH_3(CH_2)_{21}SH$ were used to form monolayers.[54] The contact angle of hexadecane for SAMs of pure dodecanthiol was 47^{o} and 46^{o} for docosanethiol. By mixing different proportions of each thiol in the adsorbing solution, Bain *et al*. were able to achieve hysteresis in the contact angle of mixed monolayer surfaces, reaching a minimum value of 10^{o} for an adsorbing solution ratio of 10/30 (dodecanethiol to docosanethiol). Hysterisis in the contact angle results from the formation of a heterogeneous surface in which the monolayer is not segmented into islands of docosanethiol and dodecanthiol. Therefore the longer chain component of the mixed surface is believed to "bend over" the shorter components exposing underlying methylene units and lowering the contact angle. The contact angle minimum coincides with a film thickness intermediate between the thicknesses of each pure SAM. This indicates that the two components do not undergo phase separation into macroscopic islands.[54] In a related study Bain *et al*.[55] also demonstrated that co-adsorption of mixed monolayers is under thermodynamic control. For adsorbing solutions containing mixtures of short and long chain alkanethiols and, where the concentration of the short chain component is higher, the SAMs that are formed were preferentially composed of

the longer chain component.[55] This preference seems to be directly related to increased Van der Waals interactions present in the longer chain alkanethiols. Increased Van der Waals interactions lead to more stable monolayer structures, which are more crystalline. Incorporation of shorter chain components decreases the stabilization from chain-chain interactions, leading to less stable and less crystalline monolayer surfaces.[55] Clearly chain length can be used to control order in SAMs and macroscopic wetting of the interface.

1.3.2 Even-Odd Chain Length Effect. Wettability is a sensitive analytical technique used to study monolayers and thin films. A small variation in alkyl chain length can result in a measurable change in water contact angles. Tao *et al*.[56]demonstrate a dependence of surface energy on the length of the alkyl chain in methyl terminated alkanethiol monolayers. Monolayers with an even number of methylene units in the alkyl chain have water and hexadecane contact angles 3^{o} higher than monolayers with an odd number of methylenes.[56] Porter *et al.*[57] illustrate the "even-odd" effect of adsorbed alkanethiols modified by contact printing interfaces where distinct regions of even and odd chain length alkanethiols are found to have measurably different surface energies. Frictional force measurements of the resulting monolayer reveal a frictional force image identical to the stamp used to modify the surface. Lee *et al*.[58]further illustrate the even-odd effect with SAMs generated from aliphatic dithiocarboxylic acids. For dithiocarboxylic acid SAMs, water and hexadecane contact angles are ~9-10^{o} higher for odd numbered chains. Odd numbered chains result in higher energy surfaces. Surface energy and contact angle are inversely related. A large contact angle is associated with a low surface energy whereas low contact angles reflect a high surface energy.

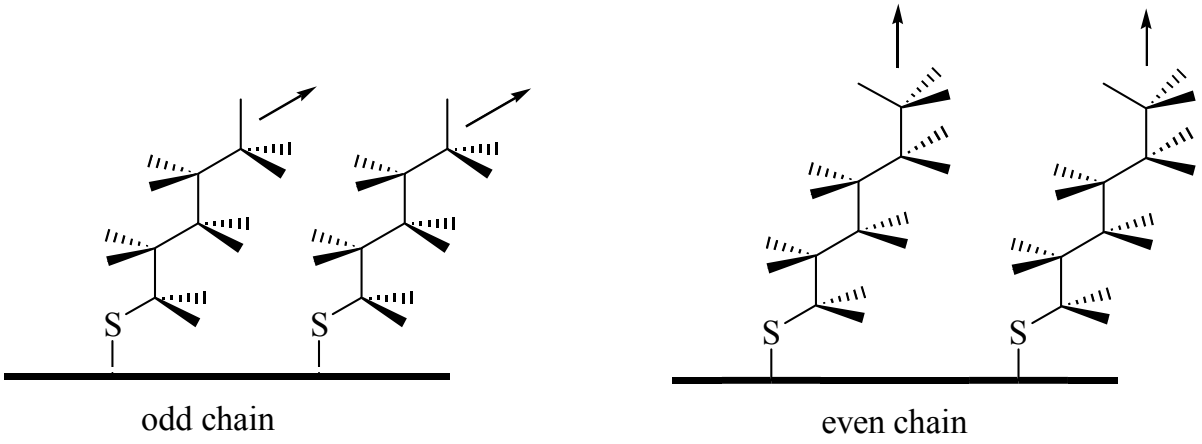

Figure 5. Projection of terminal methyl groups in even and odd numbered carbon chains of a linear alkanethiol.

This behavior is attributed the increased wettability of the underlying methylene units which are more exposed at the surface in odd number chains[58] as is illustrated in Figure 5.

A large contact angle is associated with a low surface energy whereas low contact angles reflect a high surface energy. For liquids with high surface tensions (water, glycerol, ethylene glycol) a low contact angle reflects that the surface being probed has a similar surface tension (surface energy) to the probe liquid, which causes the liquid droplet to spread. Conversely, with high contact angles the surface tension of the probe liquid and the surface are different resulting in less spreading of the liquid droplet. Hydrophilic surfaces are considered high energy surfaces whereas hydrophobic surfaces are considered low energy surfaces.

1.4 Terminal Functional Groups in Self-Assembled Monolayers

Although variations in alkyl chain length affect surface properties, a more effective method of controlling surface energy is the introduction of different functional groups onto the alkane chain terminus. Application of existing synthetic methods allows the introduction of many different functional groups. For straight chain alkanethiols, surface group steric bulk is a limiting factor. If too large, the terminal moiety can prevent the

formation of robust SAMs. Initial investigations are limited to relatively small terminal groups. In the following sections discussion of some efforts to investigate different functionalities are presented.

1.4.1 Carboxylic Acid Terminated Self-Assembled Monolayers. Interest in carboxylic acid functionalized self-assembled monolayers is significant due to their ionizable nature. By changing the pH conditions at the monolayer-liquid interface it is possible to change surface wettability. Whitesides *et al.*[59] demonstrated that water contact angles for surfaces of 11-mercaptoundecanoic are pH sensitive. At pH = 5 the surface is hydrophobic becoming completely hydrophilic at pH = 10.[59] Previous investigations[33,51,60] showed that the carboxyl moiety does not significantly disrupt alkyl chain packing and that highly ordered and densely packed monolayer surfaces are obtained.

The carboxylic acid moiety also provides increased stability due to surface hydrogen bonding.[33,51,60,61] Crooks *et al*.[62] reported hydrogen bonding of vapor-phase probe molecules to carboxyl-terminated monolayers and also significant lateral hydrogen bonding among chain termini.[62] Controlling intermolecular interactions on a surface could result in chemically sensitive monolayers or molecular recognition-based chemical sensors.[62] Other research demonstrates the reactivity of the carboxylic acid moiety. Hutt *et al*.[63] functionalized SAMs of 3-mercaptopropanoic acid with trifluoroacetic anhydride, pentafluoropropanoic anhydride, and heptafluorobutyric anhydride to obtain semifluorinated surfaces. Using the carboxylic acid terminated SAM as a template for building molecular films, sensors or other electronic devices might be synthetically accessible. It is clear that carboxylic acid terminated thiols form well-ordered SAMs and that their reactivity may be used and employed in many technologically important areas. The breadth of literature reports on these types of SAMs is extensive and only a few are covered in this section.

1.4.2 Amine And Amide Terminated Self-Assembled Monolayers. Other ionizable terminal functional groups include amines. Amides are not ionizable but can serve as H-bond acceptors like amines. Initial studies of amine and amide terminated SAMs reveal

densely packed structures similar to their methyl and carboxylic acid terminated analogs. Tam-Chang *et al*.[64] reported the synthesis of amide terminated alkanethiols and subsequent structural characterization of the SAMs, probing the extent of hydrogen bonding within the SAM structure. Inter-chain hydrogen bonding of the amide moiety for SAMs, which contained the amide functionality β to the thiolate terminus, seems to provide additional monolayer stabilization. Hydrogen bonding is responsible for the increased stabilization of the amide SAMs with respect to SAMs of butanethiol and trifluorobutanethiol, against desorption in high vacuum conditions or exchange with solutions of hexadecanethiol.[64] Other investigations by Chirakul *et al*.[65] employ amine terminated self-assembled monolayers containing diethylene glycol linkages to determine the adsorption of fibrinogen and pyruvate kinase to the SAM surface.[65] Clegg *et al*.[40-42] report that the incorporation of amide functional groups into an alkanethiols provides increased stabilization. Infrared spectroscopy of the amide containing SAMs reveals features which are exclusively due to hydrogen bonded amide groups. The SAMs are shown to be very robust and densely packed and are conceived as potential models for designing new materials and can serve as models to further understand hydrogen bonding within lipid bilayers.

Other approaches incorporate amide functional groups into SAMs via functionalization. Duevel *et al*.[66] introduce the amide functional group into the SAM by reaction of a SAM of 11-mercaptoundecanoic acid with an amine, obtaining well ordered robust SAM surfaces. It is evident that the use of amine-terminated SAMs is particularly useful in the development of chemical and biochemical sensors and reactive surfaces, and that incorporation of amides into a SAM at either the terminus or throughout the alkyl chain provides a possible avenue to new thin films and interfaces. There are many publications, which demonstrate the usefulness of amide and amine terminated SAMs, though they are beyond the scope of this review.[65]

1.4.3 Fluorine-Terminated Self-Assembled Monolayers. Fluorinated organic materials have drawn much attention due to the their low surface energies. When used to make monolayer surfaces, fluorine-terminated thiols are interesting as they are unreactive. These properties are important when designing surface modifiers.[67] There is little

reported research that focuses on semi-fluorinated n-alkanethiol monolayers, primarily because of the synthetic difficulty of preparing fluorinated thiols. Recent publications by Liu *et al.*,[68] Alves *et al.*,[69] and Motomatsu *et al.*[70] include the syntheses of semifluorinated SAMs and report chain tilt angles of 12° for $CF_3(CF_2)_{11}(CH_2)_2SH$, 20° for $CF_3(CF_2)_7(CH_2)_2SH$, and 56-76° for $CF_3CF_2(CH_2)_6SH$. Their reports indicate that greater fluorination of the alkyl chain results in lower tilt angles of the alkyl chain in the SAM. A more extensive study by Fukushima *et al.*[71] reveals that for SAMs of $CF_3(CF_2)_9(CH_2)_mSH$ (m = 2, 6, 11, 17, 33) an increase in the number of methylene units results in an increase in the tilt of the perfluorinated moiety with respect to the surface normal.[71] Naud *et al.*[67] also report that semi-fluorinated alkanethiol monolayers resist ionic permeation towards fluorides and chlorides. Miura *et al.*[43] observe that semifluorinated alkanethiol monolayers do not exhibit an "even-odd" effect in wettabilities, as is observed for methyl terminated monolayers, and attribute this variance to similar wettabilites of terminal CF_3 and chain CF_2 moieties.[43] Although only a few examples of the properties of semifluorinated alkanethiol monolayers are available in the literature, the development of new synthetic methods will likely yield more fluorinated thin films and materials with tailorable interfacial properties.

1.4.4 Hydroxyl Terminated Self-Assembled Monolayers. Hydroxyl terminated monolayers, like carboxylic acid and amine terminated monolayers, are also ionizable and can undergo surface hydrogen bonding.[61] Many initial reports on SAM chemistry and structure include ω-hydroxy thiol monolayers[34,60] because they are easily synthesized via reduction of the carboxylic acid analogs. Hydroxy-terminated SAMs are hydrophilic and consequently highly wettable. The hydroxyl group does not disrupt alkyl chain packing. Therefore, crystalline, well-ordered monolayers result when the alkyl chain has at least ten methylene units.[53] Miller *et al.*[72] report the use of ω-hydroxy SAMs as effective deterrents to electron transfer. Although defect sites are observed, hydroxy-terminated SAMs are stable under highly oxidizing conditions and withstand several minutes exposure to sulfochromic acid without an observable change to the monolayers' electrochemical properties.[72] In a subsequent publication, Miller *et al.*[73] report the use of ω-hydroxy alkanethiols as probes to determine the structural dependence of long-range

electron transfer and conclude that ω-hydroxy alkanethiol SAMs are effective electron tunneling barriers.[73]

As with carboxylic acid terminated monolayers, functionalization of hydroxy terminated SAMs is also possible. Hutt *et al*.[63] functionalize SAMs of 3-mercaptopropanol with trifluoroacetic anhydride, pentafluoropropanoic anhydride, and heptafluorobutyric anhydride and obtain CF_3- and CF_3CF_2- and $CF_3(CF_2)_2$- terminated SAMs. Crooks *et al*.[74] report the efficient reaction of hydroxyl terminated SAMs with liquid or gaseous heptanoyl chloride to form ester-linked, methyl-terminated monoalyers.[74] As with other ionizable terminal groups, ω-hydroxy terminated SAMs can serve as template surfaces for the formation of new film and materials. Numerous literature reports are available on these types of monolayers but again are too extensive to be covered in the current review.

1.4.5 Phenyl Terminated Self-Assembled Monolayers. The last major class of functional group included in the current review is phenyl and substituted phenyl terminated SAMs. Prior research reveals that gauche defects can be introduced into linear alkanethiols and can lead to increased exposure of CH_2 groups at the surface resulting in a decrease in surface energy. Computer simulations suggest that the outermost ends of the alkyl chains have more mobility than the inner portion leading to occasional gauche defects.[34] The inner most chains remain essentially crystalline.[34] For ω-substituted alkyl chains with polar groups, a significant decrease in surface energy is also observed yet conformational disorder of the alkyl chains can limit the overall contribution of the terminal moiety. In order to minimize the contributions of conformational disorder to surface energy, rigid molecules can be employed. By restricting conformational freedom, the surface energy can be exclusively dictated by the terminal group functionality.[75] Although recent publications demonstrating the usefulness of using rigid thiols for SAM formation have appeared, the major impediment to their widespread study is synthesis. [76] Sabatani *et al*.[77] report the systematic study of p-terphenyl mercaptan (TPM), p-biphenyl mercaptan (BPM) and thiophenol. Water contact angles for all three SAM surfaces reveal a greater hysteresis for thiophenol, which indicates that thiophenol forms less ordered monolayers than either biphenyl or terphenyl mercaptan. Electrochemical studies also reveal efficient

blocking of the gold surface by biphenyl and terphenyl mercaptan. As in the case of SAMs composed of linear alkanethiols, SAMS of thiophenol, TPM, and BPM form a $(\sqrt{3} \times \sqrt{3})$ R30° overlayer on gold.

Creager *et al*.[78] report that SAMs of 4-mercaptobenzoic acid are conformationally rigid. Infrared spectroscopic evidence reveals that the carboxylic acid group is not involved in surface hydrogen bonding. This behavior is in contrast with that of aliphatic carboxylic acid terminated monolayers which are flexible and can adopt conformations which allow for surface hydrogen bonding.[78] Tao *et al*.[79] report an extensive study of a series of substituted thiophenols, benzyl mercaptans, biphenylthiols and 4-biphenylmethanethiols shown in Figure 6. Hydrogen, methoxy and $OC_{16}H_{33}$ are the three functional groups incorporated into the para position of the four aromatic thiols.

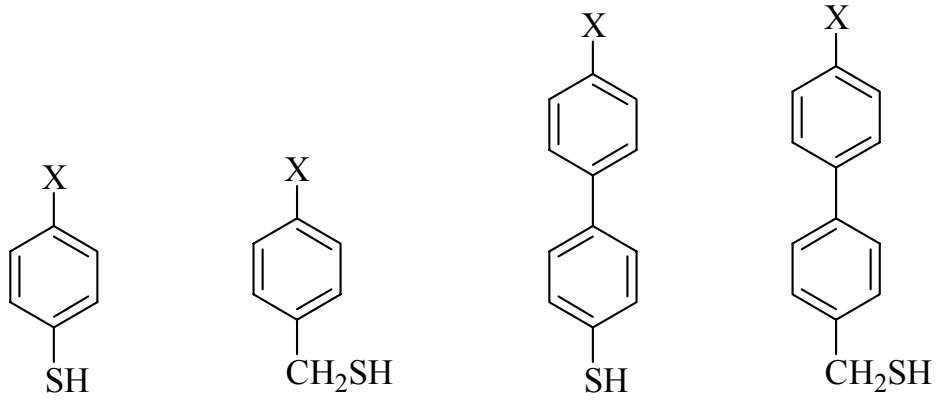

X= H, OCH_3, $OC_{16}H_{33}$

Figure 6. Aromatic thiols used by Tao *et al*.

Electrochemical data, water contact angle measurements and infrared spectra reveal that the resulting SAMs fall into two major categories.[79] The first category includes benzyl mercaptans and 4-biphenylmethanethiols, both of which have a CH_2 group between the aromatic ring and the sulfur. Calculated coverages reveal well-ordered, densely packed monolayer surfaces, also evidenced by STM imaging.[79] The second category includes the thiophenols and biphenylthiols. Calculated coverages are much lower than for SAMs in the first category and the desorption peak widths are much larger.[79] They concluded

that SAMs formed from thiophenol and biphenylthiols are not as ordered or densely packed,[79] in agreement with results reported by Sabatani.[77] Presumably the sulfur adopts sp^3 hybridization in the SAMs; therefore thiophenol must tilt significantly relative to the surface normal. For benzyl mercaptans, orbital hybridization of the sulfur does not force the aromatic ring to tilt (Figure 7) and therefore the aromatic ring is more perpendicular to the surface.[79]

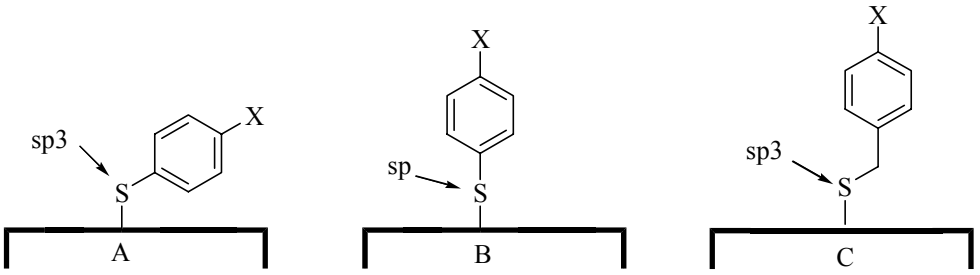

Figure 7. Possible hybridization of thiophenol (A, B), and benzylmercaptan (C)

Whelan *et al*.[80] recently found that benzenethiols are oriented almost perpendicular to gold surfaces. HREELS, XPS, and electrochemical measurements reveal an initial adsorption of thiophenols to Au where the aromatic ring is significantly tilted with respect to the surface normal. A subsequent reorganization step forms islands of perpendicular thiophenols.[80] Kang *et al*.[75] also report an extensive study of a series of 4'-substituted 4-mercaptopbiphenyls on gold and silver surfaces where $-NO_2$, $-COCH_3$, and $-CO_2CH_2CH_3$ are the three functional groups at the 4' position of the biphenyl. Infrared spectroscopy and Eulerian angle analysis reveals surface tilt angles ranging from 14-20^o for the the thiols on gold and tilt angles ranging from 8-21^o for the three thiols on silver surfaces.[75] The reported tilt angles are significantly lower than the corresponding alkanethiol SAMs.[75] Kang *et al*.,[81,82] in two recent reports, investigate the stability of mixed monolayers of rigid mercaptobiphenyl thiols, specifically 4'-methyl-4-mercaptobiphenyl and 4'-hydroxy-4-mercaptobiphenyl. It appears that, unlike the case for mixed linear alkanethiols, mixed monolayers of rigid biphenyls do not undergo contact angle hysteresis and the SAM structure remains constant over a period of 16 months.[81] Rigid substituted phenyl and biphenyl mercaptans give well-organized SAM

surfaces and could be used in various areas such as corrosion protection, adhesion and thin film formation yet synthetic difficulties limit the number of mercaptans that can be used for SAM formation.

Although there are several areas such as phosphate functionalized SAMs, azobenzene containing SAMs, and epoxide terminated SAMs which are not covered in this review, a summary of the main areas, is provided, including the most relevant publications for the various surface functional groups used and also the most important publications of SAM structure available in the literature.

1.5 Substrate Surfaces for SAM Formation

Most of the SAMs reported in the literature use gold as the metal substrate. Gold does not easily form a surface oxide and is easy to handle and clean. Other noble metals such as silver and copper readily form surface oxides, which are unsuitable for formation of self-assembled monolayers. Although gold is the most commonly used metal for SAMs investigations, there are several reports of formation of SAMs on silver, copper and even non-metals such as silicon. The following sections provide a limited review of what is reported in the literature concerning SAMs on metal surfaces other than gold and what effect substrate changes have on SAM properties.

1.5.1 Silver Substrates. Even though silver is in the same period as gold, its properties are slightly different even though its atomic radius is nearly identical. Since silver forms surface oxides more easily than gold, substrate preparation is more involved and is done in oxygen free environments prior to formation of SAMs. Laibinis *et al*.[31,83,84] are the first to report a study of the differences between SAMs prepared on silver and gold. They conclude from contact angle measurements, XPS, and infrared spectroscopic data that long chain alkanethiols are more densely packed on silver than on gold and that the alkyl chain is less tilted relative to the surface normal. The average tilt angle for gold is reported to be ~30^{o} whereas with silver the average tilt angle is ~12^{o}. The differences are attributed to greater interchain spacings for SAMs on gold. The spacing is imposed by the epitaxial metal/sulfur interaction, which, in the case of silver, allows for closer

packing of the alkyl chains of the thiols in the SAM.[31,83] Walczak *et al*.[85] also report similar results with a wider series of straight chain alkanethiols that include various chain termini. They report an average tilt angle of ~13° and also observe more densely packed SAM structures than the corresponding gold SAMs. SAMs on silver also seem to provide a more efficient barrier to ion transport to the metal surface which is of particular interest to surface modification of electrodes, although reproducible preparation of thiol monolayers is more difficult on silver than on gold.[85] The limited number of SAM literature reports using silver as the metal substrate is mainly due to the difficulty of clean substrate preparation.

1.5.2 Copper Substrates. Copper is also in the same group as silver and gold, and when used as a substrate for SAM formation, the properties of the resulting monolayer resemble those of silver more than gold. Laibinis *et al*.[31,83,84] report a series of studies which include copper as a substrate and find that the tilt angle for alkanethiol chains is ~ 12° and that the chains contain fewer gauche defects than SAMs on gold. The results are nearly identical to those found for silver and suggest that the SAMs are more densely packed and better ordered on copper and silver. The main drawback is that copper readily forms a surface oxide layer, even under stringently oxygen and water-free conditions, limiting the reproducibility of SAM formation.[83] The interest in SAMs on copper is significant.[14] Copper is a cheaper metal and can be used in microelectronics applications if appropriately passivated against surface corrosion. Again, as in the case of silver, there are few reports in the literature concerning the effects copper substrates have on SAM structure and is likely due to the difficulty in preparing clean surfaces as well as difficulty in reproducibly generating SAM surfaces.

1.5.3. Silica and Silicon Substrates. The last classes of substrates included in the current review are silica (SiO_2) and silicon. Both are discussed together since silicon dioxide is formed from oxidation of silicon (Figure 8). Silicon derived monolayers are of technological importance and widely used in chromatographic and electronics applications.[86]

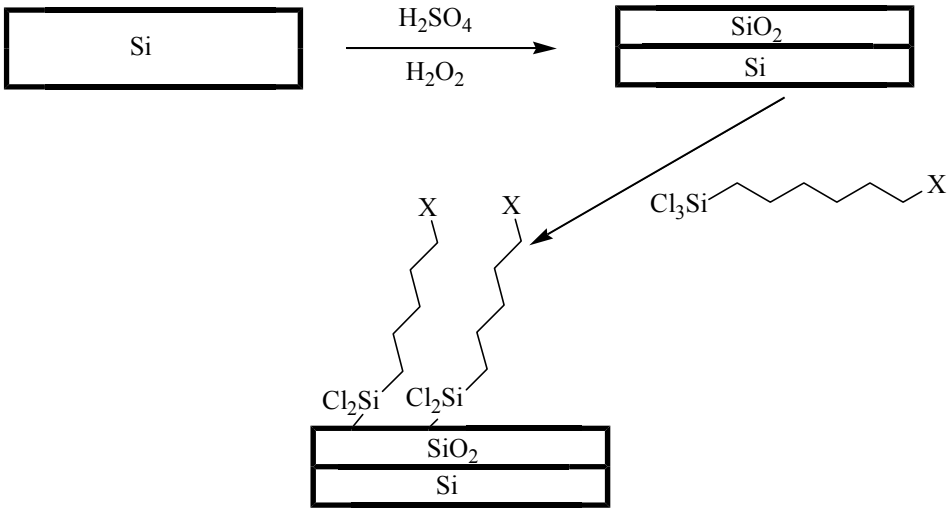

Figure 8. Monolayar formation on Si/SiO_2 substrates

Wasserman *et al*.[87] and Allara *et al*.[88] report that alkylsiloxanes form well-ordered highly robust monolayers when adsorbed on silicon-silicon dioxide substrates. Contact angle measurements, XPS, and infrared spectroscopy reveal that the alkyl chains in long chain alkylsiloxanes are tilted ~10^o and contain significant gauche defects in the chain termini.[87, 88] Other recent reports by Abdelghani *et al*.[89] report the formation of highly ordered monolayers of octadecyltrichlorosilane (OTS) on silicon electrodes.

In an attempt to develop an understanding of how to develop semiconductor biosensors, Aldelghani and co-workers oxidized n-doped silicon substrates to form a layer of SiO_2, which is subsequently functionalized with OTS.[89] Ellipsometric measurements confirm monolayer formation which is in accord with impedance measurements performed on the functionalized electrode. Infrared spectroscopic measurements confirm a well-ordered densely packed arrangement of alkyl chains.[89] Figure 9 illustrates what is believed to be the structure of OTS monolayers on SiO_2. Baptiste *et al*.[90] report the formation of self-assembled multilayer silane films on Si. The silicon surface is oxidized prior to functionalization (Figure 10).

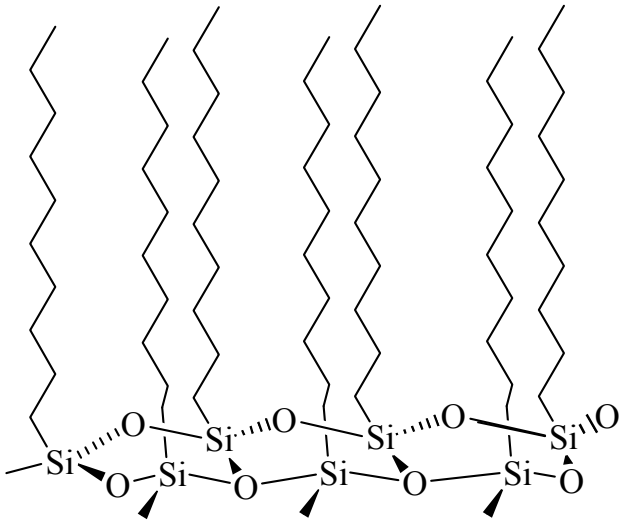

Figure 9. A schematic representation of OTS on SiO_2.

Infrared spectroscopy, Raman spectroscopy, and X-ray reflectivity measurements confirm the formation of multilayers by the synthetic path detailed above. Baptiste and coworkers demonstrate that planned multilayer architectures (Figure 10) of alkylsilanes can be achieved with a high degree of order and uniformity.[90]

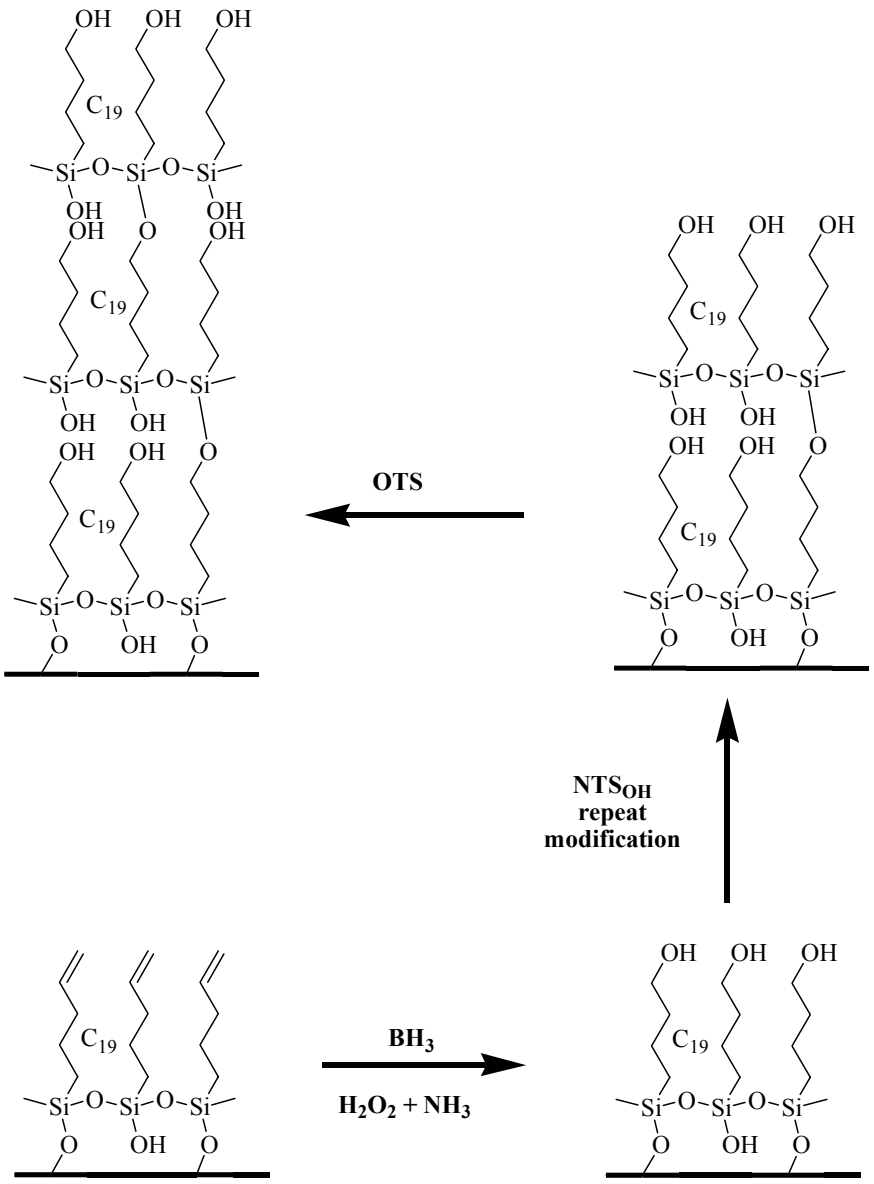

Figure 10. Diagram of multilayer formation with OTS on SiO_2 surfaces.

Near edge X-ray photoelectron studies of OTS monolayers seem to confirm the nearly perpendicular arrangement of the alkyl chains of SAMs of OTS on SiO_2.[91] There are numerous examples reported in the current literature of monolayers on silicon and SiO_2 substrates. It is evident from the previous examples that Si and SiO_2 are important substrates for SAMs and are expected to be more important in the near future in the development of new biosensors, synthetic bilayers, or surfaces appropriate for biomolecule attachment.[3]

1.6 Concluding Remarks on SAM Literature Review

Although not comprehensive, the preceding review is meant to convey the breadth of work which has been carried out in the past 15 years on self-assembled monolayers and the impact these developments have had on current technology. Also, it is important to understand the approach that investigators have taken to establish structure-property relationships in monolayers, in order to better understand the approach the author and coworkers have used to further the understanding of structure property relationships in phenyl terminated self-assembled monolayers.

Although many challenges and problems have been encountered and addressed in SAM chemistry, many aspects of structure-property relationships remain to be explored. A limited number of reports in the literature discuss efforts directed toward understanding how small atomic changes affect structure and interfacial properties.[36,92] It is hoped that through a series a systematic studies, involving the synthesis of new molecules, an understanding of structural factors controlling orientation and structure of surface bound species can be obtained. As mentioned in the previous sections, most studies have altogether changed surface functional groups in linear alkanethiols or in substituted phenyl-terminated thiols. Very few have varied the substitution pattern on the terminal aromatic moiety and still fewer have combined the use of long chains with phenyl substitution. The goal of this research is to understand the role of functional group regiochemistry on interfacial structure, surface energy, and reactivity of aryl-terminated alkanethiol self-assembled monolayers (SAMs) on gold. The relationship between SAM structure, interfacial surface energy, and reactivity reveals factors influencing corrosion passivation and adhesion of phenyl-terminated SAMs. As the regiochemistry is changed, the reactivity and projection of the terminal functional groups is altered. Eight compounds were prepared and characterized by solution NMR, IR, and MS. Their respective SAMs were prepared and characterized by reflectance absorbance infrared spectroscopy (RAIRS), impedance spectroscopy, reductive desorption cyclic voltammetry, and contact angle goniometry. RAIRS spectra provided a means of establishing the spatial orientation of the surface phenyl ring and the terminal –OH group.

By examining the position and intensity of the vibrational features of the RAIRS spectra for SAMs **1**-**8** (Figure 12), a series of spectroscopic "fingerprints" were recognized and used to develop an interfacial structure model for each of the monolayer surfaces. Reductive desorption measurements were used to determine surface coverage and desorption potentials for each monolayer. By examining the desoprtion potential, relative stabilities towards desorption for each surface could be established. Sessile drop contact angle goniometry further elucidated surface structure and interfacial surface free energy. Impedance spectroscopic measurements provided a means of establishing a relationship between interfacial structure and corrosion resistance of each SAM on gold. Chapter 2 describes our SAM surface design and the synthesis and characterization of the eight specific alkanethiols adsorbed on gold. Chapter 3 describes the characterization of the SAMs by RAIRS, the use of reductive desorption measurements to calculate surface coverage, and the use of contact angle goniometry to calculate surface energy for all SAM surfaces. Chapters 4-6 describe the conversion of hydroxyphenyl-terminated SAMs to trialkylsiloxy-terminated SAMs (silanization) and the effect the functional group transformation has on RAIRS spectra, SAM thickness, and surface energy of each monolayer.

Chapter 2 Alkanethiol Design and Synthesis

Introduction

In order to investigate the effect changes in regiochemistry and alkyl chain length have on surface energy, we needed a system that would allow synthetic control over the various structural features of the component compounds of the SAM. Section 2.1 shows how we developed our design and which structural features of the SAM we could systematically vary. Section 2.2 and 2.3 describes the synthesis of each of our target compounds. Sections 2.4 and 2.5 detail how SAMs of compounds **1**-**8** were prepared and functionalized.

2.1 Monolayer Design Features

The design of our surfaces was simply a long or short chain thiol terminated in a phenyl or a phenoxy group. Figure 11 illustrates our generic template. Each of the labeled components can be varied systematically. The length of the alkyl chain (n) is 5 or 11 -CH_2- units. The linker "L" can be -CH_2- or -O- and can vary the orientation of the terminal groups or possibly engage in hydrogen bonding affecting surface packing and SAM ordering.

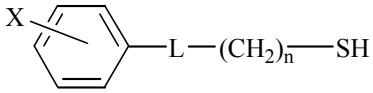

Figure 11. Template for SAM surfaces

The terminal group (X) can also be varied, and is either –H or –OH for these studies. The position of X can be para or meta to L. Other substituents can be incorporated onto the arene ring and serve as additional spectroscopic "handles", or alter the manner in which the surface groups pack.

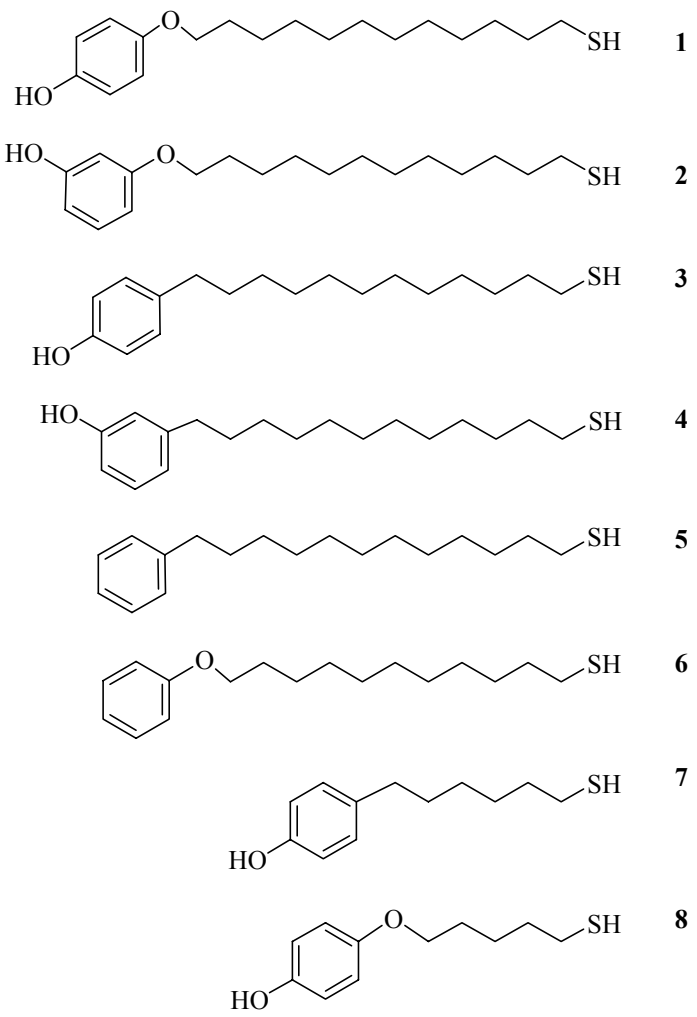

Figure 12 Structures of compounds 1-8.

Of many possible embodiments of the general template, thiols **1-8** (Figure 12) were the easiest to prepare from commercially available starting materials.

2.2 Results and Discussion

2.2.1 Synthesis of 4-(12-mercaptododecyloxy)phenol (**1**)

The first step in the synthetic scheme shown in Figure 13 involves coupling hydroquinone with 1,12-dibromododecane to establish the O-C linkage.

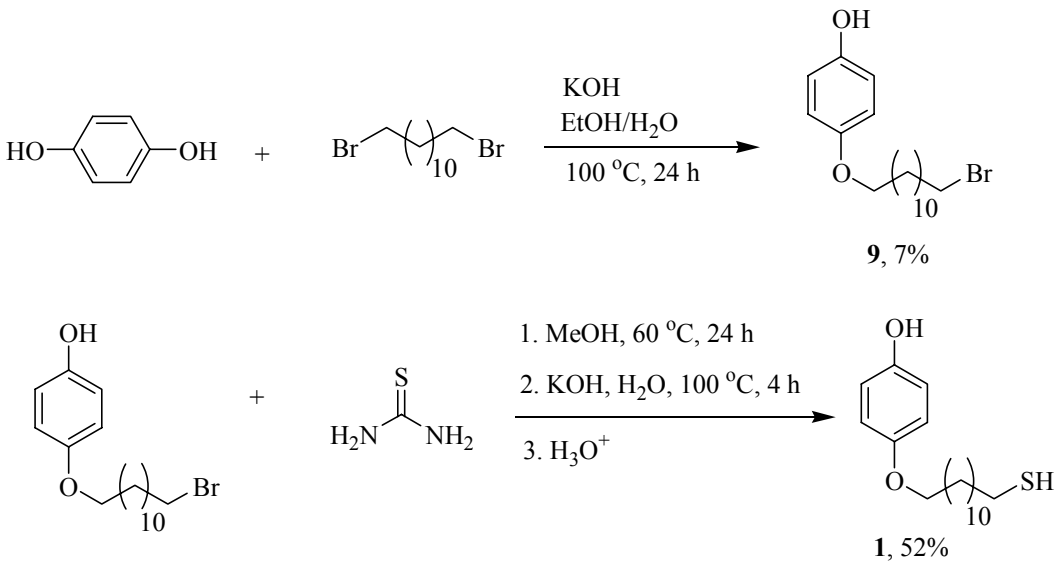

Figure 13. Synthesis of 1

The intermediate alkyl bromide (**9**) is converted to the corresponding mercaptan (**1**). The yield for the first step was 7%. Starting materials were recovered upon chromatographic purification of **9** indicating an incomplete reaction. Side reactions and byproducts (e.g., **A** in Figure 14) could also account for the low isolated yields. The identity of (**9**) was established by ^{1}H NMR.

The yield for the final step was 52%. Byproducts from incomplete alkaline hydrolysis (e.g., **B** in Figure 14) could account for the reduced yields. The identity of (**1**) was established by ^{1}H NMR, ^{13}C NMR, HRMS and elemental analysis.

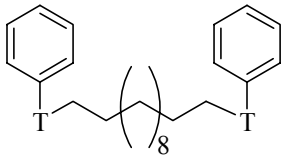

(A)

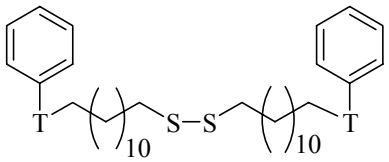

(B)

Figure 14. Putative byproducts in the synthesis of 1, 2, 6, and 8 (T=O), and 3, 4, 5, and 7 (T=CH_2)

2.2.2 Synthesis of 3-(12-mercaptododecyloxy)phenol (**2**)

The first step in the synthetic scheme shown in Figure 15 involves the coupling of resorcinol with 1,12-dibromododecane to establish the O-C linkage.

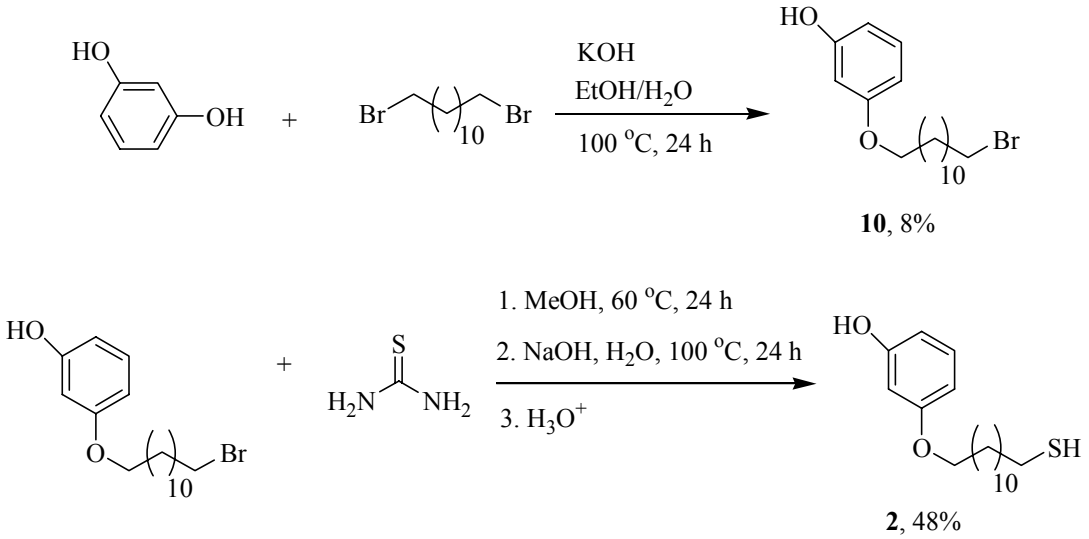

Figure 15. Synthesis of 2

The intermediate alkyl bromide (**10**) is converted to the corresponding mercaptan (**2**). Starting materials were obtained upon chromatographic purification of **10** indicating an incomplete reaction. Side reactions and byproducts could also account for the low isolated yields as in the case of compound **9**. The identity of (**10**) was established by ^{1}H NMR and elemental analysis. The identity of **2** was established by ^{1}H NMR, ^{13}C NMR and HRMS.

2.2.3 Synthesis of 4-(12-mercaptododecyl)phenol (**3**)

The first step in the synthesis of compound **3** involves the lithiation of 4-bromoanisole followed by coupling with 1,12-dibromododecane to establish the $–CH_2-$ linkage as shown in Figure 16. Compound **11** and 4-bromoanisole could not be separated using flash chromatography, so the product mixture was carried on to the following step. Conversion of the methyl ether to the phenol product allowed better separation of products, and compound **12** was obtained following chromatographic separation and characterized using ^{1}H NMR and elemental analysis.

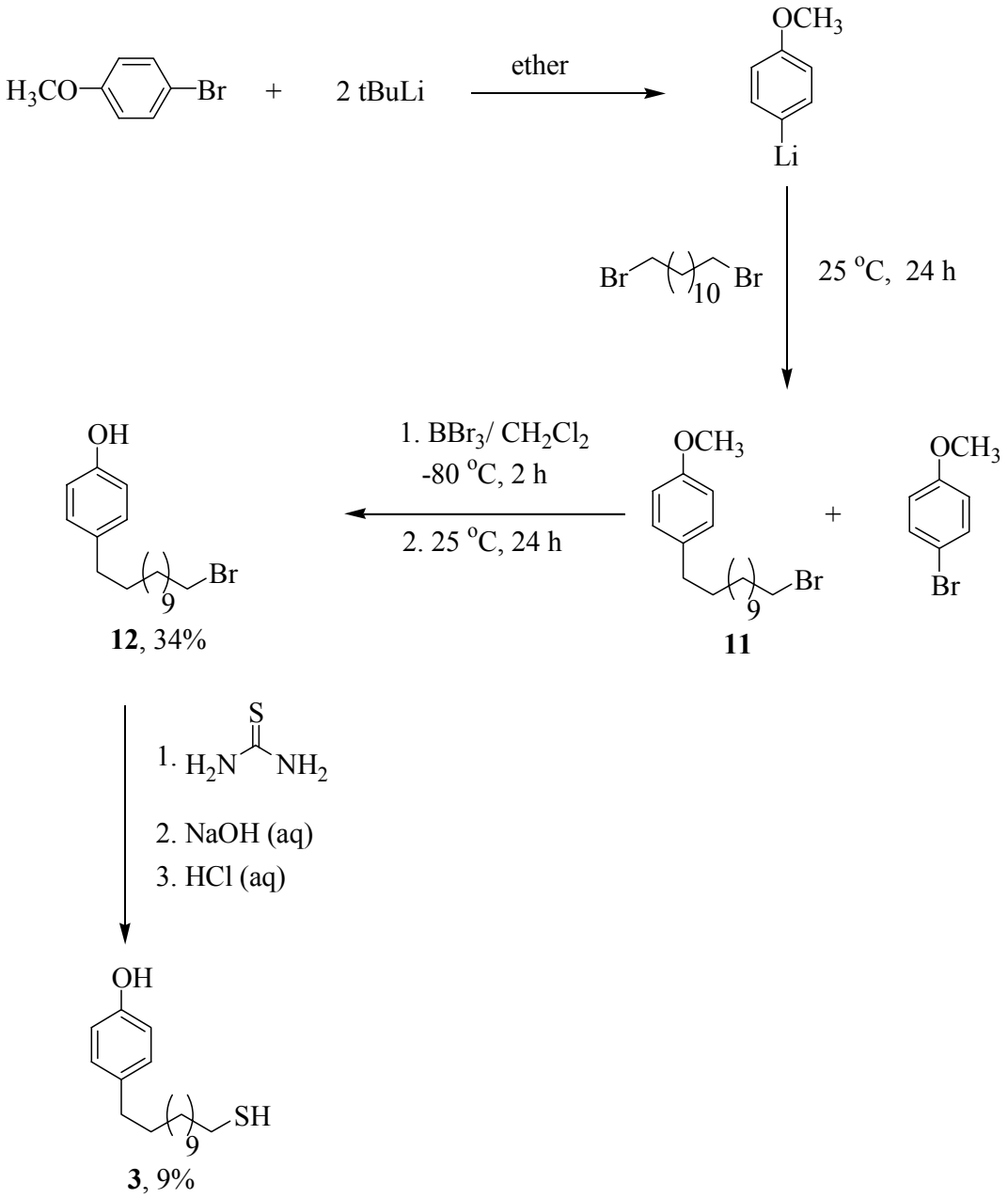

Figure 16. Synthesis of 3

As in the case of compounds **1** and **2**, the yields for each of the intermediates (**11** and **12**) and the final product (**3**) were low and likely due to side reactions resulting in byproducts structurally similar to those shown in Figure 14. The identity of (**3**) was established by ^{1}H NMR, ^{13}C NMR and HRMS.

2.2.4 Synthesis of 3-(12-mercaptododecyl)phenol (**4**)

The initial step in the synthesis of compound **4** involves the lithiation of 3-bromoanisole followed by coupling with 1,12-dibromododecane to establish the $–CH_2-$ linkage as shown in Figure 17. Compound **13** and 3-bromoanisole could not be separated using flash chromatography so the product mixture was carried on to the following step. Conversion of the methyl ether to the phenol product allowed better separation of products, and compound **14** was obtained following separation by flash chromatography and characterized using ^1H NMR. The identity of thiol **4** was established by ^1H NMR, ^{13}C NMR and HRMS.

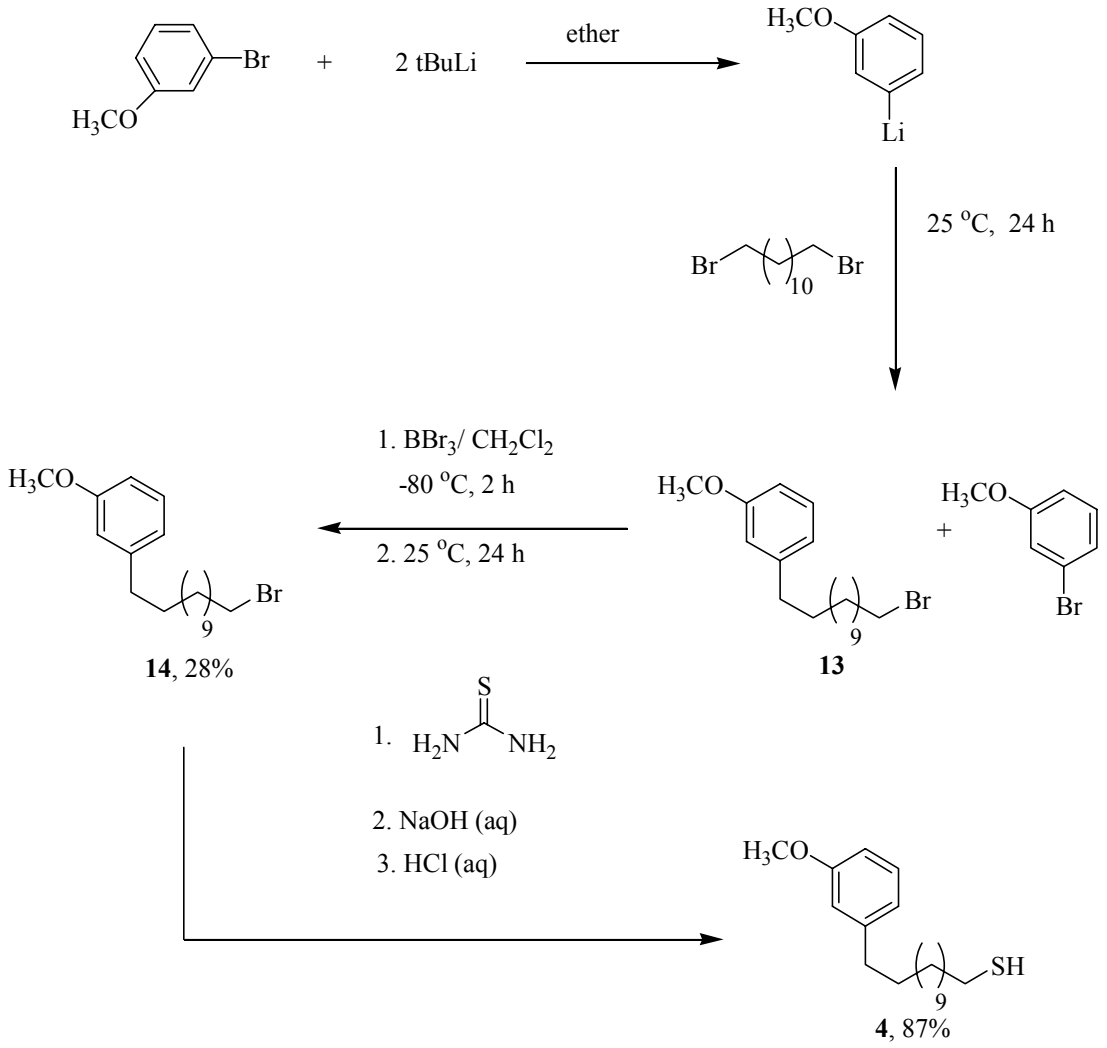

Figure 17. Synthesis of 4

2.2.5 Synthesis of 12-phenyldodecylmercaptan (**5**)

The first step in the synthesis of compound **5** is the coupling of phenyllithium with 1,12-dibromododecane to form the $–CH_2-$ linkage as shown in Figure 18. Compound **15** could not be isolated by either flash chromatography or vacuum distillation. The mixture of products were carried on to the next synthetic step. Incomplete alkaline hydrolysis in the presence of thiourea gave the thiol (**5**) in 49% yield. As in the case of compounds **1, 2, 3,** and **4**, the yield for the intermediate (**15**) was low and likely due to side reactions resulting in byproducts structurally similar to those shown in Figure 14. The identity of compound **5** was established by ^1H NMR, ^{13}C NMR and HRMS and elemental analysis.

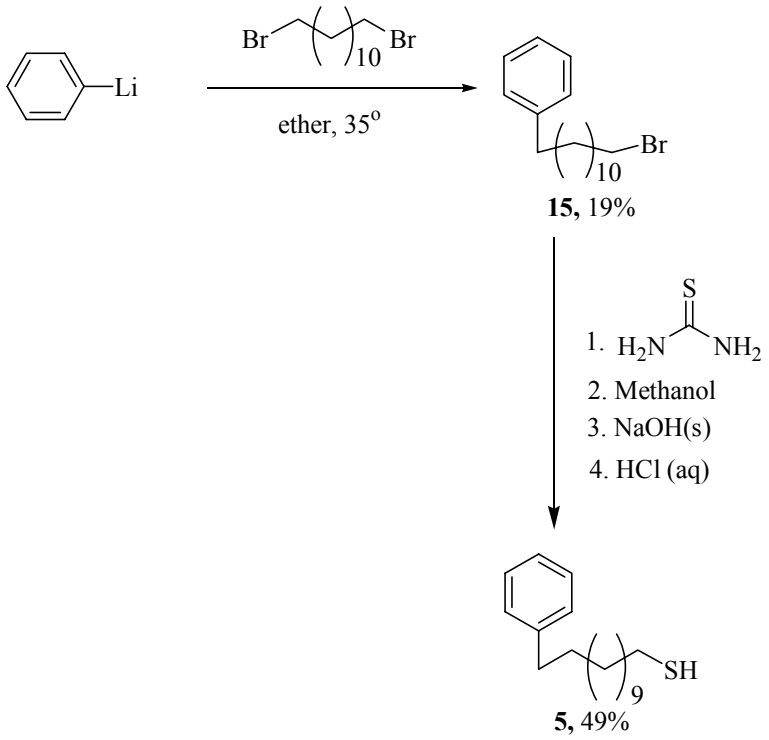

Figure 18. Synthesis of 5

2.2.6 Synthesis of 12-Phenoxyundecylmercaptan (**6**)

The initial step in the synthesis of **6** is the reaction of phenol with NaH followed by coupling of the resulting phenoxide anion with 1,11-dibromoundecane to establish the C–O linkage as shown in Figure 19. Compound **16** could not be isolated in pure form by flash chromatography. Following several separations removing 1,11-dibromoundecane, the mixture of compounds **16**

and **17** was carried on to the next step. Alkaline hydrolysis in the presence of thiourea gave a separable mixture of **6** and **17**. The identity of compound (**6**) was established by ^{1}H NMR, ^{13}C NMR and HRMS.

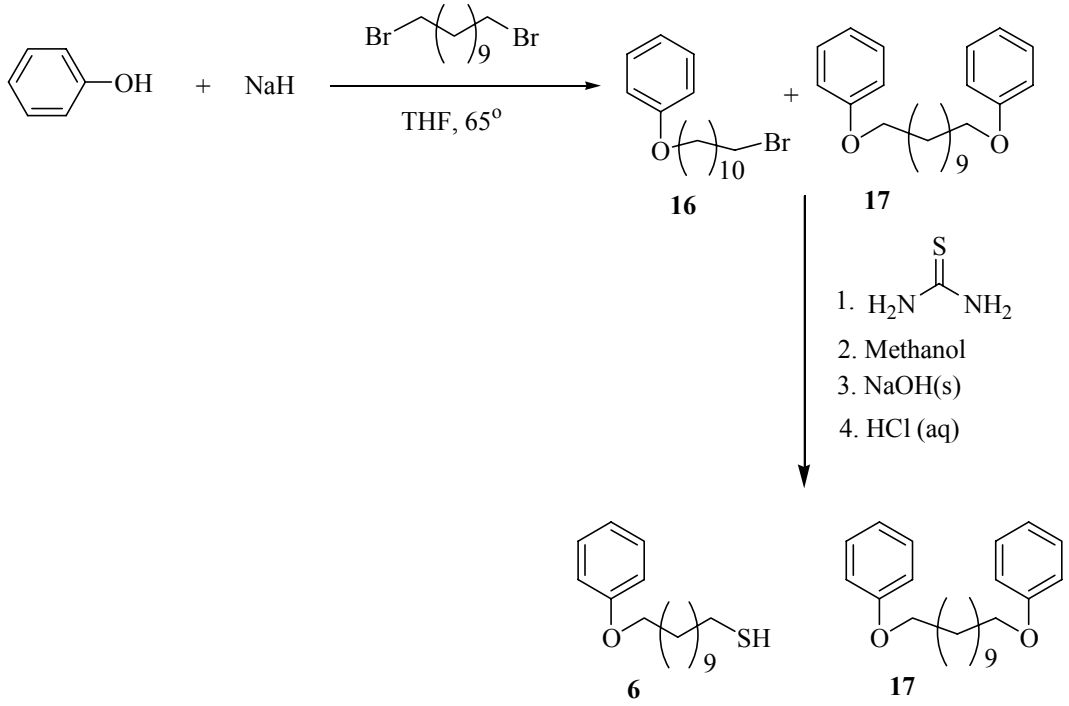

Figure 19. Synthesis of 6

2.2.7 Synthesis of 4-(6-mercaptohexyl)phenol (**7**)

The initial step in the synthetic scheme shown in Figure 20 involves the lithiation of 4-bromoanisole followed by coupling with 1,6-dibromohexane to establish the $-CH_2-$ linkage. Compound **18** and 4-bromoanisole could not be separated using flash chromatography so the product mixture was carried on to the following step. Conversion of the methyl ether to the phenol product allowed better separation of products, and compound **19** was obtained following separation by flash column chromatography and characterized using ^{1}H NMR and elemental analysis. The identity of thiol **7** was established by ^{1}H NMR, ^{13}C NMR and HRMS.

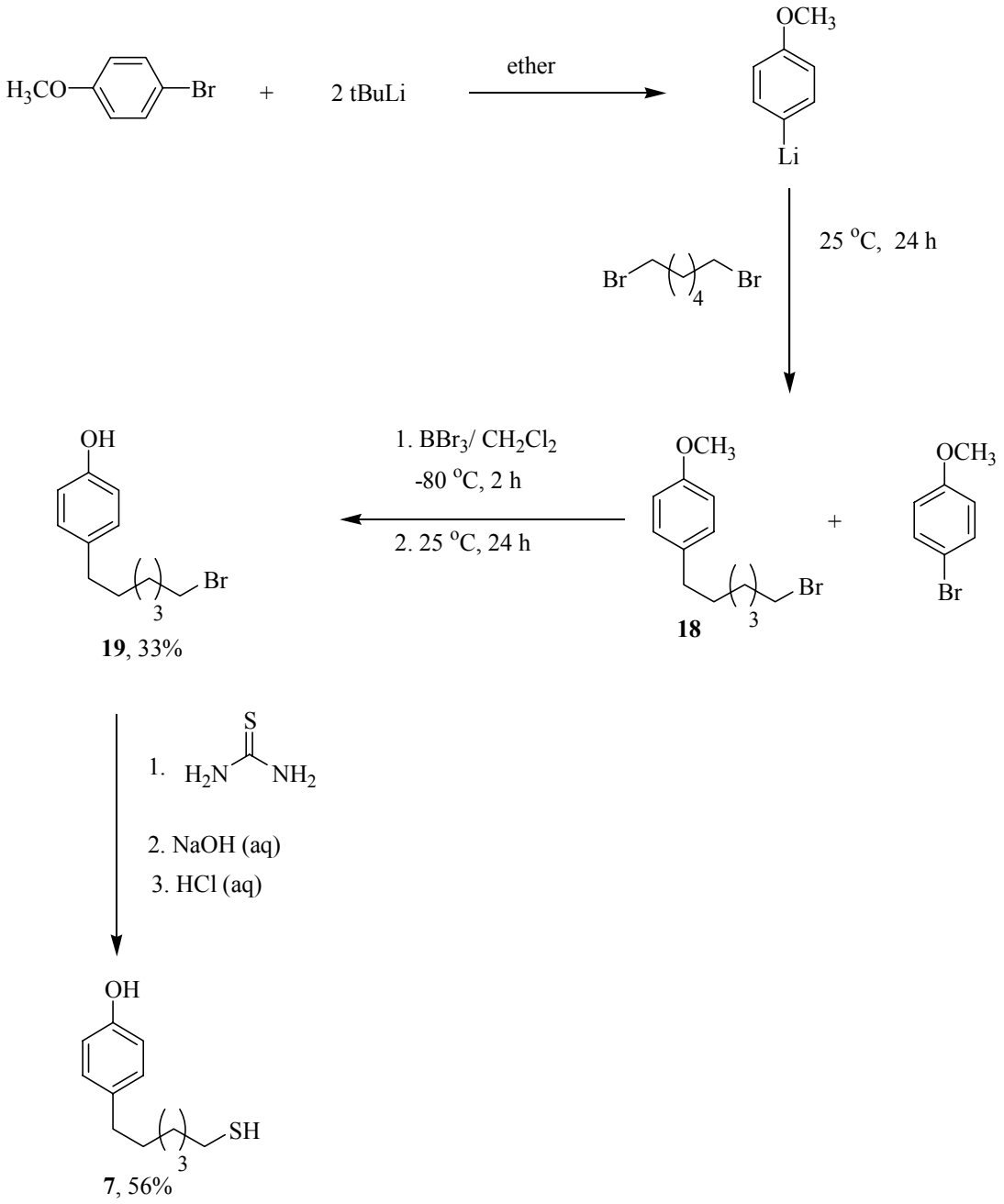

Figure 20. Synthesis of 7

2.2.8 Synthesis of 4-(6-mercaptopentyloxy)phenol (**8**)

The first step in the synthetic scheme shown in Figure 21 involves the coupling of hydroquinone with 1,5-dibromopentane to establish the O-C linkage.

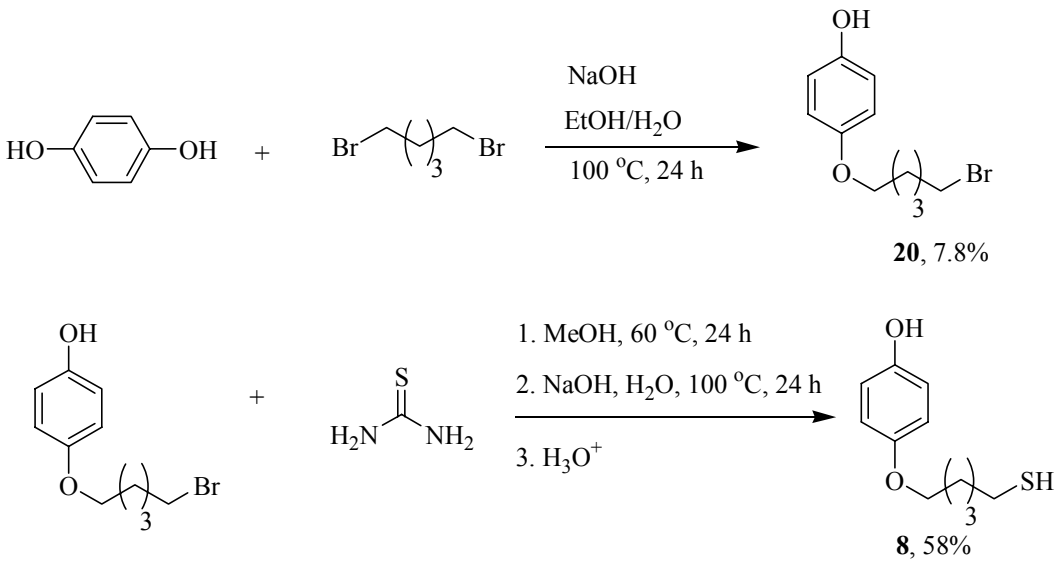

Figure 21. Synthesis of 8

The intermediate alkyl bromide (**20**) is converted to the corresponding mercaptan (**8**). The yield for the first step was 8%. Starting materials were recovered following the purification of compound **20** by flash chromatography indicating an incomplete reaction. The identity of **20** was established by ^{1}H NMR. The yield for the final step was 58%. The identity of thiol **8** was established by ^{1}H NMR, ^{13}C NMR and HRMS.

2.3 Experimental Section

2.3.1 General Synthetic Methods. Hydroquinone, resorcinol, 1,12-dibromododecane, 1,11-dibromoundecane, 1,6-dibromohexane, 1,5-dibromopentane, 4-bromoanisole, 3-bromoanisole, tert-butyllithium in hexane, thiourea, octadecyltrichlorosilane, BBr_3, and BH_3 in THF were used as received from Aldrich. Potassium hydroxide, sodium hydroxide, and anhydrous magnesium sulfate were obtained from Mallinckrodt and used as received. HPLC grade ether, THF, and dichloromethane were obtained from Aldrich and were degassed and dried with alumina columns prior to use.[93] Triethylamine was obtained from Aldrich and distilled from calcium hydride prior to use. Sodium hydride was obtained as a mineral oil dispersion from Fisher, washed with several portions of hexane, dried under vacuum, and stored in a nitrogen glove box. Phenol was obtained

from Aldrich, dissolved in ether, and dried over alumina prior to use. All reactions were carried out under a nitrogen atmosphere using standard inert-atmoshere techniques. NMR spectra were obtained on a Varian Inova 400 MHz spectrometer. High resolution mass spectra were obtained on a JEOL HX100 spectrometer.

2.3.2 Synthesis of 4-(12-bromododecyloxy)phenol (**9**) Hydroquinone (15.0 g, 0.136 mol) was dissolved in ethanol (75 mL) in a 200 mL Schlenk flask under nitrogen. A solution of 1,12-dibromododecane (10.0 g, 0.0305 mol) in 100 mL of deoxygenated ethanol was added using a syringe. A condenser was fitted, and the mixture was stirred and refluxed for 1 h under nitrogen. KOH (2.22 g, 0.0396 mol) was added to the mixture, and the reaction was refluxed overnight. The solvent was then evaporated. The product (crude **9**) was collected and dissolved in 100 mL of benzene. The solution was refluxed overnight using a Dean-Stark apparatus to remove water. Benzene was then evaporated and the white solid placed in the thimble of a Soxhlet apparatus and extracted with pentane. After evaporation of the pentane, NMR analysis confirmed a complex mixture of products which was then separated using flash chromatography on silica gel, eluting with, 10% ethyl acetate in hexane to afford 0.70 g (7%) of the brominated product (**9**). ^{1}H NMR (CD_2Cl_2, 400 MHz): δ 6.77 (m, 4H, Ph) , 4.33 (s, 1H, OH), 3.84 (t, 2H, CH_2-OPh), 3.40 (t, 2H, CH_2Br), 1.49 (p, 2H, (CH_2-CH_2Br)), 1.72 (p, 2H, -(CH_2-CH_2-OPh)), 1.27 (m, 16H, -$(CH_2)_8$-).

2.3.3 Synthesis of 4-(12-mercaptododecyloxy)phenol (**1**) The intermediate alkyl bromide (**9**, 0.70 g, 0.00196 mol) was dissolved in 50 mL of deoxygenated methanol in a 100 mL Schlenk flask. A solution of thiourea (0.72 g, 0.00947 mol) in methanol (25 mL) was added by syringe. The resulting solution was heated under reflux for 24 h under N_2. Methanol was then evaporated, and a white solid was collected. The solid was dissolved in 100 mL of 2M aqueous NaOH and refluxed for 4 h. Aqueous HCl (2 M) was then added to acidify the product mixture. The mixture was then extracted with hexane for 48 h using a continuous liquid-liquid extraction apparatus. The collected hexane was then evaporated to afford a crystalline white solid (crude **1**). The compound was then purified using flash chromatography on silica gel, eluting with 10% ethyl acetate in hexane. The

thiol was obtained in a 52% yield (0.312 g, 0.0010 mol) as a crystalline solid after evaporation of the second chromatographic fraction. ^{1}H NMR (CD_2Cl_2, 400 MHz): δ 6.77 (m, 4H, Ph), 3.88 (t, 2H, CH_2-OPh), 2.52 (q, 2H, CH_2SH), 1.74 (p, 2H, (CH_2-CH_2OPh)), 1.59 (p, 2H, -(CH_2-CH_2-SH)), 1.53 (s, 1H, -SH), 1.26 (m, 16H, -$(CH_2)_8$). ^{13}C NMR (CD_2Cl_2, 100 MHz): δ 155.27 (Ph), 117.73 (Ph), 117.33 (Ph), 70.52 (CH_2-OPh), 36.04 (CH_2), 31.46 (CH_2), 31.41 (CH_2), 31.39 (CH_2), 31.29 (CH_2), 31.29 (CH_2), 31.29 (CH_2), 30.27 (CH_2), 30.97 (CH_2), 27.92 (CH_2), 26.46 (CH_2-SH). HR-MS m/z: 310.1935 a.m.u. Calculated m/z: 310.1967 a.m.u. Anal Calcd C, 69.63; H, 9.74; S, 10.33. Found C, 70.04; H, 10.21; S, 9.80.

2.3.4 Synthesis of 3-(12-bromododecyloxy)phenol (**10**) Resorcinol (7.0 g, 0.0636 mol) was dissolved in ethanol (150 mL) in a 200 mL Schlenk flask under nitrogen. Solid 1,12-dibromododecane (8.34 g, 0.0254 mol) was added. A condenser was fitted, and the mixture was stirred and refluxed for 4 hrs under nitrogen. NaOH (1.272 g, 0.0318 mol) was added to the mixture, and the reaction was refluxed overnight under N_2. The product mixture (crude **10**) was poured into 100 mL of water and acidified to pH~3 with concentrated HCl. The acidified product mixture was then extracted with 400 mL of anhydrous ethyl ether. The ether solution was dried over anhydrous $MgSO_4$ and filtered. After evaporation of the ether, NMR analysis confirmed a complex mixture of products which was then separated using flash chromatography on silica gel, eluting with, 10% ethyl acetate in hexane to afford 0.74 g (8.2%) of the brominated product (**10**). ^{1}H NMR (CD_2Cl_2, 400 MHz): δ 7.14 (t, 1H, Ph), 6.48 (m, 3H, Ph), 4.97 (s, 1H, -OH), 3.95 (t, 2H, CH_2-OPh), 3.46 (t, 2H, CH_2Br), 1.88 (p, 2H, (CH_2-CH_2Br)), 1.77 (p, 2H, -(CH_2-CH_2-OPh)), 1.27 (m, 16H, -$(CH_2)_8$. Anal Calcd C, 60.50; H , 8.18. Found C, 61.09; H, 8.28.

2.3.5 Synthesis of 3-(12-mercaptododecyloxy)phenol (**2**) The intermediate alkyl bromide (**10**, 0.60 g, 0.00168 mol) was dissolved in 70 mL of deoxygenated methanol in a 100 mL Schlenk flask. Solid thiourea (0.655 g, 0.0084 mol) was added. After refluxing for 1 h under N_2, solid NaOH was added. The reaction mixture was refluxed for 24 h. The final product mixture was poured into 100 mL of water and acidified to pH = 3 with concentrated HCl. The mixture was then extracted with 250 mL of anhydrous ethyl

ether. The ether solution was dried over anhydrous $MgSO_4$, filtered, and evaporated to afford a crystalline white solid (crude **2**). The compound was then purified using flash chromatography on silica gel, eluting with 10% ethyl acetate in hexane. The thiol was obtained in a 48 % yield (0.250 g, 0.00084 mol) as a crystalline solid after evaporation of the second chromatographic fraction. ^{1}H NMR (CD_2Cl_2, 400 MHz): δ 7.12 (t, 1H, Ph), 6.44 (m, 3H, Ph), 4.96 (s, 1H, -OH), 3.95 (t, 2H, CH_2-OPh), 2.54 (q, 2H, CH_2SH), 1.79 (p, 2H, (CH_2-CH_2OPh)), 1.62 (p, 2H, -(CH_2-CH_2-SH)), 1.43 (s, 1H, -SH), 1.26 (m, 16H, -$(CH_2)_8$). ^{13}C NMR (CD_2Cl_2, 100 MHz): δ 160.64 (Ph), 156.83 (Ph), 129.99 (Ph), 110.34 (Ph), 106.91 (Ph), 101.85 (Ph), 68.05 (CH_2-OPh), 34.11 (CH_2), 29.52 (CH_2), 29.48 (CH_2), 29.44 (CH_2), 29.41 (CH_2), 29.34 (CH_2), 29.21 (CH_2), 29.04 (CH_2), 28.35 (CH_2), 25.97 (CH_2), 24.52 (CH_2-SH). HR-MS m/z: 310.1956 a.m.u. Calculated m/z: 310.1967 a.m.u.

2.3.6 Synthesis of 4-(12-bromododecyl)phenol (**12**) To a solution of 3.90 g (0.0212 mol) of 4-bromoanisole in 50 mL of ether in a 200 mL Schlenk flask was added tert-butylithium in hexane (24.5 mL, 1.7 M, 0.0416 mol) slowly. The reaction was stirred for 1 h. Then, a solution of 1,12-dibromododecane (6.96 g, 0.0212 mol) in 50 mL of ether was added by syringe. The mixture was stirred for 24 h. After evaporating the solvents, the crude product mixture was separated using flash chromatography on silica gel, eluting with 10% ethyl acetate/hexane. The crude intermediate (a mixture of **11** and 4-bromoanisole) was dissolved in 50 mL of dichloromethane, cooled to –80 ^{o}C, and treated with BBr_3 (5.5 g, 0.0219 mol). The reaction was stirred for 2 h at –80 ^{o}C and then allowed to warm up to room temperature overnight. The reaction was then mixed with 120 mL of H_2O. The mixture was extracted with 200 mL of ether. The ether layer was then extracted with 120 mL of 2M NaOH solution. The aqueous layer was neutralized with 2M HCl and extracted with two 200 mL portions of ether. The ether layer was dried over anhydrous magnesium sulfate, filtered, and evaporated. The product mixture (1.38 g) was purified using flash chromatography on silica gel, eluting with 10% ethyl acetate/hexane. The first fraction contained compound **12** (7.14 g, 0.00714 mol, 34%). ^{1}H NMR (CD_2Cl_2, 400 MHz): δ 7.08 (m, 2H, Ph), 6.76 (m, 2H, Ph), 3.46 (t, 2H, CH_2Br),

2.56 (t, 2H, CH_2-Ph), 1.88 (p, 2H, (CH_2-CH_2Br)), 1.59 (p, 2H, -(CH_2-CH_2-Ph)), 1.26 (m, 16H, -$(CH_2)_8$-). Anal Calcd C, 63.34; H, 8.56. Found C, 62.91; H, 8.73.

2.3.7 Synthesis of 4-(12-mercaptododecyl)phenol (**3**) The intermediate alkyl bromide (**12**, 2.00 g, 0.00586 mol) was treated with a solution of thiourea (1.38 g, 0.0181 mol) in 60 mL of methanol at 80 ^oC for 15 h. The methanol was then evaporated and treated with 150 mL of 2M KOH and refluxed for 12 h. The aqueous solution was extracted with hexane using a liquid-liquid extraction apparatus for 24 h. The hexane was then evaporated. The final product was purified using flash chromatography on silica gel, eluting with 10% ethyl acetate/hexane. The second fraction yielded 0.152 g (9% yield) of compound **3**. ^1H NMR (CD_2Cl_2, 400 MHz): δ 7.07 (m, 2H, Ph, 6.76 (m, 2H, Ph), 4.81 (s, 1H, OH), 2.55 (m, 4H, (-CH_2-Ph), (-CH_2SH)), 1.61 (m, 5H, -(CH_2-CH_2-Ph), –(CH_2CH_2SH), SH), 1.31 (m, 16H, -$(CH_2)_8$-). ^{13}C NMR (CD_2Cl_2, 100 MHz): δ 153.55 (Ph), 135.19 (Ph), 129.35 (Ph), 114.87 (Ph), 34.93 (CH_2), 34.11 (CH_2), 31.74 (CH_2), 29.57 (CH_2), 29.56 (CH_2), 29.54 (CH_2), 29.48 (CH_2), 29.46 (CH_2), 29.21 (CH_2), 29.04 (CH_2), 28.35 (CH_2), 24.52 (CH_2-SH). HR-MS m/z: 294.2037 a.m.u. Calculated m/z: 294.2017.

2.3.8 Synthesis of 3-(12-bromododecyl)phenol (**14**) To a solution of 5.00 g (0.0267 mol) of 3-bromoanisole in 90 mL of ether in a 200 mL schlenk flask was added tert-butylithium in hexane (35.6 mL, 1.7 M, 0.0534 mol) slowly. The reaction was stirred for 1 h. Then, a solution of 1,12-dibromododecane (8.757 g, 0.0267 mol) in 50 mL of ether was added by syringe. The mixture was refluxed for 12 h. After evaporating the solvents, the crude product mixture was dissolved in 250 mL of pentane and 150 mL of water. The biphasic mixture was separated and the pentane layer was kept and dried over anhydrous $MgSO_4$ and filtered. Following evaporation of the solvent the white solid was separated using flash chromatography on silica gel, eluting with 10% ethyl acetate/hexane. The crude intermediate (a mixture of **13** and 3-bromoanisole) was dissolved in 90 mL of dichloromethane, cooled to –80 ^oC, and treated with BBr_3 (10.06 g, 0.0379 mol). The reaction was stirred for 2 h at –80 ^oC and then allowed to warm to room temperature overnight. The reaction was then mixed with 100 mL of H_2O. The

mixture was extracted with 300 mL of ether. The ether layer was dried over anhydrous magnesium sulfate, filtered, and evaporated. The product mixture (7.03 g) was purified using flash chromatography on silica gel, eluting with 10% ethyl acetate/hexane. The first fraction contained compound **14** (2.15 g, 0.0063 mol, 28%). ^{1}H NMR (CD_2Cl_2, 400 MHz): δ 7.12 (t, 1H, Ph), 6.44 (m, 3H, Ph), 4.91 (s, 1H, OH), 3.46 (t, 2H, CH_2Br), 2.54 (t, 2H, CH_2-Ph), 1.87 (p, 2H, (CH_2-CH_2Br)), 1.79 (p, 2H, -(CH_2-CH_2-Ph)), 1.27 (m, 16H, -$(CH_2)_8$-).

2.3.9 Synthesis of 3-(12-mercaptododecyl)phenol (**4**) The intermediate alkyl bromide (**14**, 2.15 g, 0.0063 mol) was treated with a solid thiourea (2.458 g, 0.0351 mol) in 100 mL of methanol and refluxed at 65 ^{o}C for 24 h. Solid NaOH (0.264 g, 0.0066 mol) and reaction was refluxed for another 24 hours. The reaction mixture was the poured into 100 mL of water and acidified to pH = 3 with concentrated HCl. The aqueous mixture was extracted with 400 mL of ether. The ether layer was dried over anhydrous $MgSO_4$ and filtered. Following solvent evaporation the final product was purified using flash chromatography on silica gel, eluting with 10% ethyl acetate/hexane. The second fraction yielded 1.62 g (87%) of compound **4**. The final product was further purified by vacuum sublimation at 100 ^{o}C to yield 1.20 g (65 %) of **4**. ^{1}H NMR (CD_2Cl_2, 400 MHz): δ 7.18 (t, 1H, Ph), 6.69 (m, 3H, Ph), 4.92 (s, 1H, O<u>H</u>), 2.57 (m, 4H, (-<u>CH_2</u>-Ph), (-<u>CH_2</u>SH)), 1.61 (m, 5H, -(<u>CH_2</u>-CH_2-Ph), –(<u>CH_2</u>CH_2SH), S<u>H</u>), 1.31 (m, 16H, -$(CH_2)_8$-). ^{13}C NMR (CD_2Cl_2, 100 MHz): δ 155.60 (Ph), 145.05 (Ph), 129.25 (Ph), 120.80 (Ph), 115.17 (Ph), 112.29 (Ph), 35.72 (CH_2), 34.11 (CH_2), 31.31 (CH_2), 29.58 (CH_2), 29.53 (CH_2), 29.48 (2 CH_2), 29.45 (CH_2), 29.27 (CH_2), 29.04 (CH_2), 28.35 (CH_2), 24.52 (<u>CH_2</u>-SH). HR-MS m/z: 294.2029 a.m.u. Calculated m/z: 294.2051.

2.3.10 Synthesis of 12-phenyldodecylbromide (**15**) To a solution of phenyllithium in hexane (13.2 mL, 0.0238 mol) was added 60 mL of a solution of 1,12-dibromododecane (7.81 g, 0.0238 mol) in ether. The reaction mixture was refluxed under N_2 for 72 h. Solvent was evaporated and the solid products were separated using flash chromatography on silica gel using 2% ethyl acetate/hexane. Compound **15** was not obtained in pure form. The chromatographic fraction containing (**15**) was vacuum

distilled at 2.0 x 10^{-4} torr. Pure **15** was obtained (1.48 g, 19%) of (**15**) in the fraction collected between 120-140 ^{o}C. ^{1}H NMR (CD_2Cl_2, 400 MHz): δ 7.18 (m, 5H, Ph), 3.42 (t, 2H, $\underline{CH_2}$Br), 2.59 (t, 2H, $\underline{CH_2}$-Ph), 1.85 (p, 2H, ($\underline{CH_2}$-CH_2Br)), 1.59 (p, 2H, -($\underline{CH_2}$-CH_2-Ph)), 1.27 (m, 16H, -$(CH_2)_8$-).

2.3.11 Synthesis of 12-phenyldodecylmercaptan (**5**) The intermediate alkyl bromide (**15**, 1.48 g, 0.00455 mol) was treated with a solid thiourea (1.065 g, 0.0136 mol) in 30 mL of methanol and refluxed at 65 ^{o}C for 24 h. Solid NaOH (0.250 g, 0.00625 mol) was added to the mixture and the reaction was refluxed for another 24 h. The reaction mixture was the poured into 100 mL of water and acidified to pH = 3 with concentrated HCl. The aqueous mixture was extracted with 200 mL of hexane. The ether layer was dried over anhydrous $MgSO_4$ and filtered. Following solvent evaporation the final product was purified using flash chromatography on silica gel, eluting with 10% ethyl acetate/hexane. The first fraction yielded 0.62 grams (49%) of compound **5**. ^{1}H NMR (CD_2Cl_2, 400 MHz): δ 7.25 (m, 5H, Ph), 2.62 (t, 2H, (-CH_2-Ph)), 2.56 (p, 2H, (-$\underline{CH_2}$-SH), 1.56 (m, 5H, -($\underline{CH_2}$-CH_2-Ph), –($\underline{CH_2}CH_2SH$), S$\underline{H}$), 1.28 (m, 16H, -$(CH_2)_8$-). ^{13}C NMR (CD_2Cl_2, 100 MHz): δ 153.30 (Ph), 135.17 (Ph), 129.38 (Ph), 114.98 (Ph), 35.02 (CH_2), 35.01 (CH_2), 34.02 (CH_2), 31.69 (3 CH_2), 29.64 (CH_2), 29.63 (CH_2), 29.60 (CH_2), 29.53 (CH_2), 29.20 (CH_2), 24.64 ($\underline{CH_2}$-SH). Anal Calcd C, 77.63; H, 10.86; S, 11.51. Found C, 77.76; H, 1078; S, 11.88.

2.3.12 Synthesis of 12-phenoxy-1-bromododecane (**16**) Sodium hydride (0.381 g, 0.0159 mol) was transferred to a 200 mL Schlenck flask in a nitrogen glove box. THF (30 mL) was then syringed into the flask. With stirring 40 mL of a solution of phenol (0.995 g, 0.0106 mol) in THF was added. The mixture was stirred at 25 ^{o}C for 0.5 h. A solution of 1,11-dibromoundecane (4.00 g, 0.0127 mol), in THF (50 mL), was syringed into the flask. The reaction mixture was refluxed for 72 h. Solvent was removed and the solid product mixture was separated using flash chromatography on silica gel eluting with 5% ethyl acetate/hexane. Good separation of products was not obtained. The collected fractions were recombined, dissolved in 20 mL of pentane, and crystallized at –30^{o}C. Pentane was removed and a second flash chromatographic separation on silica gel eluting

with 5% ethyl acetate/hexane was performed on the collected solid. Two fractions were collected. Solvent was removed from the fraction containing the mixture of (**16**) and (**17**) (0.228 g). ^{1}H NMR (CD_2Cl_2, 400 MHz): δ 7.18 (m, 5H, Ph), 3.42 (t, 2H, $\underline{CH_2}$Br), 2.59 (t, 2H, $\underline{CH_2}$-Ph), 1.85 (p, 2H, ($\underline{CH_2}$-CH_2Br)), 1.59 (p, 2H, -($\underline{CH_2}$-CH_2-Ph)), 1.27 (m, 16H, -$(CH_2)_8$-).

2.3.13 Synthesis of 12-Phenoxyundecylmercaptan (**6**) A mixture of alkyl bromides (**16** and **17**) (0.228 g) was treated with a solid thiourea (0.092 g, 0.0384 mol) in 30 mL of methanol and purged with nitrogen for 0.5 h. Solid NaOH (0.250 g, 0.00625 mol) was added and the reaction mixture was refluxed for another 72 h. The reaction mixture was the poured into 100 mL of water and acidified to pH = 3 with concentrated HCl. The aqueous mixture was extracted with 250 mL of ether. The ether layer was dried over anhydrous $MgSO_4$ and filtered. Following solvent evaporation the final product was purified using flash chromatography on silica gel, eluting with 10% ethyl ether/hexane. Two mixed fractions were collected, containing 0.086 grams of **6** and **17**. ^{1}H NMR (CD_2Cl_2, 400 MHz): δ 7.02 (m, 2H, Ph), 6.71 (m, 2H, Ph), 4.73 (s, 1H, O$\underline{H}$), 2.52 (m, 4H, (-$\underline{CH_2}$-Ph), (-$\underline{CH_2}$SH)), 1.55 (m, 5H, -($\underline{CH_2}$-CH_2-Ph), –($\underline{CH_2}CH_2$SH), S$\underline{H}$), 1.26 (m, 16H, -$(CH_2)_8$-). ^{13}C NMR (CD_2Cl_2, 100 MHz): δ 159.28 (Ph), 129.31 (Ph), 120.29 (Ph), 114.39 (Ph), 67.88 (CH_2-OPh), 32.01, (CH_2), 29.77 (CH_2), 29.53 (3 CH_2), 29.49 (CH_2), 29.40 (CH_2), 29.36 (CH_2), 29.29 (CH_2), 29.22 (CH_2), 28.90 (CH_2), 26.00 ($\underline{CH_2}$-SH). HR-MS m/z: 247.2062 a.m.u. Calculated m/z: 247.2054.

2.3.14 Synthesis of 4-(6-bromohexyl)phenol (**19**) To a solution of 5.00 g (0.0267 mol) of 4-bromoanisole in 50 mL of ether in a 200 mL Schlenk flask was added tert-butylithium in hexane (31.4 mL, 1.7 M, 0.0534 mol) slowly. The reaction was stirred for 1 h. Then, a solution of 1,6-dibromohexane (6.515 g, 0.0267 mol) in 50 mL of ether was added by syringe. The mixture was refluxed for 24 h. After evaporating the solvents, the crude product mixture was separated using flash chromatography on silica gel, eluting with 10% ethyl acetate/hexane. The crude intermediate (a mixture of **18** and 4-bromoanisole) was dissolved in 50 mL of dichloromethane, cooled to –80 ^{o}C, and treated with BBr_3 (8.785 g, 0.0353 mol). The reaction was stirred for 4 h at –80 ^{o}C and then allowed to

warm up to room temperature overnight. The reaction was then mixed with 120 mL of H_2O. The mixture was extracted with 300 mL of ether. The ether layer was dried over anhydrous magnesium sulfate, filtered, and evaporated. The product mixture was purified using flash chromatography on silica gel, eluting with 10% ethyl acetate/hexane as before. The first fraction contained compound **19** (1.48 g, 0.00576 mol, 33%). ^{1}H NMR (CD_2Cl_2, 400 MHz): δ 7.08 (m, 2H, Ph), 6.76 (m, 2H, Ph), 3.46 (t, 2H, CH_2Br), 2.57 (t, 2H, CH_2-Ph), 1.88 (p, 2H, (CH_2-CH_2Br)), 1.65 (p, 2H, (CH_2-CH_2-Ph)), 1.49 (p, 2H, (CH_2), 1.39 (p, 2H, (CH_2). Anal Calcd C, 56.05; H, 6.66. Found C, 55.78; H, 6.57.

2.3.15 Synthesis of 4-(6-mercaptohexyl)phenol (**7**) The intermediate alkyl bromide (**19**, 1.32 g, 0.00513 mol) was treated with solid thiourea (2.00 g, 25.6 mmol) in 60 mL of methanol. The solution was purged with nitrogen for 0.5 h. Solid NaOH (0.246 g, 6.16 mmol) was added and reaction mixture was refluxed for 48 h. The reaction mixture was poured into 100 mL of water and acidified to pH = 3 with concentrated HCl. The aqueous mixture was extracted with 300 mL of ether. The ether layer was dried over anhydrous $MgSO_4$ and filtered. The final product was purified using flash chromatography on silica gel, eluting with 20% ethyl acetate/hexane. The first fraction yielded 0.60 grams (56%) of **7**. ^{1}H NMR (CD_2Cl_2, 400 MHz): δ 7.07 (m, 2H, Ph), 6.77 (m, 2H, Ph), 2.55 (m, 4H, (-$\underline{CH_2}$-Ph), (-$\underline{CH_2}$SH)), 1.63 (m, 4H -($\underline{CH_2}$-CH_2-Ph), –($\underline{CH_2}CH_2SH$),), 1.43 (m, 5H, -$(CH_2)_2$-), S$\underline{H}$). ^{13}C NMR (CD_2Cl_2, 100 MHz): δ 153.60 (Ph), 134.97 (Ph), 129.36 (2 Ph), 114.92 (2 Ph), 34.83 (CH_2), 34.02 (CH_2), 31.57 (CH_2), 28.60 (CH_2), 28.17 (CH_2), 24.49 ($\underline{CH_2}$-SH). HR-MS m/z: 210.1080 a.m.u. Calculated m/z: 210.1078.

2.3.16 Synthesis of 4-(6-bromopentyloxy)phenol (**20**) Hydroquinone (7.506 g, 0.0681 mol) was dissolved in methanol (120 mL) in a 200 mL Schlenk flask. Neat 1,5-dibromopentane (6.27 g, 0.0272 mol) was added. A condenser was fitted, and the mixture was stirred and refluxed for 4 h under nitrogen. NaOH (1.3 g, 0.033 mol) was added to the mixture, and the reaction was refluxed for 48 h. Solvent was evaporated. Water present in product was azeotropically distilled with benzene. Benzene was evaporated and solid remained. Product was extracted with ether using a Soxhlet

extraction apparatus. After evaporation of the ether, NMR analysis confirmed a complex mixture of products which was then separated using flash chromatography on silica gel, eluting with, 20% ethyl acetate in hexane to afford 0.55 g (7.8%) of **20**. ^{1}H NMR (CD_2Cl_2, 400 MHz): δ 6.79 (m, 4H, Ph), 4.78 (s, 1H, -OH), 3.94 (t, 2H, CH_2-OPh), 3.49 (t, 2H, CH_2Br), 1.96 (p, 2H, (CH_2-CH_2Br)), 1.81 (p, 2H, -(CH_2-CH_2-OPh)), 1.63 (p, 2H, (CH_2).

2.3.17 Synthesis of 4-(6-mercaptopentyloxy)phenol (**8**) The intermediate alkyl bromide (**20**, 0.55 g, 0.00212 mol) was dissolved in 50 mL of deoxygenated methanol in a 100 mL Schlenk flask under nitrogen. Solid thiourea (0.828 g, 0.0106 mol) was added. After refluxing for 24 h, solid NaOH (0.169 g, 0.00423 mol) was added. The reaction mixture was refluxed for 24 h. The final product mixture was poured into 150 mL of water and acidified to pH = 3 with concentrated HCl. The mixture was then extracted with 250 mL of anhydrous ethyl ether. The ether solution was dried over anhydrous $MgSO_4$, filtered, and evaporated to afford a clear liquid (crude **8**). The compound was then purified using flash chromatography on silica gel, eluting with 20% ethyl acetate in hexane. The thiol was obtained in a 58 % yield (0.260 g, 1.23 mmol) as a clear liquid after evaporation of the first chromatographic fraction. ^{1}H NMR (CD_2Cl_2, 400 MHz): δ 6.79 (m, 4H, Ph), 3.92 (t, 2H, CH_2-OPh), 2.58 (q, 2H, CH_2SH), 1.81 (p, 2H, ($\underline{CH_2}$-CH_2OPh)), 1.71 (p, 2H, -($\underline{CH_2}$-CH_2-SH)), 1.62 (m, 3H, (CH_2), (SH). ^{13}C NMR (CD_2Cl_2, 100 MHz): δ 155.27 (Ph), 117.73 (Ph), 117.33 (Ph), 70.52 (CH_2-OPh), 31.29 (CH_2), 30.97 (CH_2), 30.27 (CH_2), 27.92 (CH_2), 26.46 (CH_2-SH). HR-MS m/z: 212.0871 a.m.u. Calculated m/z: 212.0871 a.m.u.

2.4 SAM Preparation

Solutions of compounds **1-8** were prepared by dissolving a few milligrams of each compound in 50 mL of chloroform to obtain nominal concentrations of 1.0 x 10^{-3} M. Gold substrates were soaked in "piranha" solution (30% H_2O_2 and H_2SO_4) for 5 minutes, rinsed with water and dried under an N_2 stream. The substrates were then lowered into the compound solutions and allowed to soak for 24 hours. To characterize the SAM, the

slide was removed from the solution, rinsed with ethanol to remove unwanted adsorbates, rinsed thoroughly with deionized water, and dried under a nitrogen stream.

2.5 Silanization of SAMs

SAMs formed from compounds **1**, **2**, **3**, **4**, **7**, and **8** were treated with octadecyltrichlorosilane (OTS) to explore the reactivity of the terminal –OH group, to probe any structural reorganization of the SAM resulting from functionalization, and to probe the corrosion passivation properties of silane fucntionalized SAMs on gold. Each SAM was prepared as described in section 2.4. SAM modified gold substrates were immersed in a 0.1 M chloroform solution of octadecyltrichlorosilane. Each solution contained 0.2 mL of triethylamine. After 24 h the monolayers were rinsed with ethanol and water and dried under a nitrogen stream.

Chapter 3 Monolayer Characterization Techniques

Introduction

Although rigorous spectroscopic characterization of the individual compounds was carried out in solution, different characterization techniques were needed to analyze the SAMs on gold. The primary surface-spectroscopic characterization measurement was RAIRS. Spectra obtained from RAIRS were used to establish the orientation of the terminal phenyl rings and the alkyl chain of each SAM. Section 3.1 contains background on the theory of RAIRS. Section 3.2 provides some background on contact angle goniometry and the use of Zisman and Fowkes plots to determine surface energy. Section 3.3 describes the use of optical ellipsommetry to determine SAM thicknesses. Section 3.4 describes the use of voltammetric desorption measurements to determine surface coverage and relative stability of each SAM surface. Section 3.5 outlines our strategy for analyzing the SAM surfaces and determining SAM structure through the use of the previously described techniques.

3.1 Reflection-Absorption Infrared Spectroscopy (RAIRS)

RAIRS is an external reflection infrared spectroscopic technique well suited for the analysis of surface adsorbed species. RAIRS, like most modern IR methods, uses Fourier transform (FT) instrumentation for spectral data acquisition. The instrumental setup is similar to a transmission FTIR instrument, the only difference is in the sample chamber. Instead of a transmission cell, a reflection attachment is used to direct the IR radiation onto the sample surface (Figure 21).

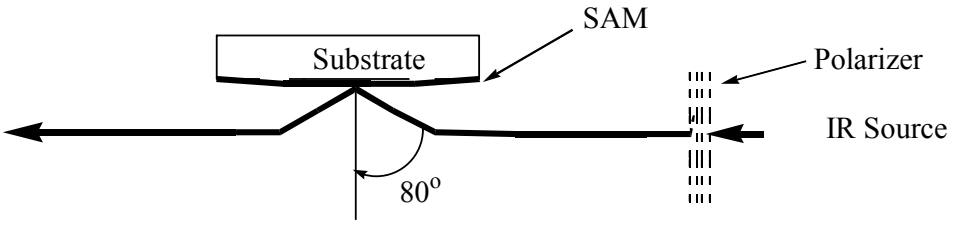

Figure 22. Reflection assembly used in RAIRS

Greenler found that the component of the electric field vector normal to the surface excites dipole-active vibrations of a molecule on the surface.[94,95] His findings give rise to a "surface selection rule": Only vibrations having a component of their transition dipole moment perpendicular to the substrate surface are observed in the reflection infrared spectrum. He also showed that vibrational excitation is only likely to occur at high incidence angles, and therefore grazing angles must be used to obtain surface spectra.[94,95]

Greenler also found that only p-polarized radiation will excite a transition dipole moment. p-Polarized radiation has its electric field vector parallel to the plane of incidence. Upon reflection, p-polarized radiation adds vectorially to its emitted vector. On the other hand, s-polarized radiation, when reflected, does not vectorially add to its emitted vector. The incident vector due to s-polarized radiation is perpendicular to the plane of incidence of radiation; and, when reflected, is phase shifted 180^{o}.[94] This phase shift is important because only transition dipole moments of "A" symmetry can produce an IR active signal; and, therefore, only transition dipole moments that are perpendicular to the surface can interact with incident radiation, and consequently, only with p-polarized light.[94] Figure 23 illustrates the behavior of s- and p-polarized light when reflected from a plane.

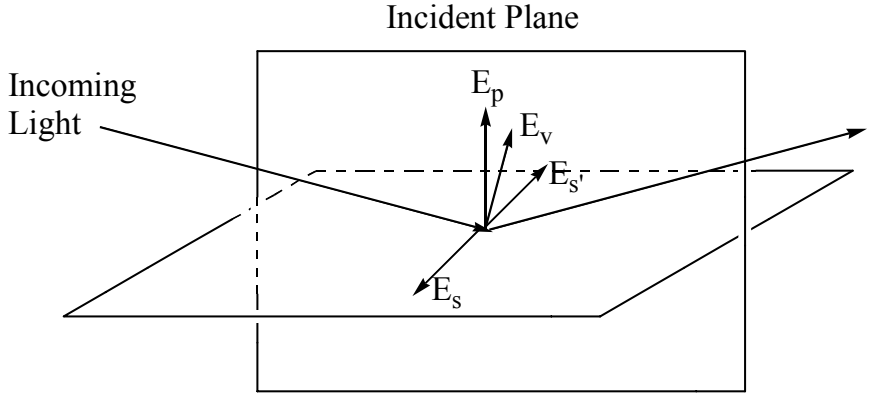

Figure 23. Schematic definition of s and p polarized light. s-Polarized light's E field is parallel to reflection surface (E_s and $E_{s'}$). p-Polarized light's E field is perpendicular to the reflection plane (E_p). The E field of a vibration (Ev) can only couple to the E field of p polarized light

Combining the surface selection rule with experimental signal intensities, the orientation of the organic molecules composing the SAM can be determined with respect to the substrate surface.

Resolution in RAIRS spectra is determined by the heterogeneity of the surface and the nature of the surface molecule interactions rather than any experimental limitation.[96] Surfaces that are not homogeneous in composition and structure can cause an increased signal to noise ratio which lowers resolution. Surface hydrogen bonding can "soften" C-H modes of alkanethiol SAMs on gold substrates causing broadening of the C-H bands also limiting practical resolution.[96] RAIRS is ideal for the characterization of SAMs because vibrational spectra can be obtained from monolayer or submonolayer quantities of surface-adsorbed thiols.[96] For a given SAM, the spectrum obtained is simpler than the corresponding solution transmission spectrum of the chosen alkanethiol, yet direct comparison of vibrational frequencies can be made between the two spectra. RAIRS can also provide evidence for the orientation of surface groups and the packing density of molecules on the metal substrate.[96]

3.2 Surface Energy Measurements

Contact angle goniometry is one of the most widely used methods for determining surface energy.[97] There are several techniques for measuring contact angle, but only the sessile drop method was used. The technique involves placing a drop of an aqueous or non-aqueous liquid on a substrate and measuring the tangential angle at the point of contact of the drop with the surface, as is illustrated in Figure 24a.

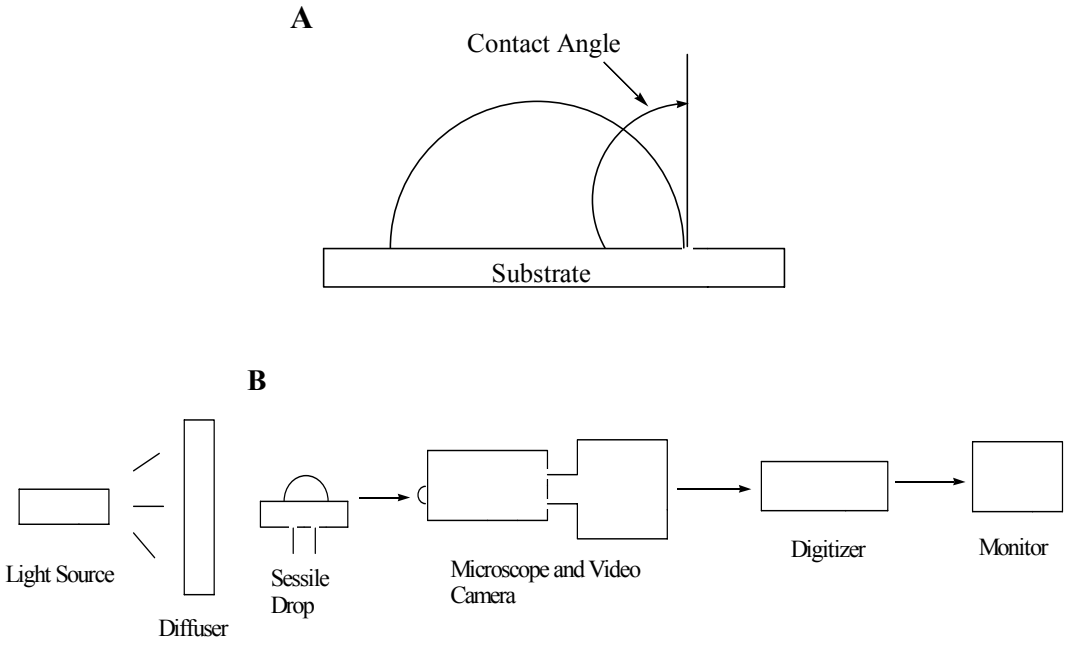

Figure 24. a)Contact Angle Measurement, b) Components of a sessile drop goniometer

If the water contact angle is greater than 90°, the liquid is said to not wet the surface and the surface is considered hydrophobic. If, on the other hand, the water contact angle of the surface is 0°, the surface is considered to be hydrophilic. A zero value is considered to be the limiting extreme in a strictly geometric sense.[97] Most surfaces have measured contact angles between 0° and 100° and are considered more or less hydrophilic based on how close they are to either limit. The instrument used to measure surface contact angles is goniometer. A diagram of a basic goniometer is shown in Figure 24b.

Young and Dupre in the 1800's established the relationship between surface energy, contact angle, and the thermodynamic work of adhesion. Equation 1 illustrates this relationship where w_{AB} is the thermodynamic work of adhesion between a substrate (A) and an adhesive (B).

$$w_{AB} = \gamma_B (1 + \cos \theta) \qquad (1)$$

In eq 1, γ_B is the surface free energy of the adhesive and θ is the contact angle between a liquid and a substrate. Inspection of equation (1) reveals that the largest value of w_{AB} is 2 times $\gamma_{B,}$ and this value occurs when θ is 0°. At this point the surface free energy of the substrate is equal to

that of the probe liquid. This point is known as the critical surface free energy (γ_B^c). We can experimentally determine the critical surface free energy for each modified substrate by measuring the contact angle of each SAM with a series of liquids having known surface tensions (γ_L). Zisman showed that plotting γ_L of each liquid versus the cosine of the determined contact angle, the critical surface free energy can be determined by extrapolating the trend line to the point where cos θ is equal to 1.[98] Fowkes extended this analysis to probe the dispersive and polar contributions of the substrate to the critical surface energy.[99] According to Fowkes, a plot of $\sqrt{\gamma_L^D}/\gamma_L$ versus the cosine of the experimental contact angle gives a line, the slope of which is $2\sqrt{\gamma_S^D}$, where γ_S^D is the dispersive component of the surface free energy and γ_L^D is the dispersive component of the surface free energy of the probe liquid. Since γ_L is the total surface free energy, the polar and dispersive components to the total surface free energy can be extracted from a combination of a Zisman and Fowkes analysis of each SAM surface. From the results of the contact angle measurements, an assessment of surface polarity as it relates to interfacial structure can be obtained. It is then possible to correlate the interfacial structure (e.g projection of functionality, lateral interactions) to the surface energy. A note of caution is necessary as it relates to the Zisman and Fowkes analyses. Errors associated with the Zisman analysis are larger than the errors associated with the Fowkes analysis. Values for the dispersive and polar contributions to the surface energy from the Fowkes analysis are not be taken as absolute quantities as well as the values for the total surface free energy obtained from the Zisman analysis. There are assumptions made with in the Fowkes and Zisman analyses which limit the accuracy of the obtained energy values but nonetheless conclusions can be drawn based on trends in the obtained values.[97,100,101]

3.3 Optical Ellipsometry

One of the most widely used methods for determining SAM or thin film thickness is optical ellipsometry. In order to be able to use ellipsometry, the surface being analyzed must be reflective (*e.g*. gold). Reflection of linearly polarized light from a surface produces elliptically polarized light. The perpendicular and parallel components of linearly polarized light reflect differently from surfaces, causing a relative phase shift in either component which leads to elliptically polarized light following reflection. The phase shift of both components of linearly

polarized light can be measured and used to characterize the reflecting surface.[102] The technique relies on changes in the refractive index and absorption coefficients of the substrate to determine film thicknesses. There are two ellipsometric parameters which are monitored and used to determine film thickness. The difference in phase angle between the leading and trailing components of light is designated as Δ. The ratio of electric field amplitudes between the two components of light is designated ψ. A plot of Δ versus ψ is generated for the clean metal substrate. The plot has a set period different for different substrates. Each point on the plot corresponds to measured ψ, Δ, and n (refractive index). By determining ψ and Δ for a monolayer a refractive index value can be extracted, from the substrate ψ versus Δ plot, and used to calculate a film thickness.[103] A diagram of an ellipsometer is shown in Figure 25.[102]

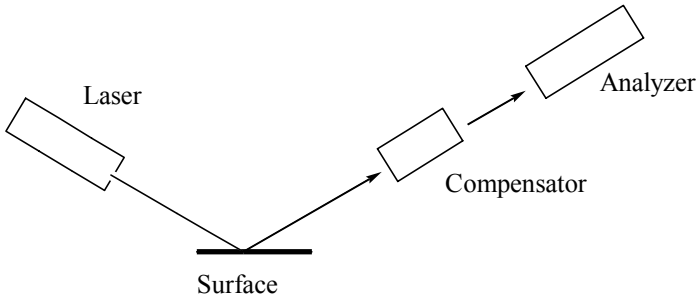

Figure 25. Diagram of the components of an ellipsometer

Measurements are made at a single wavelength and at a single incidence angle. Changing the angle of incidence of the measurement, ambiguities in the measured refractive indeces can be eliminated.

Ellipsometry is also widely used to study film growth on various surfaces.[102] For the study of SAM surfaces, ellipsometry can be used to establish that a single monolayer is formed and help to asses the extent of reaction following the addition of other layers to a modified substrate.

3.4. Reductive Desorption

Cyclic voltammetry is another useful analytical technique for the analysis of surface bound compounds. Applications of cyclic voltametry to the study of SAMs by Porter *et al*. lead to the use of reductive desoprtion as a method of determining several properties of SAM surfaces.[49,104] For alkanethiolates on gold, the reduction of the gold

bound sulfur can be achieved at reasonable potentials (1.0-1.4 V relative to Ag/AgCl). By using the substrate surface as the working electrode, desorption of the molecules is achieved with the formation of an (RS^-), which diffuses into solution. The reduction process is irreversible and has been shown, spectroscopically, to remove the monolayer from the gold surface.[49,105,106]

Reductive-desoprtion measurements of alkanethiolate monolayers provide information regarding the strength of the lateral interactions within a given monolayer.[105] Shifts in the peak potential are characteristic of changes in the stabilization energy due to varying lateral interactions of the molecules comprising the monolayer. Monolayers that are prepared with molecules which have additional stabilizing lateral interactions (hydrogen bonding, π-π interactions) will have their desorption potentials shifted to more negative potentials. According to Imabayashi, a shift in desorption potentials to more negative values is characteristic of increased stabilization of the monolayer relative to a reference surface.[105] By assuming Butler-Volmer kinetics and a Frumkin adsorption isotherm, the relationship between desorption peak potential and monolayer stabilization energy is given by equation 2:

$$zu_{11} = -2F\,\Delta E_p \qquad (2)$$

where u_{11} is the interaction energy, z is the number of nearest neighbors in the monolayer, F is Faraday's constant and ΔE_p is the peak potential difference between the sample and the reference potential (reference surface desorption potential).[105] It is imperative that the molecules being compared have comparable surface densities if a difference in potential is to be attributed to increased lateral stabilization. Likewise, disruptive interactions, such as gauche defects or small structural changes, can also be determined by a shift in peak potential. The evaluation of trends in the desorption peak potentials allows for interpretation of the effect structural changes have on lateral stabilization within SAMs.

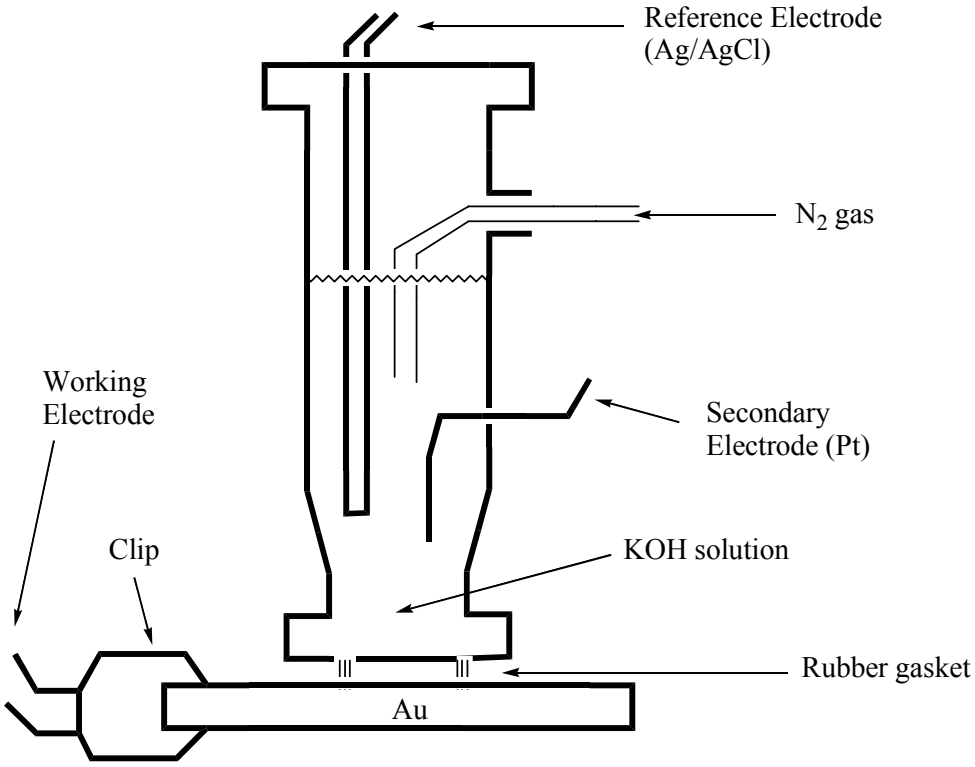

Figure 26. Diagram of reductive desorption experimental setup

A diagram of the setup used to carry out the reductive desorption measurements is shown in Figure 26.

3.5 Impedance Spectroscopy

The last analytical technique used to analyze the SAM surfaces is impedance spectroscopy. Impedance spectroscopy is a common technique used for monitoring the influence that interfacial layers have on the electrochemical properties of the substrate.[9,12,107] The current response of an electrochemical cell to applied potential can be modeled by an electrical circuit composed of resistors and capacitors. These resistors and capacitors represent different contributions to the current reponse, e.g. double layer charging, solution resistance, charge transfer resistance. The impedance measurement investigates how the interfacial layer impacts the values of these individual circuit components.

In the impedance for a modified surface, an equivalent circuit is proposed to model the electrochemical cell. From the equivalent circuit model, the current response is calculated, and the value of the components of the model circuit adjusted until the calculated current closely approximates the experimental rsponse. There are several types of equivalent circuit models proposed and used in the literature.[108-111] One of the most widely used equivalent circuits is shown in figure 27. Bruening et al.[112] and Jennings et al.[108] use the equivalent circuit shown to model systems which are very different. Janek et al.[111] also use this circuit to determine the influence different SAM surfaces have on the corrosion protection of gold substrates.

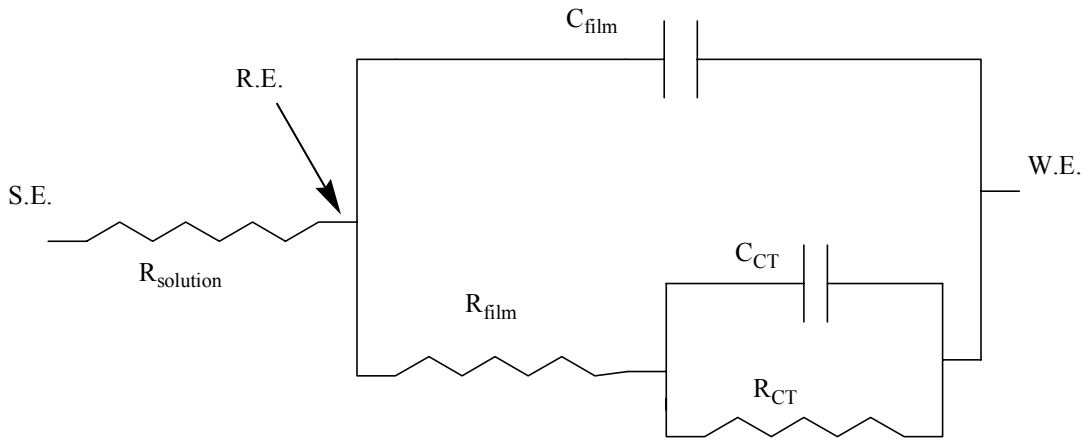

Figure 27. Equivalent circuit diagram proposed by Bruening for modeling impedance spectroscopic results

The values of the resistance and capacitance terms can be extracted from the theoretical fit of the equivalent circuit to the impedance data, and can be used to assess the resistive or capacitive nature of the modified substrate being analyzed.

$R_{solution}$ corresponds to the resistance of the solution and should be independent of the nature of the monoalyer. The solution contains an electroactive couple. In most cases, reported in the literature, the redox couple is a dilute solution of an equal molar mix of $Fe(CN)_6^{-3/-4}$.[113] C_{CT} and R_{CT} are the capacitance and resistance terms associated with the charged double layer. Because the monolayer film alters the interface, the charge transfer terms should be influenced by the nature of the monolayer film. R_{film} and C_{film} are the resistance and capacitance terms due to the film on the substrate surface and will likely vary significantly for the different monolayers.

In the analysis, a sinusoidal signal of set frequency is applied at the working electrode surface (at a set potential) and the current response is monitored. During the course of the measurement,

the analysis frequency is varied from 10 kHz down to 1 Hz, collecting 15 data points per decade change in the frequency. Because of the capacitance, the current response will have a phase shift relative to the input voltage waveform. This phase shift will be a function of the frequency of the input voltage. Figure 28a illustrates the relationship between alternating current and voltage across (at a given frequency) a resistor and a capacitor in series. There is a phase shift of the current response with respect to the voltage signal. The in-phase and out-of-phase current responses can be measured; and from this data, the real and imaginary portions of the electrochemical cell impedance determined. From a simple circuit composed of resistors and capacitors, the in-phase impedance is the contribution from resistance, and the out-of-phase impedance is the contribution due mainly to capacitance.[102] There are several methods of graphically presenting impedance data for a given system. One commonly used method is the complex impedance plot (Figure 28b) in which Z' and –Z" are plotted against one another.

(A)

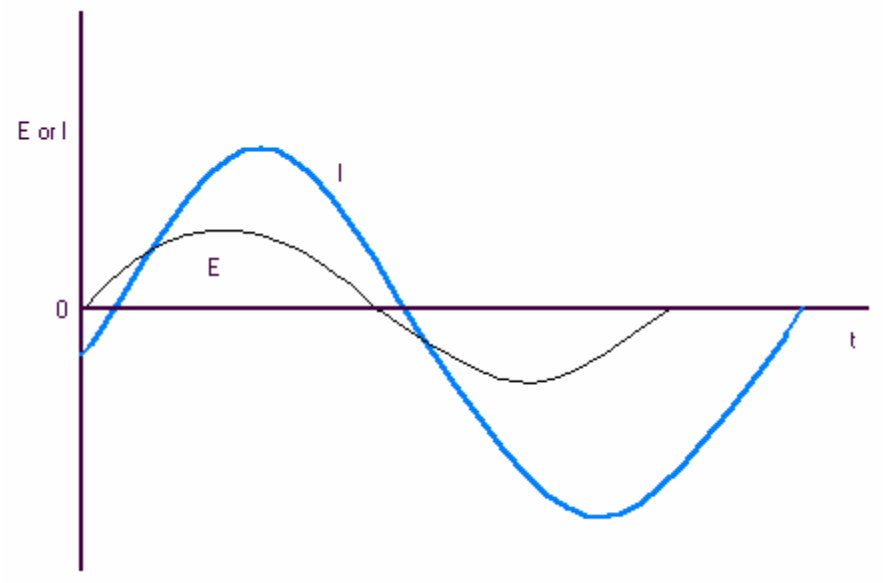

(**B**)

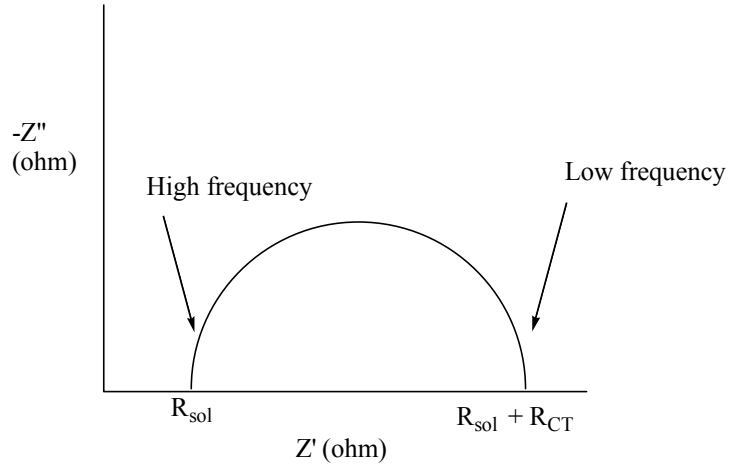

Figure 28. (A) Phasor Diagram for current (blue line) and voltage (black line). (B) Diagram of a Complex Impedance Plot

Z' (Z_{Re}) is the real component of the impedance for the cell and –Z" (Z_{Im}) is the imaginary component of the impedance. Z is the total impedance and is a series combination of Z' and Z".[102] By fitting the data that is obtained to the theoretical response of the equivalent circuit, the values for each resistance and capacitance component of the circuit can be approximated and comparisons between different monolayer systems made.

Because comparisons between resistance and capacitance terms can be made, these measurements combined with data from RAIRS, reductive desorption, and contact angle goniometry should provide information about the role of structure on the interface properties. Through this

correlation we can determine how effective our SAMs are at preventing corrosion and which structural changes increase or diminish the corrosion protection efficiency.

Chapter 4 Surface Characterization Results: SAMs 3, 4, 5 and 6

Introduction

In order to better understand the effect that regiochemistry has on surface energy, surface structure, and corrosion resistance all eight SAM surfaces should not be considered together. To better understand the role that L (linkage) and X (terminal group) play in determining surface structure it is necessary to consider changes to either factor within a homologous series. SAMs **3**, **4**, **5**, **6** will be considered in this chapter since the chain length for each compound is the same. Also, the effect that regiochemistry has on interfacial surface structure can be ascertained more clearly by comparing monolayers with no substitution on the aromatic ring to monolayers which incorporate ring substitution. Sections 4.2-4.5 present and discuss the spectral characterization of all four thiols and SAMs. Spectra of silanized SAMs **3** and **4** is also discussed. Section 4.6 presents and discusses the reductive desorption data for all four SAMs. Section 4.7 discusses the ellipsometry results for SAMs **3**, **4**, **5**, **6**, as well as the silane functionalized surfaces. Section 4.8 presents the contact angle data, Zisman plots, and Fowkes plots for the SAMs. Contact angle data for silanized SAMs of **3** and **4** is also included. Section 4.9 presents and discusses the impedance spectroscopic results for all four SAMs.

4.1 Experimental Details

Gold substrates for SAM preparation were purchased from Evaporated Metal Films Inc. (Ithaca, NY). The substrates consist of a 1" x 1" glass slide coated with ~ 60 Å of chromium as an adhesive layer. Gold (~ 1000 Å) was deposited onto the chromium layer. Substrates were cleaned prior to use by soaking in "piranha" solution (3:1/ H_2O_2: H_2SO_4). Concentrated sulfuric acid and 30% hydrogen peroxide were obtained from VWR and used as received.

4.1.1 Infrared Spectroscopy RAIRS spectra were obtained using a Nicolet model 710 infrared spectrometer (Madison WI) using a liquid nitrogen cooled HgCdTe detector. For RAIRS, the spectrometer was fitted with a Spectra-Tech model FT-80 fixed grazing angle specular reflectance sample apparatus at an incident angle of 80°. The infrared

source light was p-polarized using a Zn-Se wire grid polarizing filter. Reflection spectra of the monolayers were collected at 2 cm^{-1} resolution and 512 interferometer scans. Vibrational band assignments used in the analysis were aided using normal mode calculations conducted with Titan molecular modeling software (Wavefunction, Irvine CA).

Transmission IR spectra were obtained using a Midac model M Fourier transform infrared spectrophotometer (Irvine, CA) equipped with a Sensir dura scope diamond ATR sampling attachment. All samples were analyzed as pure solids or as neat liquids on the ATR sampling attachment at 4 cm^{-1} resolution and 64 interferometer scans.

4.1.2 Reductive Desoprtion Reductive desoprtion experiments were conducted with a CH Instruments model 600A potentiostat (Austin, TX) and a drop electrochemical cell similar to that described by Chidsey.[60] With this electrochemical cell, the contact area that a drop of electrolyte solution makes with the modified substrate, 0.65 cm^2 for these measurements, defines the surface area of the working electrode. Surface roughness was found to be 1.2 using Porter's method, and surface coverages are reported accounting for this roughness.[49] Solution resistance was compensated 90-100% using positive feedback IR compensation for all measurements. A potassium hydroxide solution (Electronic grade, Aldrich) (0.05 M) was used as the electrolyte. The potential was swept between 0 and –1.4 V versus a Ag/AgCl reference electrode at a rate of 100 mV/s. All solutions were dearated with N_2 for 5 minutes prior to measurement.

4.1.3 Contact Angle Measurements Contact angle data was collected using an FTA model 125 goniometer (Portsmouth VA) equipped a camera for video capture. FTA drop shape analysis software was used to collect and calculate contact angles for each SAM analysis. Glycerol, ethylene glycol, and formamide were obtained from Aldrich and used as received. Deionized water from a Barnstead Nanopure II water purification system with a measured resistivity of 17.4 $M\Omega \cdot cm$ was used for water contact angle measurements.

4.1.4 Optical Ellipsometry Ellipsometric measurements were conducted using a Beaglehole picometer ellipsometer (Wellington, New Zealand) equipped with a photoelastic birefringence modulator. Modulation frequency was set at 50 KHz and phase locked signal detection was used. A HeNe laser (632.8 nm) was used as light source and an end on photomultiplier was used for detection. Measurements were performed every 1^{o} between 70^{o} and 80^{o}. Beaglehole system software was used to calculate Δ and ψ and to obtain ellipsometric thickness for each SAM and silanized SAM surface.

4.1.5. Impedance Spectroscopy Impedance spectroscopic measurements were conducted using a Schlumberger Solatron model 1170 frequency response analyzer (Hampshire, England) interfaced to a JAS instrument systems (Salt Lake City, UT) model J-1600-B potentiostat. A variable frequency sine wave was used as the input voltage. Frequency amplitude was set to 10 mV and the frequency was swept from 10,000-10 Hz at 15 points per decade. The instruments were thoroughly calibrated by measuring the impedance of electrical circuits constructed from high precision resistors and capacitors. Current output was detected both for the in-phase (real) and out-of-phase (imaginary) components. From the in-and out-of-phase current measurements the complex impedance is determined.

A conventional three-electrode cell was used with a perforated Teflon cap for electrode insertion and N_2 purge. All experiments were conducted at 25 ^{o}C. Aqueous solutions containing 0.05 M $NaH_2PO_4 \cdot H_2O$ (electrolyte), 0.05 M $Fe_2(CN)_6$, and 0.05 M $Fe_3(CN)_6$ (redox couple) were deaerated for 5 minutes prior to data acquisition. A Ag/AgCl reference electrode was used and a platinum wire served as secondary electrode. A gold electrode (BAS, Lafayette, IN) was used as working electrode. This electrode was soaked in 2 M H_2SO_4 solution while being continuously electrochemically oxidized and reduced for 4 minutes to prepare the surface. Following electrochemical cleaning, the electrode was polished and rinsed thoroughly with deionized water, dried, and immersed in millimolar solutions of each thiol for 24 h. Following SAM formation and prior to analysis, the electrode is rinsed with ethanol and water.

4.2 IR and RAIRs Spectra of Compounds 3-6

4.2.1 Relevant IR Vibrational Modes As previously mentioned, only vibrations which have a significant portion of their transition dipole moment normal to the surface are observed in RAIRS. Figure 29 illustrates the transition dipole moment for three aromatic ring stretching modes which are important for the determination of the orientation of the aromatic ring at the monolayer/air interface. All the bands are strong and characteristic of substituted benzene rings.[114] Importantly, in the case of vibrations 19a and 19b the transition dipoles are orthogonal to each other. It should be noted that ring vibrational modes of benzene and substituted benzenes have a number and letter associated with them. This numbering convention was developed by E.B. Wilson[115] to simplify vibrational assignments. This convention will be used throughout the rest of this thesis.

Transition dipole moments are important in RAIRS, since the presence or absence of certain vibrations can assist in determining the projection of surface functional groups.

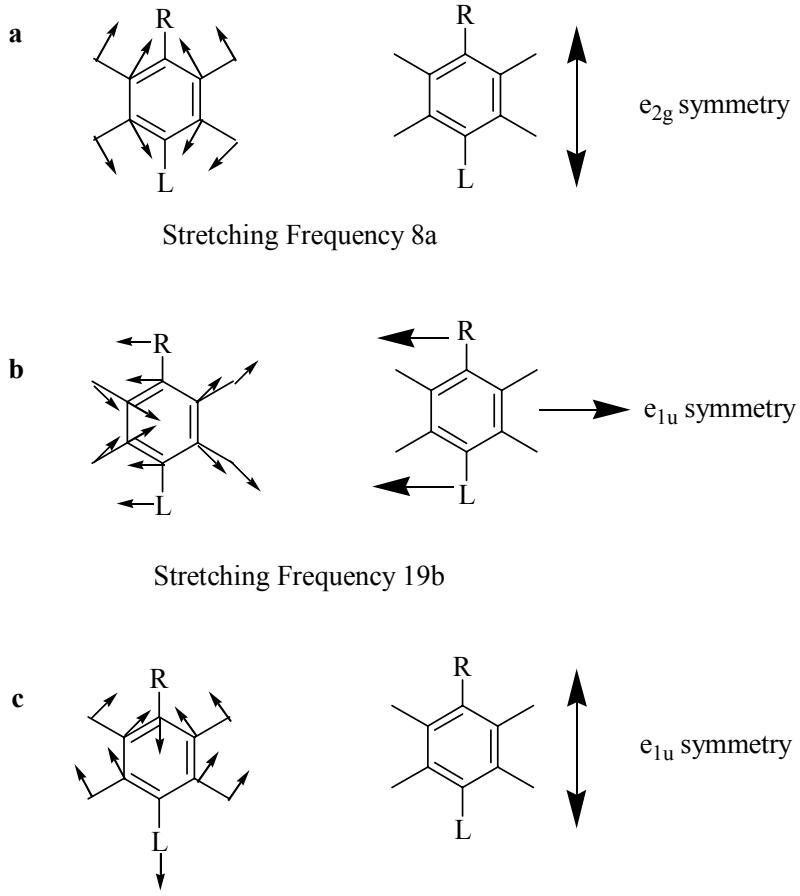

Figure 29. Orthogonal vibrations of a substituted benzene ring[114]

As determined by Varsanyi each of the vibrational modes in Figure 29 has a corresponding frequency range. The vibrational frequencies are sensitive to extent of substitution of the aromatic ring as well as sensitive to regiochemistry. A graphical summary of these vibrational ranges is shown in Figure 30.

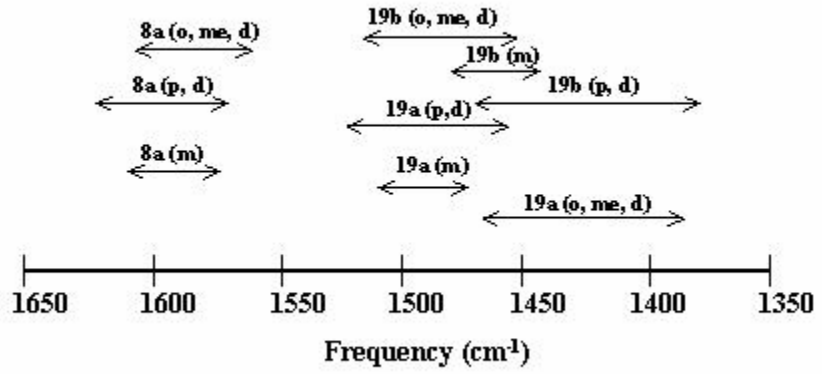

Figure 30. Vibrational Frequency Ranges for Aromatic C-C Stretching Modes (o = ortho-substitution, p = para-substitution, me = meta-substitution, m = monosubstituted, d = disubstituted).

All of these vibrations were used to determine the orientation of the terminal phenyl ring. In several cases, more than one vibrational mode, of the three mentioned above, are absent from any given RAIRS spectrum. Table 1 contains vibrational frequency assignments for some known compounds which can serve as structurally similar models for compounds **1**-**8**.

Table 1. Vibrational Assignments Reported in the Literature

Compound	Vibrational Frequencies (cm-1)	Wilson's Notation
6-phenyl-n-hexanethiol (neat)[116]	1604 1496 1453	8a 19a 19b
6-phenyl-n-hexanethiol(Au/SAM)[116]	1606 1498 1450	8a 19a 19b
6-(p-vinylphenyl)-n-hexanthiol(neat)[116]	1609 1511	8a 19a
6-(p-vinylphenyl)-n-hexanthiol(Au/SAM)[116]	1608 1511	8a 19a

	1422	19b

4.2.2 Transmission and RAIRS spectra of 4-(12-mercaptododecyl)phenol(**3**) The transmission IR spectrum of thiol **3** is shown in Figure 31 and the RAIRS spectrum of SAM 3 is shown in Figure 32. The spectra are clear and no vibrational features attributable to CO_2(g) are observed in the RAIRS spectrum. Vibrational assignments for both spectra are summarized in Table 3.

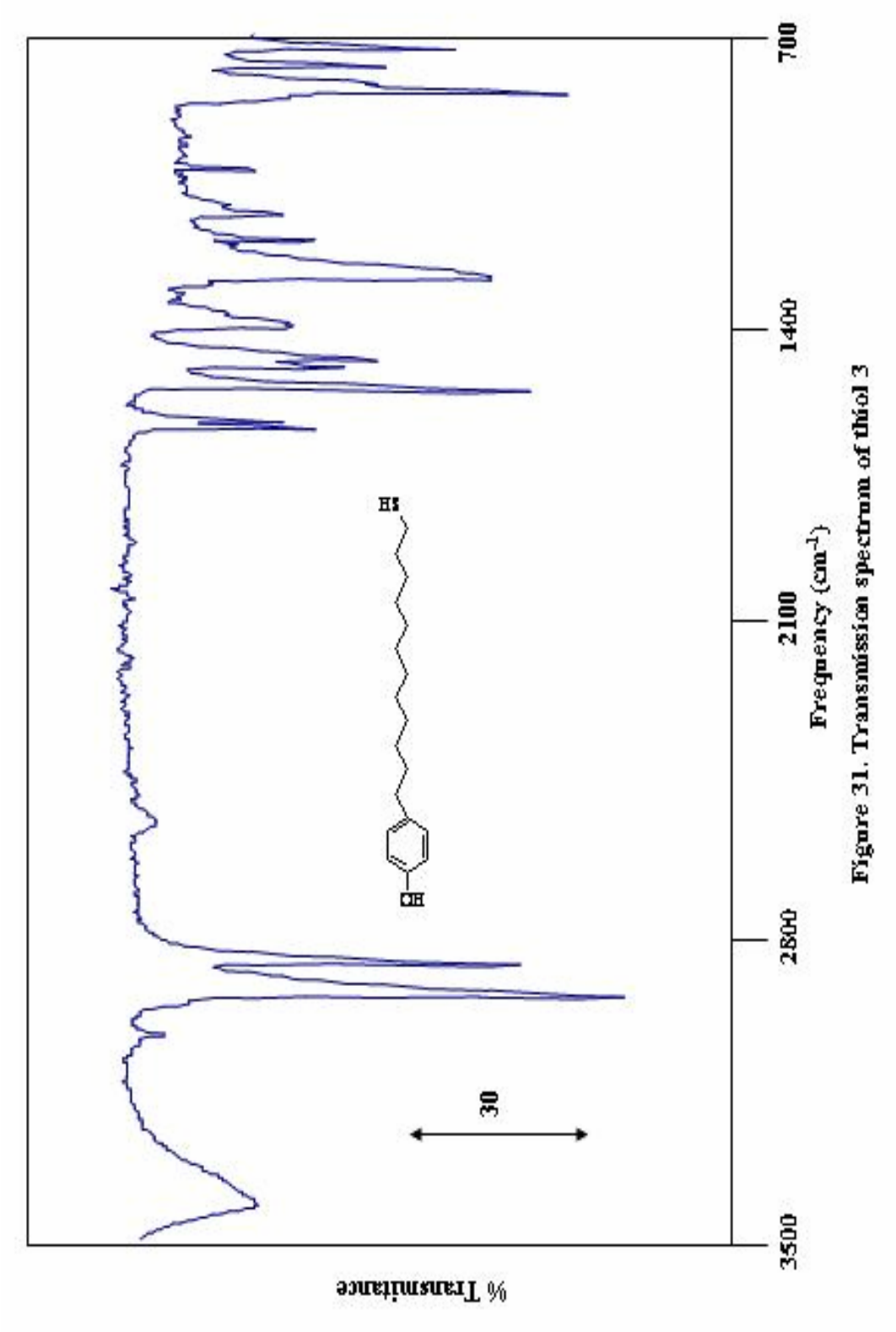

Figure 31. Transmission spectrum of thiol 3

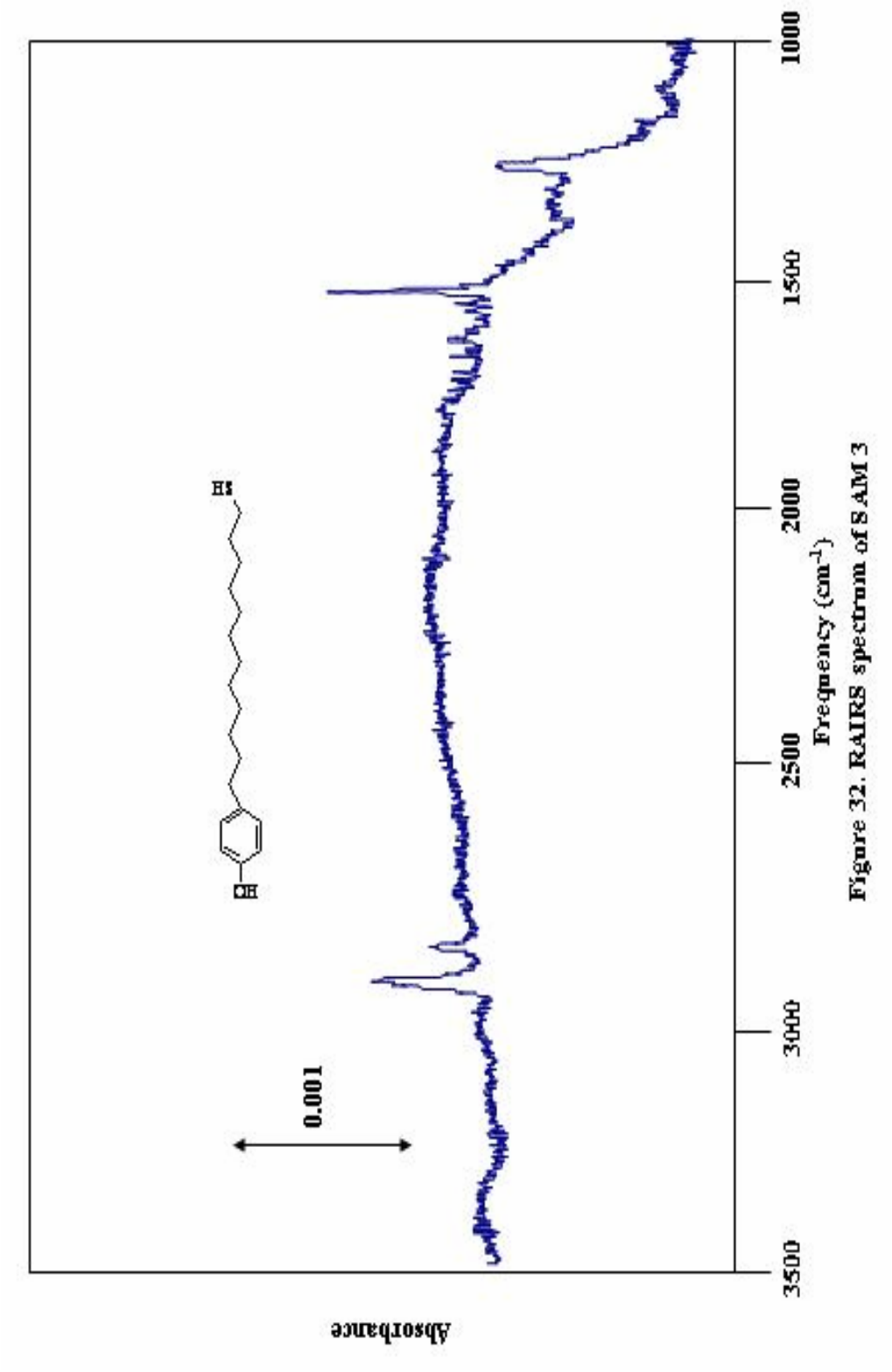

Figure 32. RAIRS spectrum of SAM 3

Table 2. Assignment of the transmission IR spectrum of thiol (3) (Figure 31) and the RAIRS spectrum of thiol (3) on gold (Figure 32).

Transmission (cm-1)	RAIRS (cm^{-1})	Assignment	Wilson Notation
3432(br)	----	OH stretch	----
2915(s) 2850(s)	2923(s) 2852(m)	ν_{as}-$(CH_2)_n$- ν_s-$(CH_2)_n$-	---- ----
1600(m)	1606(m)	νC-C(ring stretch)	8a
1512(s)	1515(s)	νC-C(ring stretch)	19a
1220(s)	----	νC-O	----

As can be seen in Table 2 above, there is good agreement between the vibrational frequencies observed in transmission spectrum and the RAIRS spectrum. The intensity of vibration 8a and 19a indicates that the plane of the phenyl ring along the C1-C4 axis is largely perpendicular to the substrate surface. Vibration 19b is not observed in the RAIRS spectrum which suggests the plane of the phenyl ring is not twisted in a fashion where either edge of the aromatic ring, along C1-C2 or C5-C6, is protruding at the monolayer/air interface.

4.2.3 Transmission and RAIRS spectra of 3-(12-mercaptododecyl)phenol(**4**). The transmission IR spectrum for thiol **4** is shown in Figure 33 and the RAIRS spectrum of SAM **4** is shown in Figure 34. The vibrational assignments for both spectra are summarized in Table 4. Again, the spectra are clear and there are no vibrational features in the RAIRS spectrum which can be attributed to CO_2(g).

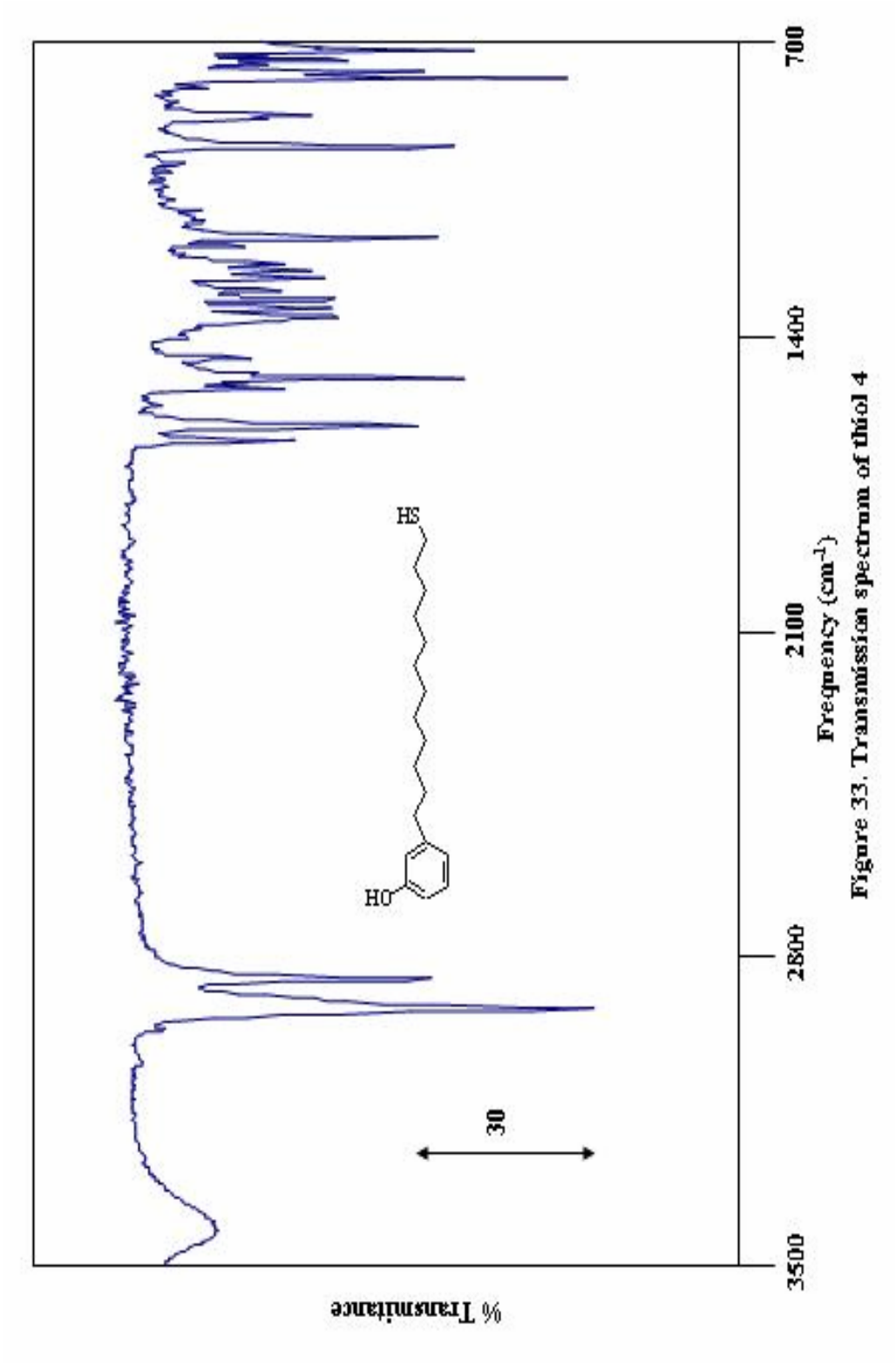

Figure 33. Transmission spectrum of thiol 4

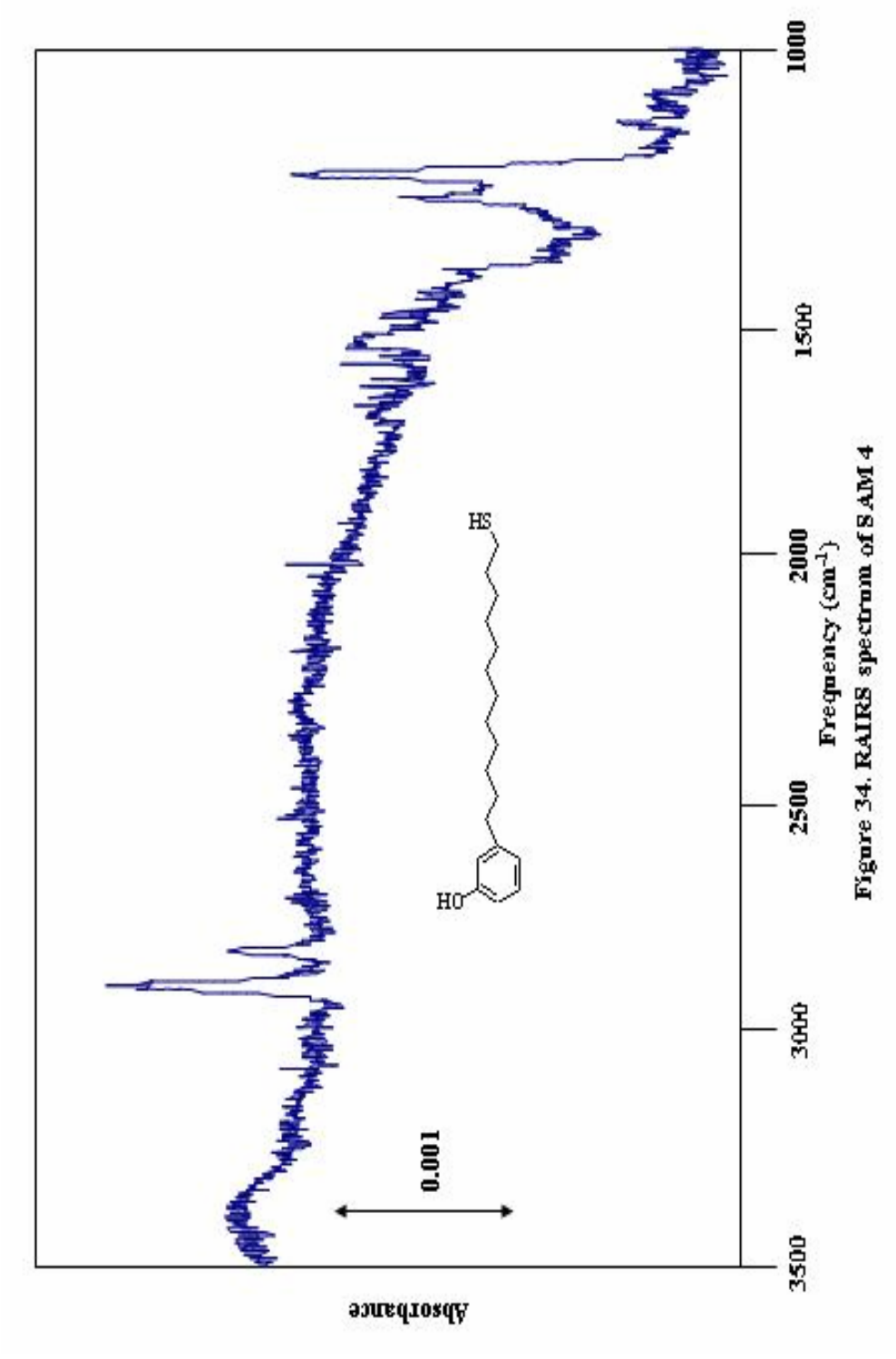

Figure 34. RAIRS spectrum of SAM 4

Figure 34. RAIRS spectrum of SAM 4

Table 3. Assignment of the transmission IR spectrum of thiol (4) (Figure 33) and the RAIRS spectrum of thiol (4) on gold (Figure 34).

Transmission (cm-1)	RAIRS (cm^{-1})	Assignment	Wilson Notation
3448(br)	----	OH stretch	----
2916(s)	2924(s)	ν_{as}-$(CH_2)_n$-	----
2850(s)	2852(m)	ν_s-$(CH_2)_n$-	----
1581(3)	1608(w)	νC-C(ring stretch)	8a
1470(s)	1496(w)	νC-C(ring stretch)	19a
1150(s)	----	νC-O	----

There is good agreement between the transmission IR and RAIRS vibrational frequencies summarized above. Unlike in the case of SAM **3**, the RAIRS spectrum of SAM **4** does not show medium or strong intensities for vibrations 8a and 19a, indicating that the plane of the phenyl ring is largely parallel to the substrate surface. Vibration 19b is also not observed which indicates no ring canting is taking place. It appears from comparison of the RAIRS spectra of SAM **3** and SAM **4** that meta substitution of the ring forces the plane of the aromatic ring to adopt a different packing arrangement. The intensities of the C-H stretching modes due to the alkyl chain remain constant indicating the packing of the alkyl chain is not altered by changes in substitution regiochemistry.

4.2.4 Transmission and RAIRS spectra of 12-phenyldodecylmercaptan(**5**) The transmission spectrum of thiol **5** is shown in Figure 35 and the RAIRS spectrum for SAM 5 is shown in Figure 36. The vibrational assignments are summarized in Table 4. In the RAIRS spectrum there are features at ~2400 cm^{-1} attributed to the presence of gaseous CO_2 in the reflectance chamber of the IR spectrometer.

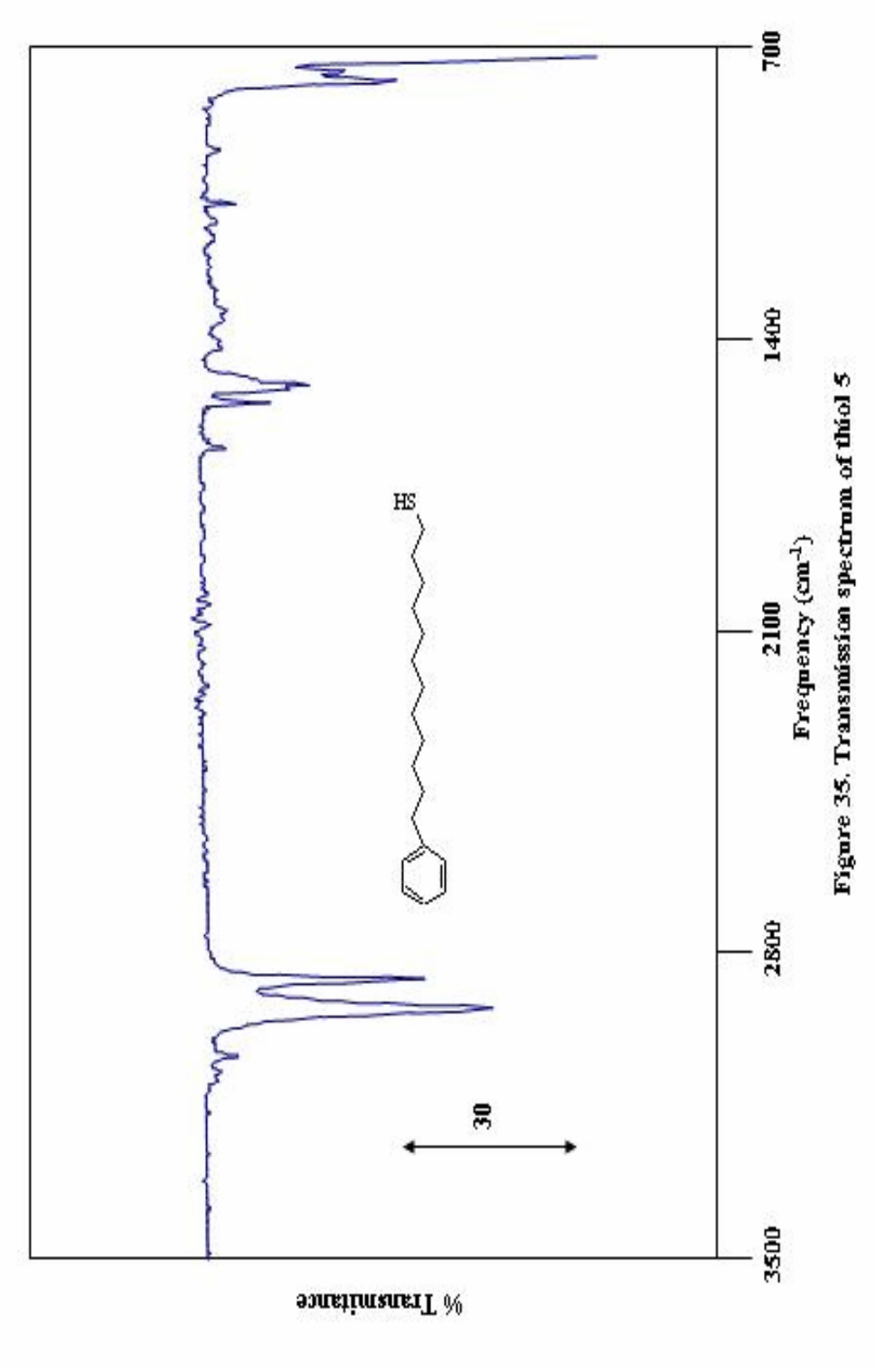

Figure 35. Transmission spectrum of thiol 5.

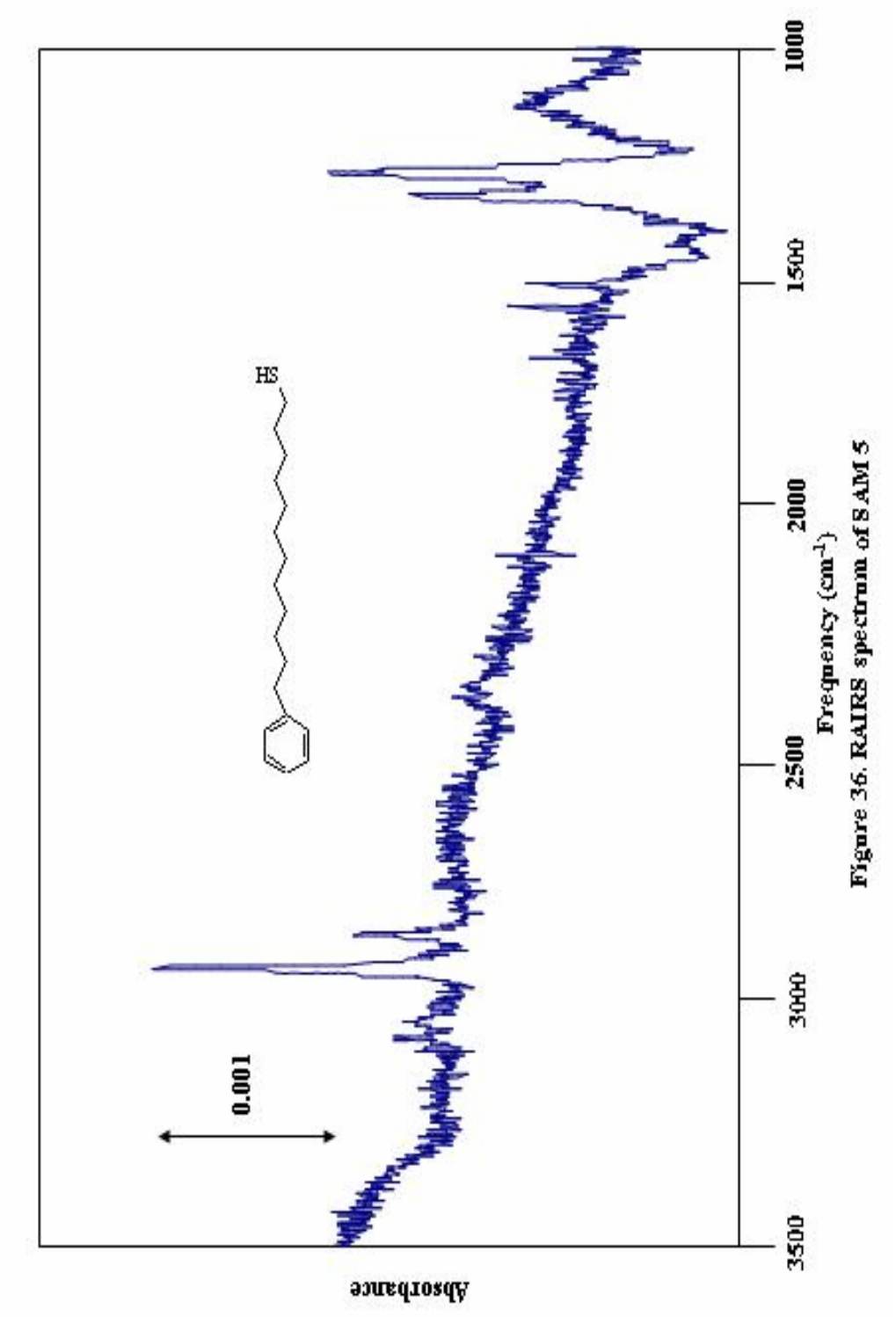

Figure 36. RAIRS spectrum of SAM 5

Figure 36. RAIRS epctrum of SAM 5

Table 4. Assignment of the transmission IR spectrum of thiol (5) (Figure 35) and the RAIRS spectrum of thiol (5) on gold (Figure 36).

Transmission (cm-1)	RAIRS (cm^{-1})	Assignment	Wilson Notation
3062(w)	3070(w)	νC-H (ring)	----
2923(s)	2920(s)	ν_{as}-$(CH_2)_n$-	----
2850(s)	2850(m)	ν_s-$(CH_2)_n$-	----
1604(w)	1610(w)	νC-C(ring stretch)	8a
1496(m)	1508(m)	νC-C(ring stretch)	19a

There is good agreement between the vibrational frequencies observed in the transmission and RAIRS spectra of thiol **5** and SAM **5**. Unlike in the case of SAMs **3** and **4**, the RAIRS spectrum of SAM 5 shows vibrational features attributed to aromatic C-H stretching modes. These features are also observed by Lee *et al*.,[36] and are attributed to possible edge-to-face π-π interactions amoung the terminal phenyl rings. The increased stabilization allows for increased stability resulting in a more crystalline packing arrangement of the molecules in the monolayer.[36] The intensity of vibrations 8a and 19a are lees than those observed for SAM **3**, but are larger than those observed for SAM **4**, indicating that the plane of the phenyl ring is not perpendicular to the substrate surface but is at an intermediate angle between SAM **3** and SAM **4**. Vibration 19b is also not observed. It appears that the absence of substitution of the aromatic ring allows for intermediate tilt angles of the aromatic moiety. The intensity of the C-H vibrational features due to the alkyl chain remain constant relative to SAMs **3** and **4** indicating a similar chain tilt angle for SAMs **3**, **4**, and **5**.

4.2.5 Transmission and RAIRS spectra of 12-Phenylundecyloxymercaptan(**6**) The transmission spectrum of thiol **6** is shown in Figure 37 and the RAIRs spectrum for SAM **6** is shown in Figure 38. The vibrational assignments are summarized in Table 5. In the RAIRS spectrum there are features at ~2400 cm-1 attributed to the presence of gaseous CO_2 in the reflectance chamber of the IR spectrometer.

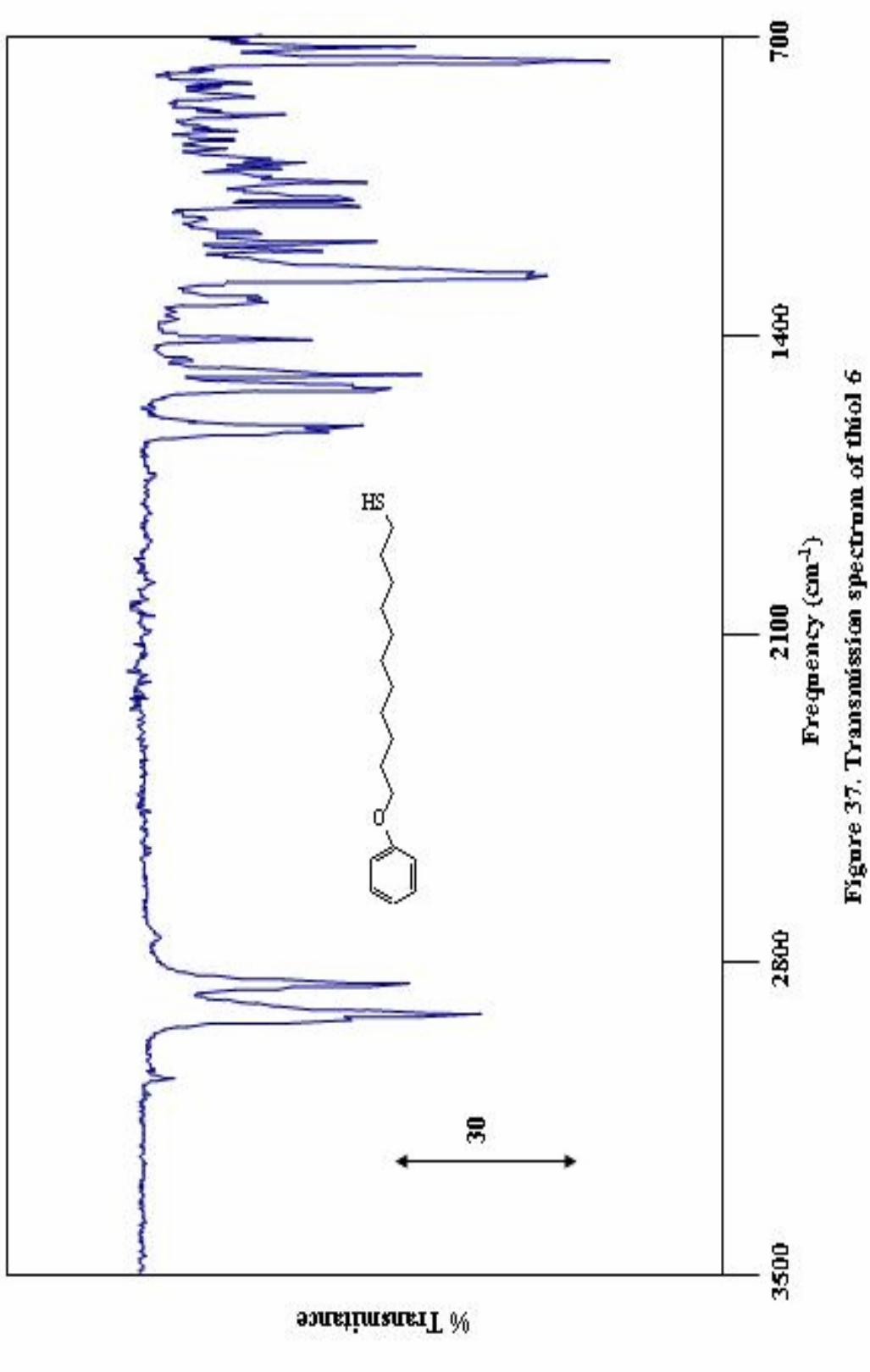

Figure 37. Transmission spectrum of thiol 6

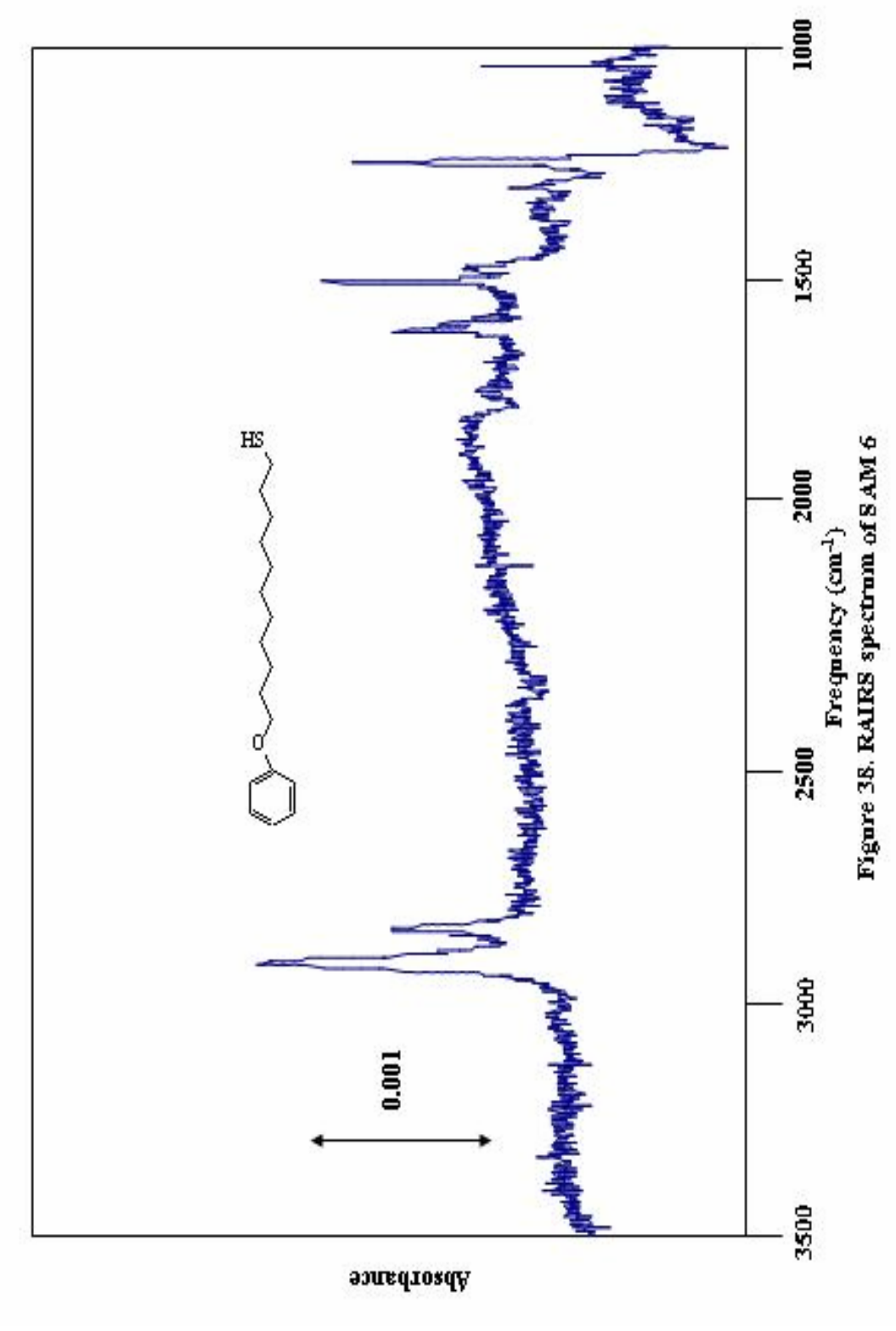

Figure 38. RAIRS spectrum of SAM 6

Figure 38. RAIRS spectrum of SAM 6

Table 5. Assignment of the transmission IR spectrum of thiol (6) (Figure 37) and the RAIRS spectrum of thiol (6) on gold (Figure 38).

Transmission (cm-1)	RAIRS (cm^{-1})	Assignment	Wilson Notation
3066(w)	----	νC-H (ring)	----
2915(s)	2925(s)	ν_{as}-$(CH_2)_n$-	----
2846(s)	2852(m)	ν_s-$(CH_2)_n$-	----
1596(s)	1608(m)	νC-C(ring stretch)	8a
1500(s)	1496(s)	νC-C(ring stretch)	19a
1486(s)	----	νC-C(ring stretch)	19b
1245(s)	----	νC-O	----

There is good agreement between the vibrational frequencies observed in the transmission IR spectrum and the RAIRS spectrum for thiol **6** and SAM **6**. Unlike in the previously shown transmission spectrum, vibration 19b is observed for thiol **6** yet it is not observed in the RAIRS spectrum of SAM **6** indicating no canting of the aromatic ring along the edge of the phenyl ring. Also, a small feature attributed to an aromatic C-H stretching mode is observed in the transmission spectrum yet absent in the RAIRS spectrum indicating that inclusion of the ether linkage does not allow for edge-to-face interactions of the terminal phenyl rings. The intensity of vibrations 8a and 19a are larger than those observed in SAMs **4** and **5** indicating that the phenyl ring is largely perpendicular to the surface although less than seen with SAM **3**. The inclusion of an ether oxygen linkage forces the unsubstituted phenyl ring into a more perpendicular arrangement relaive to the substrate surface. The intensity of the C-H stretching modes due to the alkyl chain remain constant relative to SAMs **3**, **4**, and **5** indicating a similar chain tilt angle for all four surfaces.

4.2.6 RAIRS spectra of silanized SAMs (**3**) and (**4**) SAMs **3** and **4** were reacted with trichlorooctadecylsilane (OTS) and RAIRS spectra were obtained of the functionalized surfaces following reaction. Differences in reactivity, towards OTS functionalization, for SAMs **3** and **4** were expected but not confirmed by RAIRS. Changes in spectral features, upon reaction, are attributed to changes in the interfacial structure of the monolayer.

Figure 39 shows the RAIRS spectra of SAM **3** and SAM **3** following reaction with the silane. The vibrational assignments do not vary following functionalization with OTS but variations in peak intensities are noted. The peak intensity for the asymmetric and symmetric C-H stretching vibrations significantly increased following reaction due to increased C-H vibrations due to added alkyl chains of the silane. Vibration 8a at 1606 cm^{-1} is no longer visible and vibration 19a at 1515 cm^{-1} is significantly diminished in intensity. Vibration 19b is observed at 1485 cm-1 which indicates that the plane of the aromatic ring is canted with respect to the substrate and not completely parallel with it.

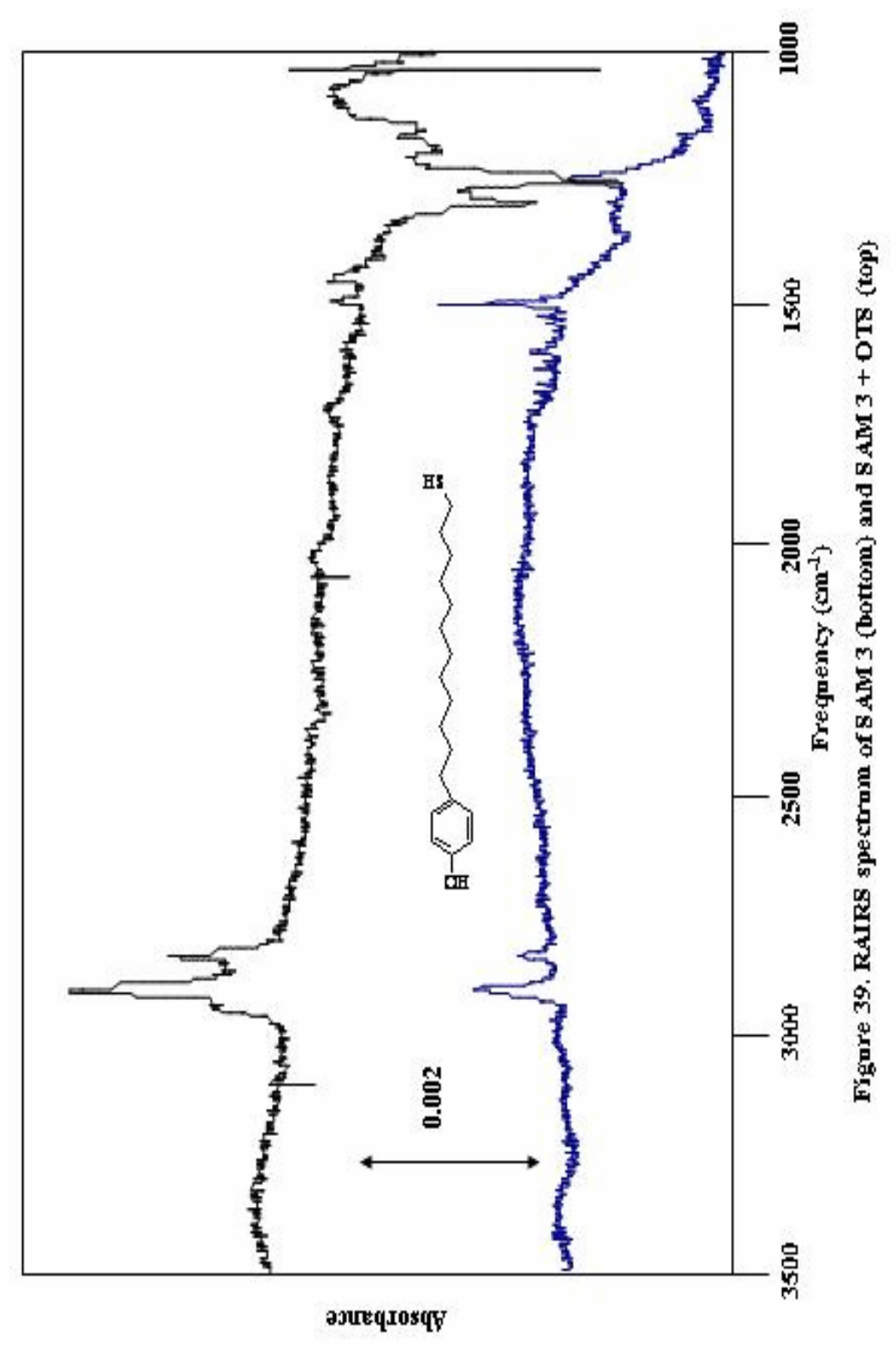

Figure 39. RAIRS spectrum of SAM 3 (bottom) and SAM 3 + OTS (top)

Figrue 39. RAIRS spectra of SAM# and SAM 3 +OTS

Figure 40 shows the RAIRS spectra of SAM **4** and SAM **4** following functionalization. Peak positions do not vary after reaction with OTS. The differences between the two spectra are in the peak intensities. The features corresponding to the C-H asymmetric and symmetric stretching vibrations increase in intensity and all other vibrational features remain the same. Unlike SAM **3**, the orientation of the phenyl ring in SAM **4** does not seem to change upon reaction with OTS.

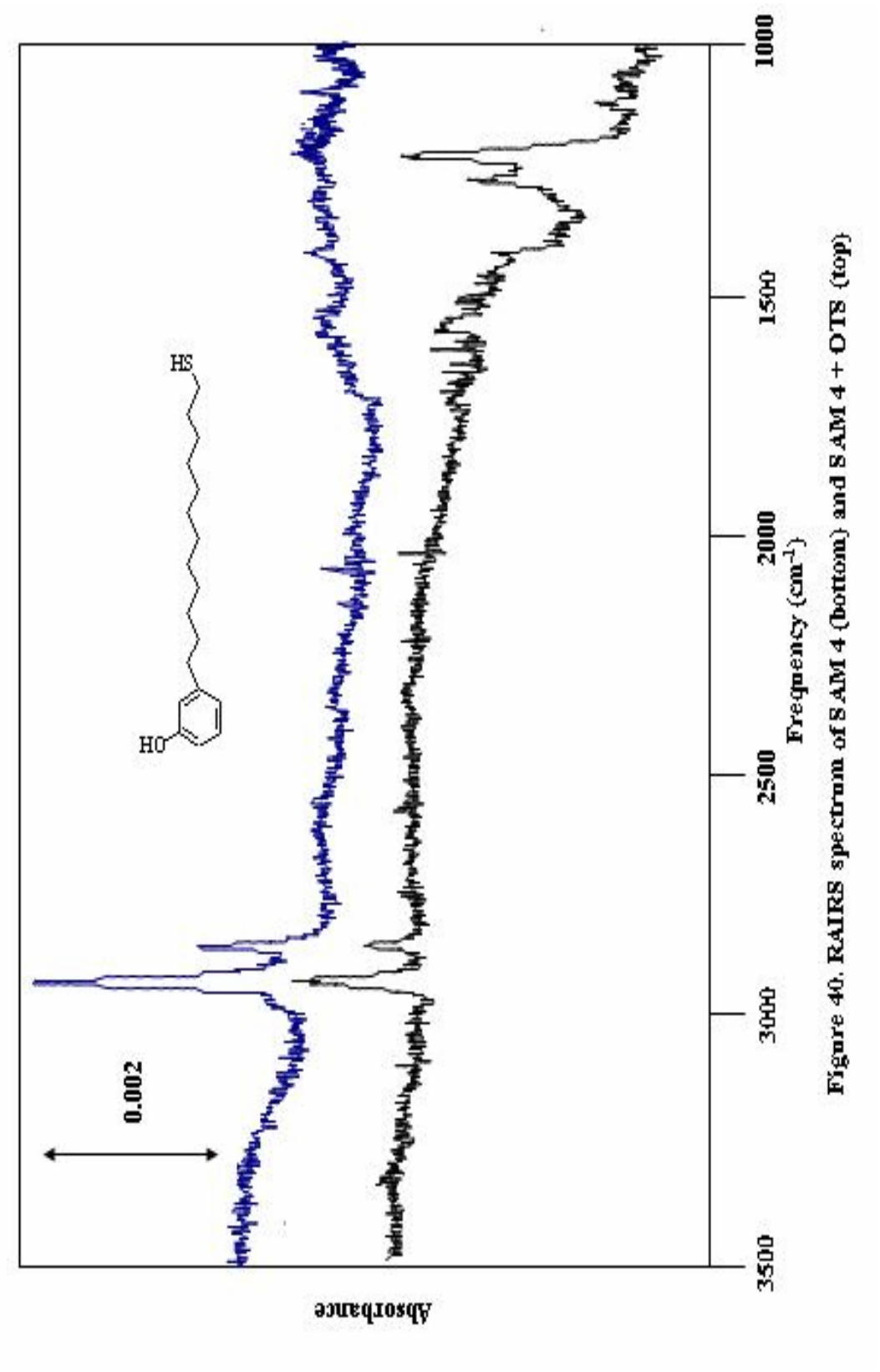

Figure 40. RAIRS spectrum of SAM 4 (bottom) and SAM 4 + OTS (top)

Figure 40. RAIRS spectrum of SAM 4 and SAM 4 + OTS

4.2.7 Discussion of IR spectra By comparing the intensities of the C-H stretching vibrations of the alkyl chain (~ 2920cm^{-1} and 2850 cm^{-1}) for SAMs **3**, **4**, **5**, and **6** it is concluded that the chain tilt angle is approximately the same for all four modified interfaces. Inspection of peak widths (FWHM) reveals noticeable differences in the asymmetric C-H vibration (Table I). Peak widths for SAMs **3**, **4**, and **6** are similar. SAM **5** has significantly lower FWHM values indicating increased order within the monolayer.[36] FWHM data for dodecanethiol is included for reference and as an example of a well ordered monolayer.

Table 6. FWHM analysis of the features due to the C-H stretching modes of the alkyl chain in SAMs 3, 4, 5, and 6.

Monolayer	**CH_2, asym position (cm^{-1})**	**CH_2, asym width (cm^{-1})**	**CH_2, sym position (cm^{-1})**
4-(12-mercaptododecyl)phenol (**3**)	2923	21	2852
3-(12-mercaptododecyl)phenol (**4**)	2924	23	2852
12-phenyldodecylmercaptan (**5**)	2920	16	2850
12-Phenylundecyloxymercaptan (**6**)	2925	22	2856
Dodecanethiol	2917	15	2850

It appears that substitution of the aromatic ring or inclusion of an –O- linkage disrupts monolayer ordering, leading to larger FWHM values for the alkyl chain C-H stretching modes and to the absence of certain aromatic C-H stretching vibrations.

The terminal aromatic ring in SAMs **3** and **6** seems to be oriented differently than the terminal ring group in SAMs **5** and **4**. Inclusion of either para-substitution or an ether linkage seems to impose a more perpendicular arrangement of the aromatic ring with respect to the substrate surface evidenced by the increase in intensity of vibrations 8a and 19a in SAM **6** relative to SAM **5**. Figure 41 illustrates what orientation each of the terminal phenyl and substituted phenyl rings are believed to adopt, and which account for

the absence of vibration 19b in the RAIRS spectra and the increased intensity of others, namely 8a, 19a.

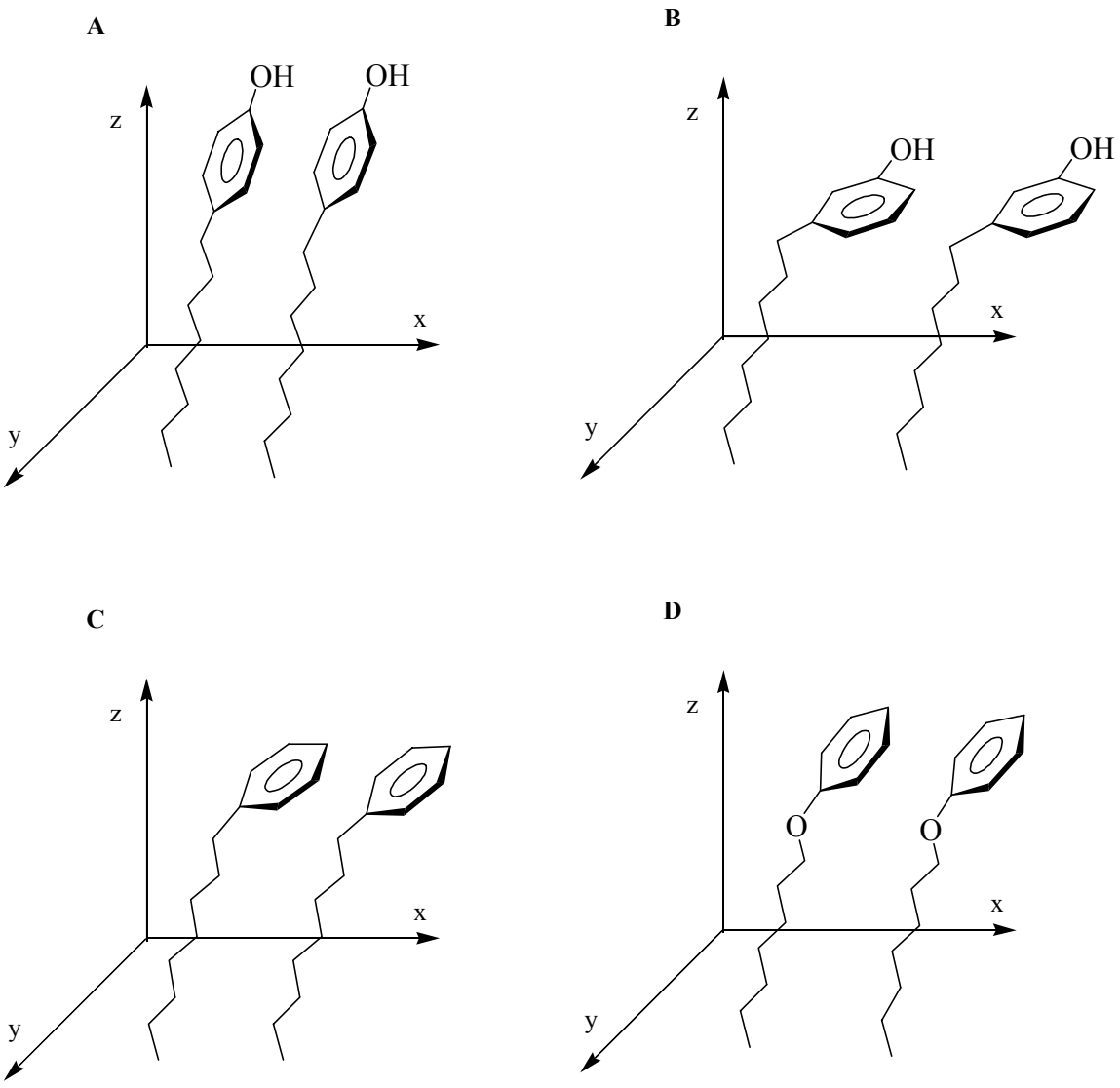

Figure 41. a) Orientation of SAM 3, b) Orientation of SAM 5, c) Orientation of SAM 6, d) Orientation of SAM 4

Figures 41 b and d illustrate how the plane of the aromatic ring is more parallel to the surface and the "face" of the ring is exposed at the surface where as Figures 41 a and b demonstrate how the tip of the aromatic ring protrudes at the surface. These orientations account for the intensity differences of vibrations 19a and 8a in the RAIRS spectra of all four SAMs.

Although transmission IR and RAIRS spectra provide a means of determining relative orientations of molecules on a surface, further analyses are needed to further establish the structure of these monolayers and to further investigate how variations in structure affect interfacial surface properties. The following section describes how the use of contact angle goniometry can be used to further investigate surface structure.

4.3 Contact Angle Goniometric Data

4.3.1 Experimental details and data The contact angle of each SAM was measured using three different liquids. The three liquids (water, glycerol, and ethylene glycol) represent a homologous series of liquids having similar properties. Of these, water has the highest surface tension and ethylene glycol the lowest. The different surface tensions result in differences in the measured contact angles and aid in the determination of the surface free energy using the Zisman analysis. Table 7 contains the experimental values for SAMs **3**, **4**, **5**, **6**, and functionalized **3** and **4**.

Table 7. SAM-liquid interfacial contact angles.

Monolayer	**Water (deg)**	**Ethylene Glycol (deg)**	**Glycerol (deg)**
4-(12-mercaptododecyl)phenol(**3**)	38(3)	18(1)	27(3)
3-(12-mercaptododecyl)phenol(**4**)	58(2)	37(3)	55(1)
12-phenyldodecylmercaptan(**5**)	89(2)	58(1)	73(2)
12-phenylundecyloxymercaptan(**6**)	85(2)	55(2)	69(2)
SAM **3** + OTS	74(3)	-----	-----
SAM **4** + OTS	82(3)	-----	-----

SAM **3** is a higher energy surface when compared to other SAMs in the above table. SAM **4** is not as high an energy surface as SAM **3** and agrees with the previously proposed model (Figure 41). SAMs **5** and **6** are completely hydrophobic since they have no polar group substitution. SAMs **3** and **4**, following silanization, become hydrophobic as expected, since OTS does not contain a polar terminal group. These results suggest that aromatic ring substitution regiochemistry influences surface energy. SAM **3** is a higher energy surface than SAM **4**. Surfaces which are hydrophobic are low energy surfaces, of which SAMs **5** and **6** are good examples. To determine the surface energy of a given surface it is necessary to obtain a Zisman plot for each monolayer.

4.3.2 Results and discussion of Zisman analyses Zisman and Fowkes analyses were elaborated for SAMs **3**, **4**, **5**, and **6**. From the graphical Zisman analyses, surface free energy values were obtained for each monolayer and are summarized in Table 8. Figure 42 shows the Zisman plot for SAMs **3**, **4**, **5**, and **6**. It is clear from Figure 42 that the point at which each line crosses the value of 1 on the y-axis is different, suggesting different surface energies for each monolayer.

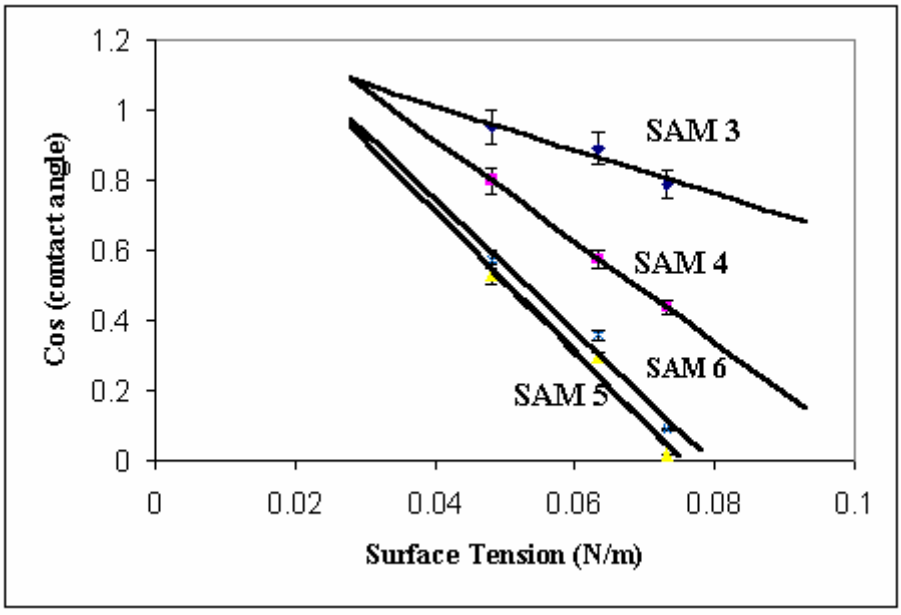

Figure 42. Zisman plots of SAMs 3, 4, 5, and 6

Visual inspection of the slopes of the lines in the above figure also indicates that intermediate surface energies can be obtained by varying the substitution regiochemistry of the aromatic ring or by removing ring substitution.

Table 8. Calculated surface free energies for SAMs 3, 4, 5, and 6. Slopes, intercepts, and R^2 values for each regression line shown in Figure 42 are included along with associated errors.

Monolayer	Slope	Error in Slope	Intercept	Error in intercept	R^2	Surface Energy (mN/m)
SAM **3**	-6.30	1.82	1.23	0.05	0.618	41.9 $\pm$ 11.8
SAM **4**	-14.47	0.18	1.49	0.01	0.999	28.6 $\pm$ 0.9
SAM **5**	-20.10	3.49	1.52	0.22	0.923	25.6 $\pm$ 3.5
SAM **6**	-19.00	3.78	1.51	0.24	0.949	26.8 $\pm$ 2.8

The calculated surface free energy for SAM **3** is 41.9 mN/m $\pm$ 11.8 mN/m indicating that SAM **3** is a relatively high energy surface. For SAM **4**, the calculated surface free energy is 28.6 mN/m $\pm$ 0.9 mN/m, which is 32 % less than SAM **3**. This is expected according to the model in Figure 41d where the orientation of the phenyl ring should increase the dispersive contribution to the total surface energy. Although the –OH moiety is accessible at the monolayer interface, dispersive contributions from the face of the aromatic ring dominate the surface energy. The calculated surface free energy for SAM **5** is 25.6 mN/m $\pm$ 3.5 mN/m. The decrease in surface energy is due to the absence of any hydrophilic group on the aromatic ring. Likewise, the calculated surface free energy for SAM **6** is 26.8 mN/m $\pm$ 2.8 mN/m similar to that for SAM **5**. It appears that inclusion of an ether linkage does not significantly affect the surface free energy value obtained for SAM **6**. The ether linkage does not seem to be accessible at the monolayer/air interface and does not contribute to the measured surface free energy. It is evident that substitution regiochemistry about the phenyl ring has a significant impact on the energy values obtained for SAMs **3** and **4**. Even though there are large errors associated with the Zisman analysis, the trend in the average surface energy values suggests that increased

tilting of the aromatic ring as a result of meta substitution results in a decrease in surface energy for SAM **4**.

4.3.3 Results and discussion of Fowkes analyses As mentioned earlier (**3.2**) the total surface free energy is described as being composed of polar and dispersive components. Following determination of the dispersive contribution, the polar contribution can be extracted. Figure 42 shows the Fowkes plot for SAM **3, 4, 5,** and **6** and Table 9 summarizes the dispersive component determinations for SAMs **3**, **4**, **5**, and **6**.

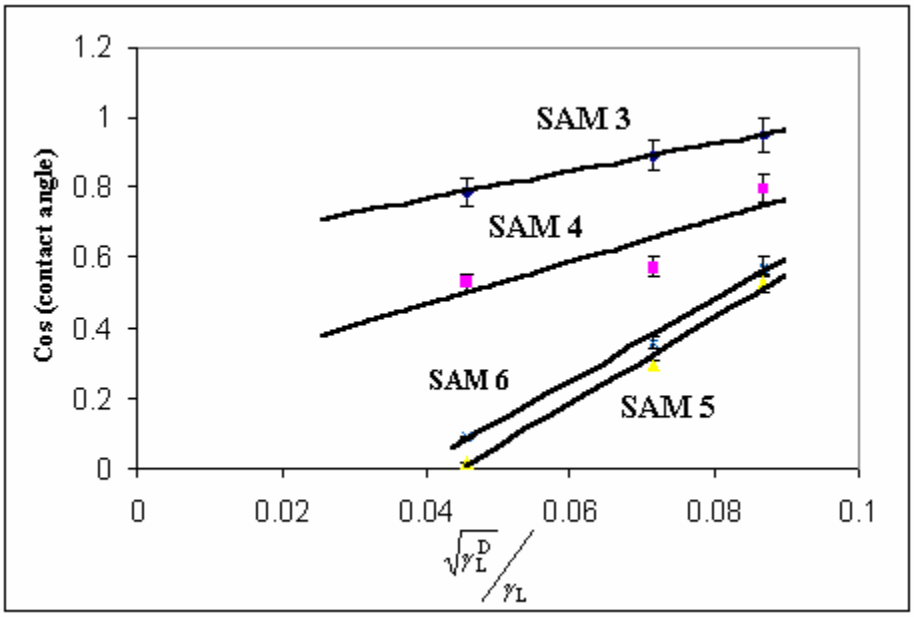

Figure 43. Fowkes plots for SAMs 3, 4, 5, and 6

Visual inspection of the slopes of the lines in the above plot reveal that differences in polar contributions to the surface energy can be achieved through variations in the structure of molecules comprising a monolayer.

Table 9. Calculated dispersive contributions for SAMs 3, 4, 5, and 6. Slopes, intercepts, and R^2 values for each regression line shown in Figure 43 are included along with associated errors.

Monolayer	Slope	Error in Slope	Intercept	Error in intercept	R^2	Dispersive Component (mN/m)
SAM **3**	3.96	0.01	0.61	----	1	3.9 $\pm$ 0.7
SAM **4**	6.02	3.44	0.23	----	0.809	9.1 $\pm$ 3.1
SAM **5**	12.26	1.30	-0.55	----	0.989	37.6 $\pm$ 2.1
SAM **6**	11.68	0.95	-0.45	----	0.993	34.1 $\pm$ 2.1

The dispersive contribution of the surface energy for SAM **3** is 3.9 mN/m $\pm$ 0.7 mN/m, which indicates that the surface free energy is primarily due to the polar component. This is in agreement with the proposed interfacial model for SAM **3** where the terminal –OH moiety is projected into the air/solid interface. The dispersive contribution to the surface energy determined for SAM **4** is 9.1 mN/m $\pm$ 3.1 mN/m supporting the conclusion that SAM **4** is significantly less polar and that the surface –OH group is less accessible at the monolayer/air interface. The dispersive contribution increases by a factor of ~2 as a result of meta-substitution of the aromatic ring. For SAM **5** the dispersive component of the surface energy is 37.6 mN/m $\pm$ 2.1 mN/m. As previously mentioned there are large errors associated with using Fowkes plots to accurately determine the disperse components of the surface free energy which may account for the large value obtained for SAM **5**. Nevertheless, the surface energy of SAM **5** is expected to be completely dispersive since it has no polar terminal group. Likewise, the dispersive contribution of the surface energy for SAM **6** is 34.1 mN/m $\pm$ 2.1 mN/m. Again, the calculated value for the dispersive contribution is larger than the total surface energy, yet this result is expected since there is no polar group present on the aromatic ring.

4.3.4 Discussion of contact angle results Zisman and Fowkes analyses of SAMs **3**, **4**, **5**, and **6** revealed that surface energy is varied by changing the substitution regiochemistry of the aromatic ring. The surface free energy for SAM **3** is primarily due to polar

contributions from the terminal –OH group. SAM **4** has a much greater dipersive component contribution to the surface free energy attributed to the different orientation of the aromatic moiety compared with SAM **3**. These values are consistent with the interpretation of the monolayer structure determined from the RAIRS spectra. SAM **5** and SAM **6** are both low energy surfaces and the surface energy is confirmed to be primarily dispersive as is expected for a surface lacking any polar functionality.

Figure 42 graphically illustrates how substitution patterns of the terminal phenyl ring affect surface energy and yield intermediate surface energy values. Figure 43 illustrates how changes in substitution regiochemistry also affect the polar and dispersive contributions to the total surface free energy.

In Table 7 it can also be seen that reaction of SAMs **3** and **4** with OTS results in a significant increase in the water contact angle indicating that partial functionalization of the terminal –OH groups took place on both monolayer surfaces. Since the terminal –OH groups in SAMs **3** and **4** reacted with OTS, it can be concluded that the projection of the terminal phenyl ring does not affect it's reactivity and that changes in surface energy for SAMs **3** and **4** can be obtained with silanization.

4.4 Reductive Desorption Results

Reductive desorption data obtained for SAMs **3**, **4**, **5**, and **6** reveal that all four surfaces have similar packing densities. Table III summarizes the calculated surface densities for each monolayer along with their corresponding desorption potentials.

Table 10. Desoprtion potentials and calculated surface densities for SAMs 3, 4, 5, and 6.

Monolayer	Desorption Potential (V)	Coverage (Ґ) (10^{-10} mol/cm^2)
4-(12-mercapto-dodecyl)phenol (**3**)	-1.047 $\pm$ (0.003)	4.9 $\pm$ 0.4
3-(12-mercapto-dodecyl)phenol (**4**)	-1.054 $\pm$ (0.006)	5.0 $\pm$ 0.5
12-phenyldodecyl-mercaptan (**5**)	-1.09 $\pm$ (0.01)	4.6 $\pm$ 0.2
12-phenylundecyloxy-mercaptan (**6**)	-0.96 $\pm$ (0.01)	4.3 $\pm$ 0.5

SAM **3** and **4** have similar desorption potentials indicating that both monolayers have similar stabilities towards desorption and that differences in substitution regiochemistry do not seem to have a significant impact on surface stability. It also reveals that despite the suspected increased tilt, of the phenyl ring in SAM **4**, the surface density is not affected. SAM **5** has the most negative desorption potential indicating the surface is more robust. The increased stability may be due to possible π-π interactions of the terminal phenyl ring.[36] This is consistent with the presence of aromatic C-H stretching modes in the RAIRS spectrum of SAM **5**. The surface density for SAM **5**, on the other hand does not suggest that the increased stabilization increases the packing density.

Inclusion of an ether linkage in SAM **6** seems to disrupt the possible π-π interactions observed for SAM **5**, leading to a more positive desorption potential. The RAIRS spectrum for SAM **6** does not show evidence for aromatic C-H stretching modes. The calculated surface density for SAM **6** is again similar to the calculated values for the other three monolayers. It is believed that the surface density is primarily dictated by the steric bulk of the terminal aromatic ring and not by ring substitution or substitution regiochemistry. The calculated surface densities for SAMs **3**, **4**, **5**, and **6** are significantly lower than surface densities which are reported for linear alkanethiol monolayers. Porter

et al. determined the maximum coverage density for a linear alkanethiol monolayer to be 7.5 - 8.0 x 10^{-10} mol/cm^2.[49]

It appears that substitution of the aromatic ring in SAMs **3** and **4** also disrupts the possible edge-to-face π-π interactions observed with SAM **5** resulting in a destabilization of the monolayer structure and a consequent decrease in desorption potentials. This observation is again consistent with the absence of aromatic C-H stretching modes in the corresponding RAIRS spectra.

4.5 Ellipsometry Results

Monolayer thicknesses were determined by ellipsometry and are summarized in Table 11. Differences between thicknesses of SAM **3** and **4** were expected and confirmed by the results obtained.

Table 11. Monolayer thicknesses obtained for SAMs 3, 4, 5, and 6 as well as for silanized SAMs 3 and 4.

Monolayer	Film Thickness(Å)	Film Thickness After Silanization (Å)
4-(12-mercaptododecyl)-phenol (**3**)	18.4 ± (1.5)	37.7 ± (3.5)
3-(12-mercaptododecyl)-phenol (**4**)	15.7 ± (0.8)	44.8 ± (2.4)
12-phenyldodecylmercaptan (**5**)	18.5 ± (1.4)	-------
12-phenylundecyloxy -mercaptan (**6**)	19.3 ± (2.4)	-------

The suspected tilt of the aromatic ring from the RAIRS spectrum of SAM **4** is confirmed in the monolayer thickness being measurably smaller. The film thicknesses also confirm that the alkyl chain tilt is largely the same, and differences in the linkage (L) do not affect the determined thickness for SAMs **5** and **6**; although a slight difference was expected

due to the suspected increased planarization of the aromatic ring with respect to the substrate surface in SAM **5**. The reaction of OTS with SAMs **3** and **4** is also confirmed since the determined thickness more than doubles in magnitude. It also seems that the reaction of OTS with SAM **3** does not lead to monolayer thicknesses as large as SAM **4**, possibly indicating the alkyl chains from added OTS have a greater tilt angle than the added OTS chains on SAM **4**. It is also possible that addition of OTS forces the plane of the phenyl ring into a largely parallel arrangement with respect to the substrate surface. The RAIRS spectrum for SAM **3** + OTS indicates that the plane of the aromatic ring becomes largely parallel to the substrate surface. Vibrations 8a and 19a largely disappear following silanization. The monolayer thicknesses for the silanized SAMs also confirm the contact angle results, which indicate that the surface energy decreases as a result of OTS addition.

4.6 Impedance Spectroscopy Results

Each SAM was modeled using the equivalent circuit model shown in Figure 27. Following data collection, complex impedance plots were prepared for each SAM. Fitting of the complex impedance plots with LEVM 7.11 (Solatron) software, yielded the resistance and capacitance values associated with each monolayer, and are summarized in Table 12.

Table 12. Film resistance and capacitance values determined for SAMs 3, 4, 5, and 6 following fitting of experimental data to the equivalent circuit model shown in Figure 27.

Monolayer	Monolayer Resistance (KΩ)	Monolayer Capacitance (μF)
4-(12-mercaptododecyl)-phenol (**3**)	3.91 $\pm$ 0.29	0.81 $\pm$ (0.02)
3-(12-mercaptododecyl)-phenol (**4**)	1.28 $\pm$ 0.2	0.94 $\pm$ (0.03)

12-phenyldodecylmercaptan (**5**)	2.04 ± 0.01	0.54 ± (0.01)
12-phenylundecyloxy-mercaptan (**6**)	3.54 ± 0.08	0.18 ± (0.01)

The other terms in the equivalent circuit model such as: solution resistance, resistance due to charge transfer (double layer resistance), and capacitance due to charge transfer (double layer capacitance) are not included in the above table for clarity. Suffice it to say the values are similar for all four SAM surfaces and do not significantly increase or decrease from one monolayer to another.

The resistance values obtained for SAMs **4**, **5**, **6** are similar within experimental error. SAM **3** does not seem to be as resistive to electron transfer. The capacitance values indicate that SAMs **3**, **4**, and **5** are the most capacitive monoalyers. SAM **6** is the least capacitive monolayer. This trend may indicate a relationship between the tilt of plane of the aromatic with respect to the surface normal and the monolayer resistance. As the tilt angle increases, film resistance seems to decrease. The resistance values for SAMs **3**, **4**, **5**, and **6** also suggest a relationship between monolayer structure and stability, evidenced both in the RAIRS spectra and also in the desorption potentials obtained for each monoalyer.

An overlay of the complex impedance plots for SAMs **3**, **4**, **5**, and **6** is shown in Figure 44. The plots are prepared with the results of the mathematical fit of the experimental data. Experimental data points are omitted for clarity.

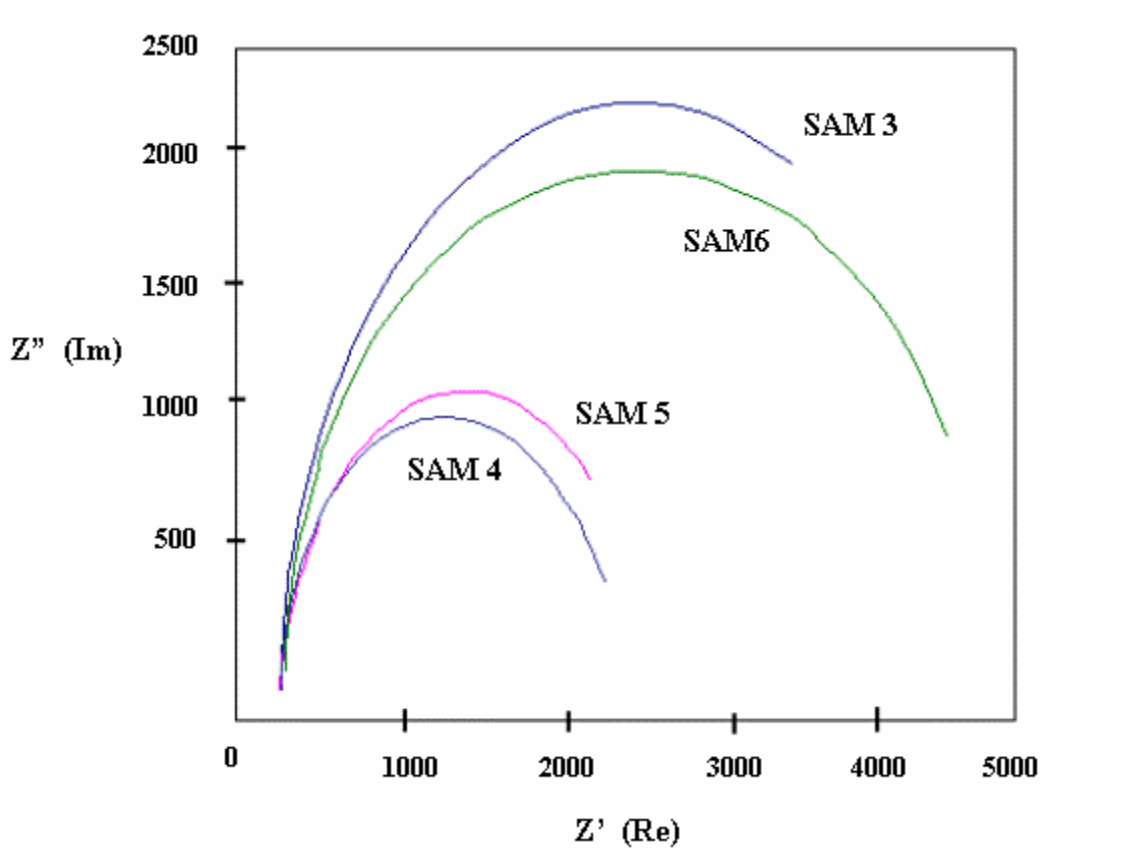

Figure 44. Complex Impedance Plots for SAMs 3, 4, 5, and 6

From visual inspection of the above plot there do not seem to be significant differences between SAMs **3** and **6** and between SAMs **4** and **5;** yet there are large noticeable differences between both pairs of data. This is consistent with the RAIRS spectra for each monolayer, which suggests that the plane of the phenyl ring SAMs **3** and **6** is more perpendicular to the substrate surface than the plane of the phenyl ring in SAMs **4** and **5**. The tilt angle of the aromatic ring seems to disrupt the ability of the monolayer to resist electron transfer. It also appears that monolayer stabilites, as determined from desorption peak potentials and RAIRS, do not have an impact on a monolayers resistive properties.

4.7 Chapter Conclusions

It is clear from the RAIRS spectra that the substitution, substitution regiochemistry, and inclusion of an ether linkage have a significant impact upon the projection of the terminal

aromatic ring as well as on the resultant projection of the terminal –OH group in SAMs **1**-**4**. It appears that meta-substitution in SAM **4** has the effect of forcing the plane of the aromatic ring into a largely parallel configuration with respect to the substrate surface. This change in orientation lowers the surface free energy of the interface and increases the dispersive contribution to the surface energy. On the other hand, meta-substitution does not seem to disrupt monolayer stability as reflected by the similarity in the desorption potentials for SAMs **3** and **4**. This suggests that the desorption potentials for SAMs **3** and **4** are primarily dictated by alkyl chain van der Waals interactions and less influenced by interactions of the terminal aromatic group.

The RAIRS spectra and desorption potential for SAM **5** suggest that this monolayer is more stable than SAMs **3**, **4**, and **6**. The terminal phenyl rings are believed to be involved in face-to-edge π-π interactions, which lead to greater stability towards desorption and contribute to the appearance of aromatic C-H stretching modes in the RAIRS spectrum. Substitution of the aromatic ring and inclusion of an ether linkage seems to disrupt these interactions and leads to more positive desorption potentials and the disappearance of the aromatic C-H vibrational modes as evidenced by the results obtained for SAMs **3**, **4**, and **6**. Impedance measurements suggest that the orientation of the terminal moiety has an impact on the resistance properties of the monolayer. Increasing tilt angles for the plane of the aromatic ring, relative to the surface normal, lowers the ability of monolayers **4** and **5** to resist electron transfer to the substrate.

It appears from the results obtained for SAMs **3**, **4**, **5**, and **6** that substitution regiochemistry and linkage atom, have a significant impact on the structural, and resistance properties of the resulting interfaces, as well as on the surface energy of each monolayer.

Chapter 5 Surface Characterization Results: SAMs 1 and 2

Introduction

SAMs of thiols 1 and 2 allow direct comparison of terminal aromatic regioisomerism. Both thiols have an ether linkage between the alkyl chain and the terminal functional group. However these SAMs are considered separately here because the total chain length is "odd" (12 CH_2 + L = O) and are one unit longer than the monolayers discussed in Chapter 4.

5.1 IR and RAIRS spectra of compounds 1 and 2

5.1.1 Transmission and RAIRS spectra of 4-(12-mercaptododecyloxy)phenol(**1**) The transmission IR spectrum of thiol **1** is shown in Figure 45 and the RAIRS spectrum of SAM **1** is shown in Figure 46. The vibrational feature assignments are summarized in Table 13. The spectra are clear and there are no vibrational features present in the RAIRS spectrum of SAM **1** attributable to CO_2 (g).

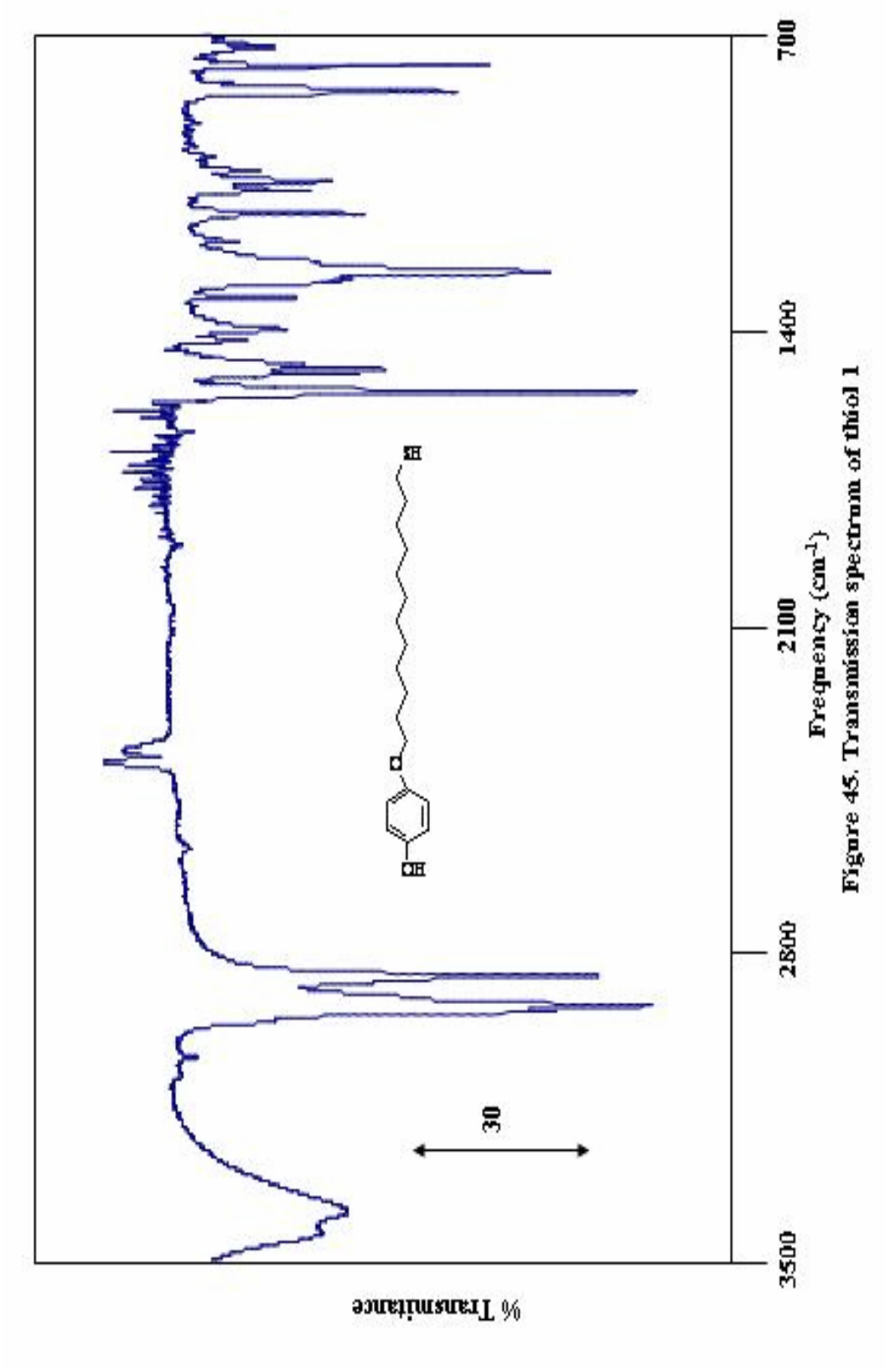

Figure 45. Transmission spectrum of thiol 1

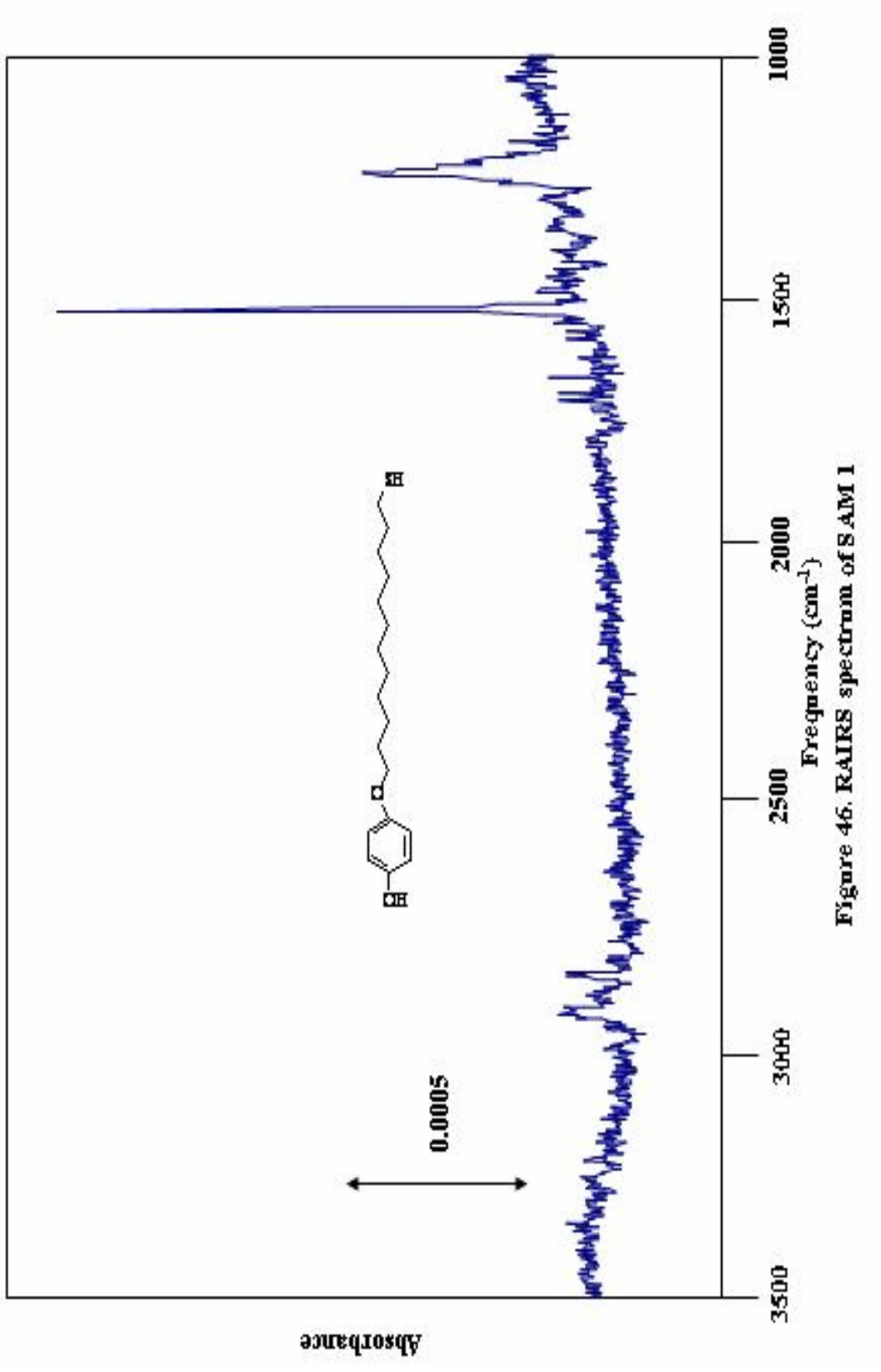

Figure 46. RAIRS spectrum of SAM 1

Table 13. Assignment of the transmission IR spectrum of thiol (1) (Figure 45) and the RAIRS spectrum of thiol (1) on gold (Figure 46).

Transmission (cm-1)	RAIRS (cm^{-1})	Assignment	Wilson Notation
3402(br)	----	OH stretch	----
3060(w)	----	νC-H (ring)	----
2920(s)	2924(w)	ν_{as}-$(CH_2)_n$-	----
2852(s)	2856(w)	ν_s-$(CH_2)_n$-	----
1516(s)	1515(s)	νC-C(ring stretch)	19a
1478(m)	----	νC-C(ring stretch)	19b
1245(s)	----	νC-O	----

There is good agreement between the transmission IR vibrational features and the RAIRS vibrational features. A feature at 3060 cm^{-1} attributed to an aromatic C-H stretching mode is observed in the transmission IR but is absent in the RAIRS spectrum indicating that there are no face-to-edge interactions in SAM **1**. Vibration 19b is also observed in the transmission spectrum but absent in the RAIRS spectrum indicating there is no canting of the aromatic ring, with respect to the substrate surface, along the C2-C3 or C5-C6 edges. The RAIRS of SAM **1** is almost featuresless in the aromatic region of the spectrum. The low intensity of the alkyl chain C-H stretching modes, relative to SAMs **3**, **4**, **5**, and **6**, indicates that the tilt angle of the alkyl chain is significantly less than in the previously mentioned SAMs. The intensity of vibration 19a is significantly larger than vibration 19a n SAM **3**. This indicates that the plane of the phenyl ring in SAM **1** is largely perpendicular to the substrate surface and more so than in SAM **3**. This may be attributable to both a decreased alkyl chain tilt angle, and a decreased tilt angle of the phenyl ring resulting from the inclusion of an ether linkage into thiol **1**.

5.1.2 Transmission and RAIRS spectra of 3-(12-mercaptododecyloxy)phenol(**2**) The transmission spectrum of thiol **2** is shown in Figure 47 and the RAIRS spectrum for SAM **2** is shown in Figure 48. The vibrational feature assignments are summarized in Table 14. There are vibrational features in the RAIRS spectrum at ~ 2400 cm^{-1} attributable to gaseous CO_2 present in the reflectance chamber of the IR spectrometer.

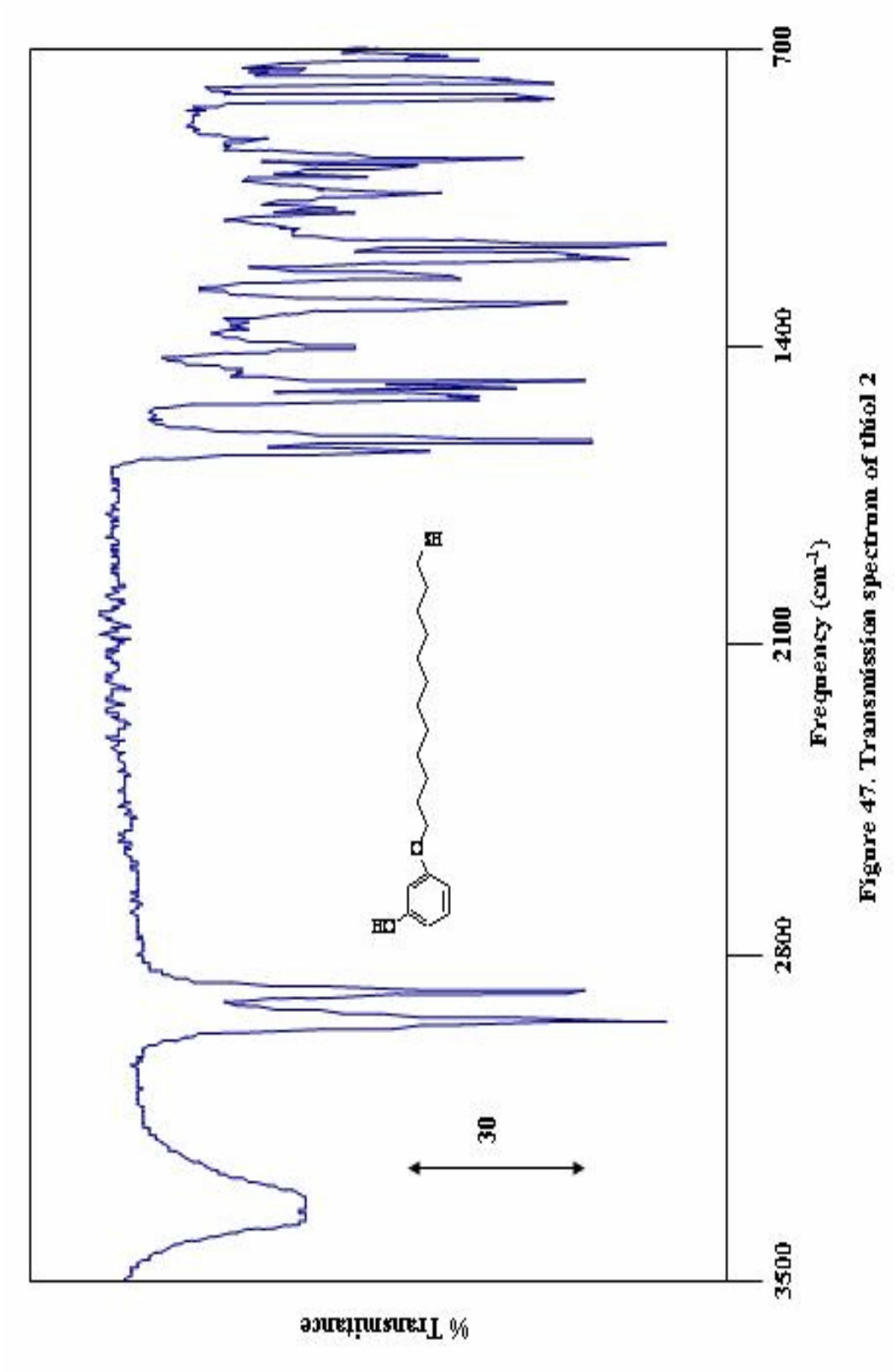

Figure 47. Transmission spectrum of thiol 2

Figure 47. Transmission Spectrum of thiol 3

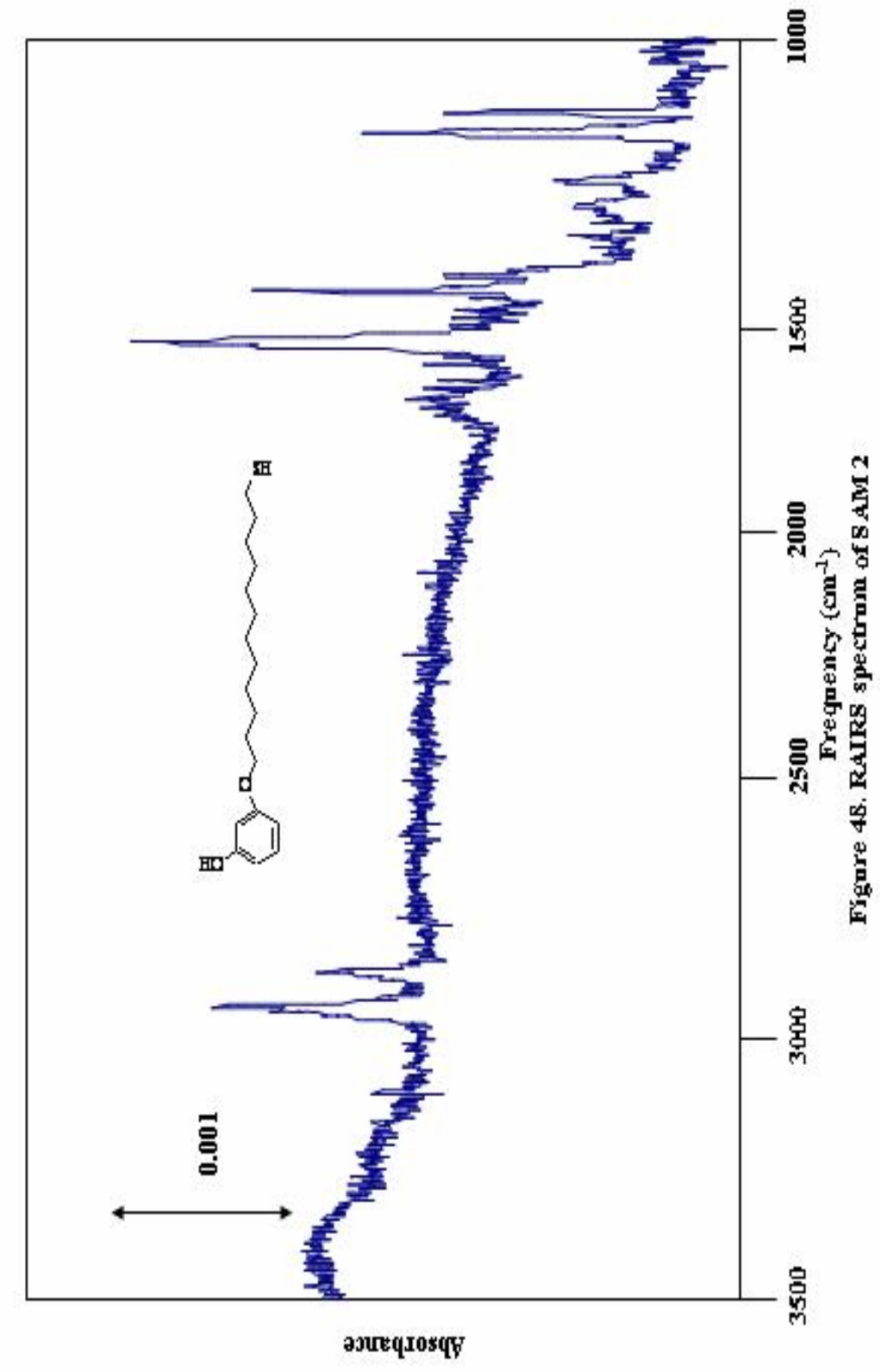

Figure 48. RAIRS spectrum of SAM 2

Table 14. Assignment of the transmission IR spectrum of thiol (2) (Figure 47) and the RAIRS spectrum of thiol (2) on gold (Figure 48).

Transmission (cm-1)	RAIRS (cm^{-1})	Assignment	Wilson Notation
3367(br)	----	OH stretch	----
2916(s)	2923(m)	ν_{as}-$(CH_2)_n$-	----
2850(s)	2854(w)	ν_s-$(CH_2)_n$-	----
1596(s)	1610(s)	νC-C(ring stretch)	8a
1504(s)	1510(m)	νC-C(ring stretch)	19a
1485(s)	----	νC-C(ring stretch)	19b
1280(s)	----	νC-O	----

There is good correspondence between the vibrational features in the transmission IR spectrum of thiol **2** and the vibrational features in the RAIRS spectrum of SAM **2**. Unlike in SAM **1** there is no vibration in the transmission spectrum observed for an aromatic C-H stretching mode. Vibration 19b is observed in the transmission spectrum for thiol **2** but absent in the RAIRS spectrum for SAM **2**, indicating no canting of the plane of the aromatic ring with respect to the substrate surface. The intensities of the alkyl chain C-H stretching modes in the RAIRS spectrum are similar in intensity to those observed for SAM **1** indicating the tilt angle of the alkyl chains is similar to that of SAM **1**. The intensity of vibration 19a is lower in SAM **2** than in SAM **1** indicating the tilt angle of the plane of the phenyl ring, with respect to the substrate, is larger than in SAM **1** and is likely the result of meta- substitution. This is consistent with the RAIRS spectrum for SAM 4, in which the intensity of vibration 19a decreases significantly as a result of meta substitution. It is also known that the intensity of vibration 19a in meta substituted benzenes is similar to the intensity of 19a in para substituted benzenes so the difference in intensity seems to be attributable to differences in orientation. The projection of the phenyl ring at the air/monolayer interface is different because of the change in ring substitution regiochemistry. Vibration 8a is observed in the RAIRS spectrum but it's intensity, relative to SAM **3,** is lower. The decrease in intensity may be attributable to a small overall change in the dipole moment for vibration 8a associated with para-substitution with similar functional groups on either end of the aromatic moiety.

5.1.3 RAIRS spectra of silanized SAMs (**1**) and (**2**) SAMs **1** and **2** were also reacted with OTS and RAIRS spectra obtained following silanization. Figure 49 shows the RAIRS spectra of SAM **1** and SAM **1** following reaction with OTS. Assignments of the various vibrational features remain as specified in section 5.1.1. The intensity of the C-H stretching modes of the alkyl chain increases following silanization as expected, due to added alkyl chains. The intensity of vibration 19a at 1515 cm^{-1} remains largely unchanged suggesting the orientation of the aromatic moiety remains the same after addition of an OTS layer. These observations suggest that the terminal –OH moiety is accessible for reaction at the surface of the monolayer and that addition of more layers does not significantly alter the underlying monolayer structure.

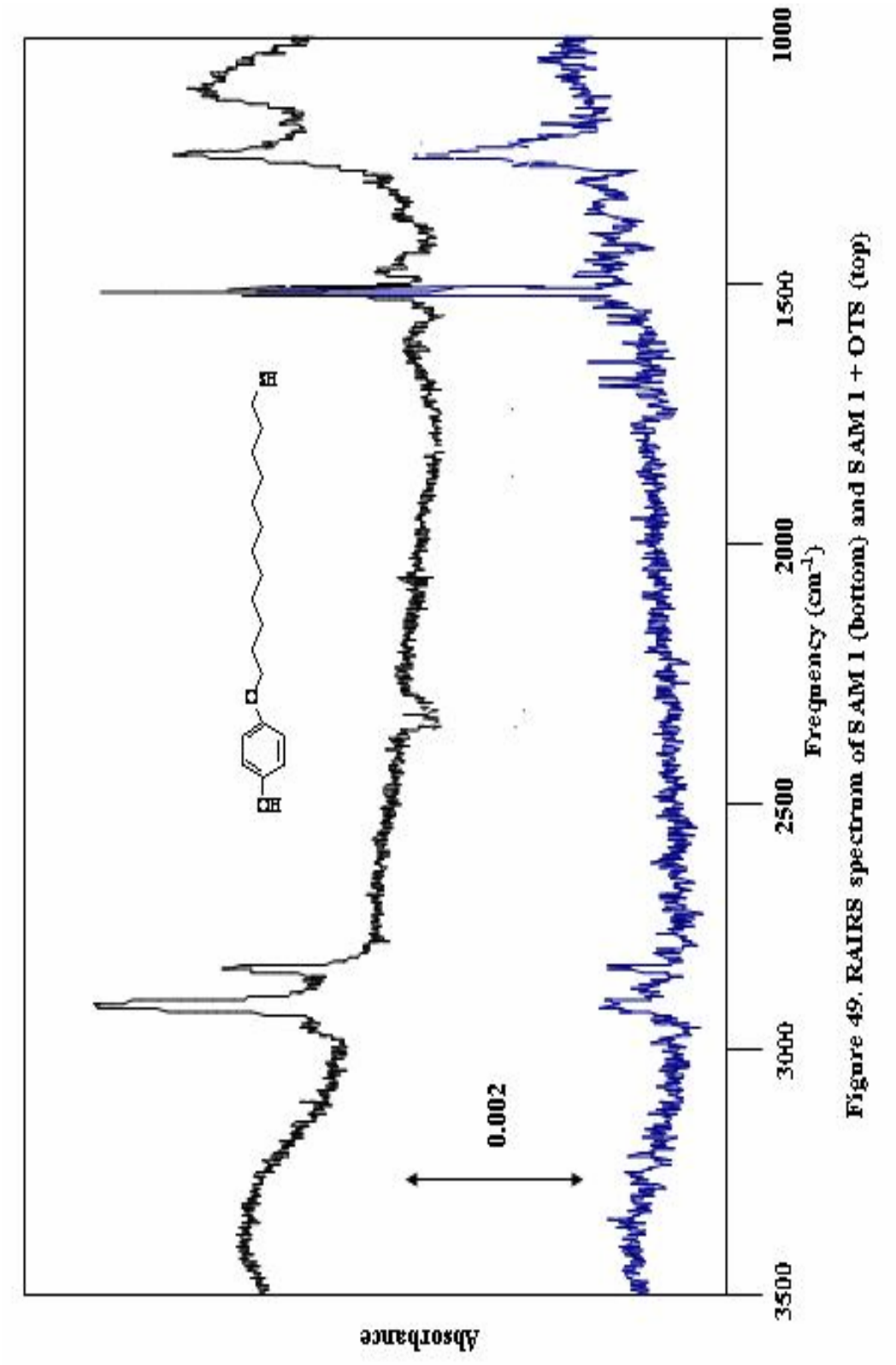

Figure 49. RAIRS spectrum of SAM 1 and SAM 1+OTS

The RAIRS spectrum of SAM **2** shows significant changes following silanization. Figure 50 shows the RAIRS spectra of SAM **2** and SAM **2** following silanization. The asymmetric and symmetric C-H stretching vibrations increase in intensity primarily due to the added number of alkyl chains from OTS with a possible contribution from increased tilting of the SAM alkyl chains following silanization. Vibrations 8a and 19a are no longer visible which suggests that upon functionalization the plane of the aromatic ring becomes largely parallel to the substrate surface. The larger tilt angle of the phenyl ring in SAM **2**, relative to the ring tilt angle in SAM **1**, does not significantly alter the reactivity of the terminal –OH moiety. Unlike with SAM **1**, the tilt angle of the phenyl ring in SAM **2** becomes larger following addition of OTS evidenced by the decrease in the intensity of vibrations 19a and 8a.

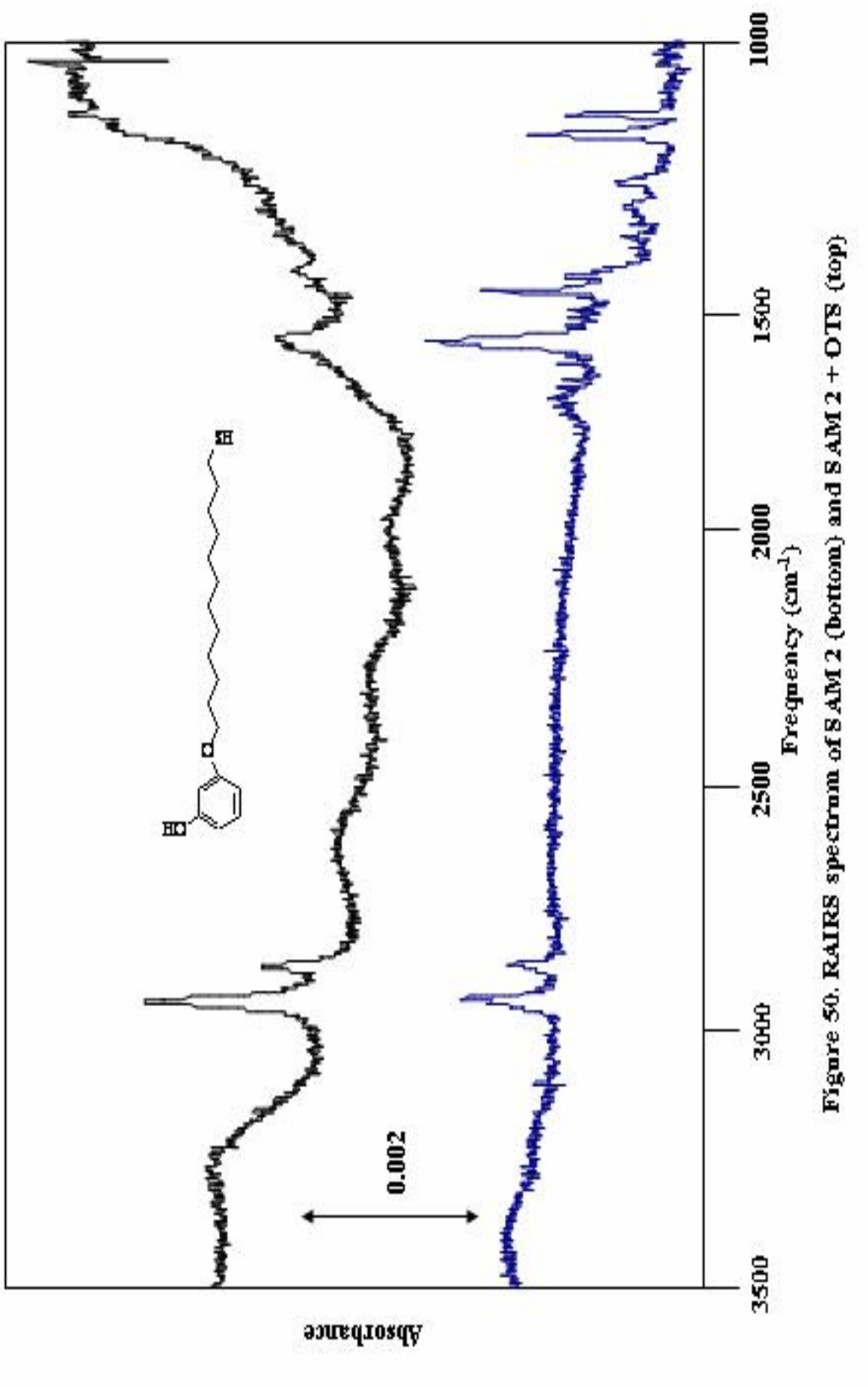

Figure 50. RAIRS spectrum of SAM 2 (bottom) and SAM 2 + OTS (top)

Figure 50. RAIRS spectrum of SAM 2 and SAM 2+OTS

5.1.4 Discussion of IR spectra It appears from the RAIRS spectra that inclusion of an ether linkage, to make an "odd" chain length, decreases the tilt angle of the alkyl chains relative to the substrate surface. Like with SAMs **3** and **4**, changes in ring substitution regiochemistry, alter the tilt angle of the plane of the phenyl ring. As with SAM **4**, meta-substitution in SAM **2** forces a change in the packing conformation of the terminal moiety, and forces the phenyl ring into a more parallel arrangement relative to the substrate surface. The orientation of the plane of the aromatic ring in SAM **1** seems to be almost completely perpendicular to the substrate leading to an uncharacteristically large feature at 1515 cm^{-1}. Figure 51 models what is thought to be the structure of SAMs **1** and **2** based on their RAIRS spectra.

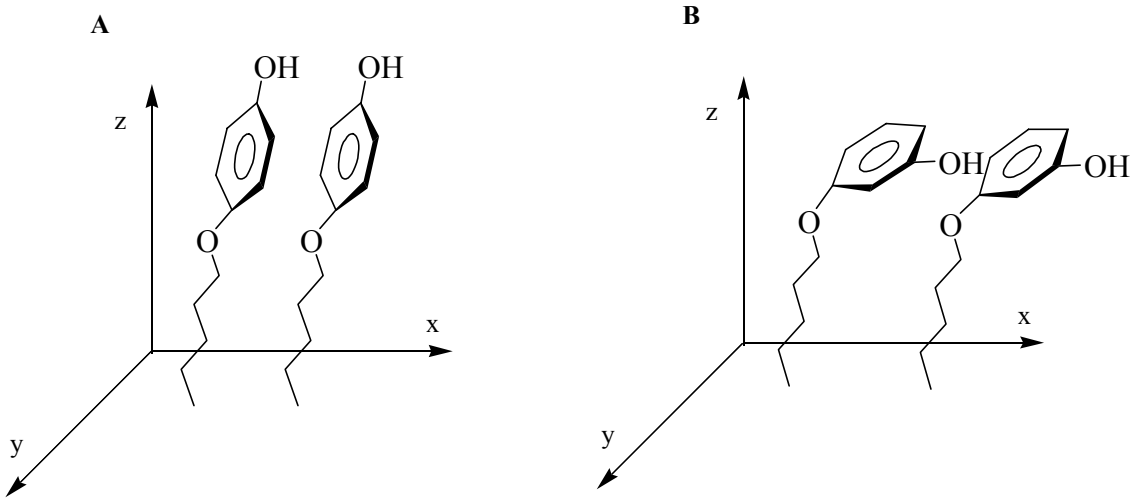

Figure 51. a) Orientation of SAM 1, b) Orientation of SAM 2

Reaction with OTS does not seem to affect the orientation of the aromatic ring in SAM **1** whereas silanization of SAM **2** forces the aromatic ring into a more parallel orientation with respect to the substrate surface as evidenced by the decrease in the intensities of vibrations 8a and 19a.

5.2 Contact Angle Results

5.2.1 Experimental details and data Contact angle data were obtained for SAMs **1** and **2** as well as for the corresponding silanized surfaces. Table 15 summarizes the contact

angle results obtained using water, ethylene glycol, and glycerol. SAM **1** has a lower contact angle than SAM **2,** and consequently, is the more hydrophilic surface. The surface –OH group according to the structure model proposed in Figure 51 suggests that SAM 2 is a less polar surface since the terminal –OH is not projected into the monolayer/air interface as it is in SAM **1**.

Table 15. SAM-liquid interfacial contact angles for SAMS 1, 2, and silanized SAMS 1 and 2.

Monolayer	Water (deg)	Ethylene Glycol (deg)	Glycerol (deg)
4-(12-mercapto-dodecyloxy)phenol (**1**)	47(2)	33(3)	47(3)
3-(12-mercapto-dodecyloxy)phenol (**2**)	68(2)	48(2)	63(2)
SAM **1** + OTS	63(3)	-----	-----
SAM **2** + OTS	73(2)	-----	-----

Following functionalization with OTS, water contact angles for SAM **1** increase as expected. The water contact angle for silanized SAM **2** does not increase significantly, although SAM **2** is more hydrophobic prior to functionalization. Both silanized surfaces behave as expected following addition of alkyl chains to the monolayer surface. These results support the conclusions drawn from the RAIRS spectra of each SAM and also support the proposed structure model shown in Figure 51.

5.2.2 Results and discussion of Zisman analyses Zisman plots were prepared for SAMs **1** and **2**. The combined Zisman plot for SAM **1** and **2** is shown in Figure 52. From the graphical Zisman analyses, surface free energy values were obtained for each monolayer and are summarized in Table 16. Visual inspection of the Zisman plot reveals that the point at which each line intercepts the value of 1 on the y axis is different, indicating the surface free energies for each SAM surface are different.

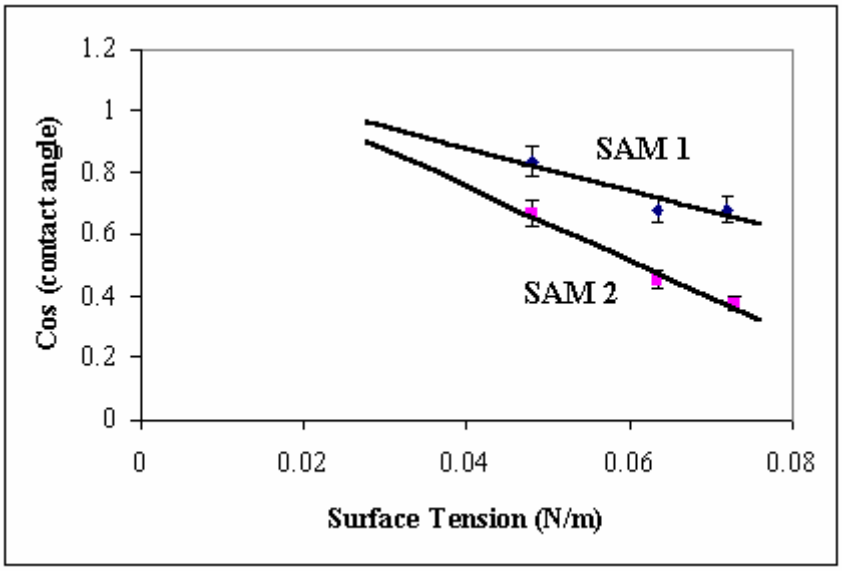

Figure 52. Zisman Plot for SAMs 1 and 2

The calculated surface free energy for SAM **1** is calculated to be 23.1 mN/m $\pm$ 13.2 mN/m, which is comparable to the value obtained for SAM **3**. The surface free energy for SAM **2** is 19.8 mN/m $\pm$ 5.4 mN/m, which is similar to the surface energy of SAM **1**. It appears that meta-substitution of the ring, as in the case of SAM **4**, decreases the surface energy of SAM **2** relative to SAM **1**.

Table 16. Calculated surface free energies for SAMs 1 and 2. Slopes, intercepts, and R^2 values for each regression line shown in Figure 52 are included along with associated errors.

Monolayer	Slope	Error in Slope	Intercept	Error in intercept	R^2	Surface Energy (mN/m)
SAM **1**	-6.98	2.65	1.03	0.06	0.333	23.1 $\pm$ 13.2
SAM **2**	-12.01	1.57	1.19	0.06	0.832	19.8 $\pm$ 5.4

Even though there are large errors associated with the Zisman analysis the trend that is observed when comparing the surface energies of SAMs **1**, **2**, **3**, and **4** is that meta substitution of the aromatic ring decreases the calculated values for surface free energy

although, this difference is larger in the case of SAMs **3** and **4**. This conclusion is also supported by the RAIRS spectral results obtained for the monolayers in question.

5.2.3 Results and discussion of Fowkes analyses The dispersive contributions to the surface free energy were determined for SAMs **1** and **2** from the combined Fowkes plot shown in Figure 53. A summary of the results and error analyses for the Fowkes analyses is provided in Table 17. Visual inspection of Figure 53 reveals that changes in the dispersive contribution, to each surface energy in SAMs **1** and **2**, is also achieved by changing the aromatic ring substitution regiochemistry.

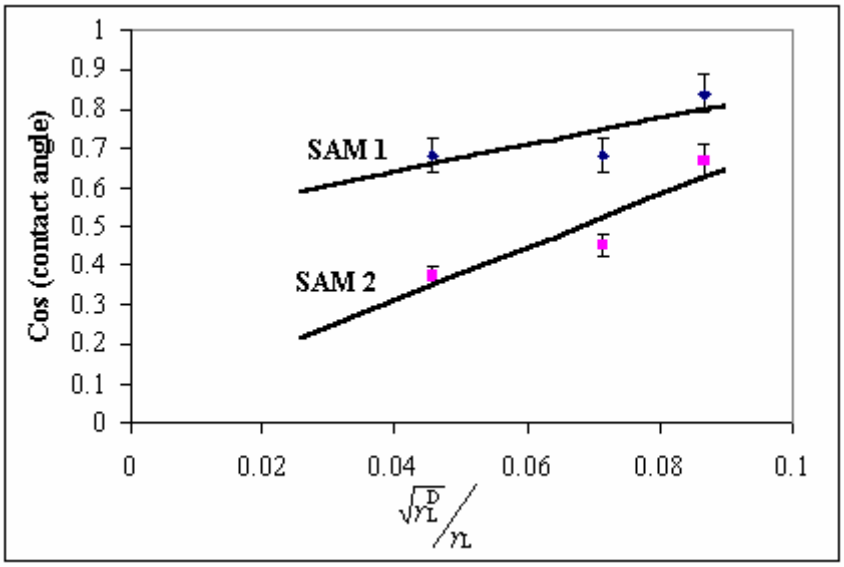

Figure 53. Fowkes Plot for SAMs 1 and 2

The calculated dispersive contribution for SAM **1** is 3.7 mN/m $\pm$ 0.4 mN/m, which is 16 % of the total surface free energy. The dispersive contribution is small and similar in magnitude to that of SAM **3**.

Table 17. Calculated dispersive components for SAMs 1 and 2. Slopes, intercepts, and R^2 values for each regression line shown in Figure 53 are included along with associated errors.

Monolayer	Slope	Error in Slope	Intercept	Error in intercept	R^2	Dispersive Component (mN/m)
SAM **1**	3.41	2.71	0.51	----	0.613	3.7 ± 0.4
SAM **2**	6.73	2.91	0.04	----	0.843	11.3 ± 2.2

The dispersive component calculated for SAM **2** is 11.3 mN/m $\pm$ 2.2 mN/m, which is 57% of the total surface free energy. Meta-substitution of the ring, as with SAM **4**, increases the dispersive contribution since the tilt angle of the plane of the phenyl ring increases, relative to the surface normal. Consequently, the face of the ring is more exposed at the monolayer/air interface increasing the hydrophobicity of the monolayer. These observations agree with and support the proposed structure model for SAMs **1** and **2** shown in Figure 51.

5.2.4 Discussion of the contact angle results Large differences for the calculated surface free energies for SAMs **1** and **2** were not found, yet significant differences in the dispersive contribution were discovered. The experimental results agree with the proposed orientation model (Figure 58) for SAMs **1** and **2** in which meta-substitution of the aromatic ring leads to a greater tilt angle of the plane aromatic ring with respect to the surface normal. Increased exposure of the plane of the aromatic ring at the air solid interface leads to an increased dispersive contribution to the surface energy and limits the contribution due to the terminal –OH moiety in SAM **2**. Likewise, increased exposure of the terminal hydroxide and limited exposure of the plane of the aromatic ring at the interface should lower the dispersive contribution, which is observed for SAM **1**. It appears that inclusion of an ether linkage to make an "odd" chain does not significantly affect the values obtained for surface free energy nor does it affect the dispersive contribution to the surface free energy.

5.3 Reductive Desorption Results

Desorption data for SAMs **1** and **2** is summarized in Table 18. The desorption potential for SAM **1** is more negative than the desorption potential for SAM **2** by 139 mV. The large difference can only be accounted for based on packing arrangement. It is assumed that the alkyl chains are disordered and are not in a crystalline environment. The steric bulk of the terminal aromatic ring limits the intractions of the alkyl chains and lowers the stabilization energy which may result from increased van der Waals interactions. Following these assumptions, the interactions of the head group largely dictate the desorption potential; consequently, meta-substitution seems to disrupt head group interactions leading to a more positive desorption potential. From the RAIRS spectra, the aromatic ring in SAM **1** is believed to be more perpendicular to the surface, this could lead to increased Van der Waals interactions within the alkyl chain and increased stability towards desorption. The desorption potential for SAM **1** is also higher than that obtained for SAM **5** which indicates that even though no edge-to-face π-π are evidenced by the RAIRS spectra, monolayer stability is also a function of monolayer structure and does not rely solely on interactions between the terminal functional groups.

Table 18. Desoprtion potentials and calculated surface densities for SAMs 1 and 2.

Monolayer	**Desorption Potential (V)**	**Coverage (Ґ) (10^{-10} mol/cm^2)**
4-(12-mercaptodo-decyloxy)-phenol (**1**)	-1.19 + (0.07)	4.6 $\pm$ (0.5)
3-(12-mercaptodo-decyloxy)phenol (**2**)	-1.055 $\pm$ (0.005)	4.5 $\pm$ (0.3)

Unlike in the case of SAMS **3** and **4**, meta substitution in SAM **2** seems to disrupt the monolayer stability observed for SAM **1**.

The calculated surface densities are similar to the surface densities obtained for the previous four SAMs (Chapter 4), indicating that the packing density of SAMs **1** and **2** do

not measurably change due to inclusion of an ether linkage or by increasing the length of the alkyl chain. As is the case for the monolayers discussed in Chapter 4, the major structural factor dictating coverage densities is the steric bulk of the terminal phenyl ring. Substitution regiochemistry of the aromatic ring seems to seriously affect the desorption potential of SAMs **1** and **2**. This trend was not observed in SAMs **3** and **4** and suggests that SAM **1** is particularly stable towards desorption.

5.4 Ellipsometry Results

SAM thicknesses were obtained for SAMs **1** and **2** and for the corresponding silanized analogs and are summarized in Table 19. There are no observable differences in film thicknesses for SAMs **1** and **2** and the suspected increased tilt of the aromatic ring in SAM **2** is not corroborated by the ellipsometric thicknesses. The monolayer thicknesses are larger than the thicknesses observed for SAMs **3**, **4**, **5**, and **6** suggesting that the decreased alkyl chain tilt angles observed in the RAIRS spectra for SAMs **1** and **2** are reflected in the film thicknesses.

Table 19. Monolayer thicknesses obtained for SAMs 1 and 2 as well as for silanized SAMs 1 and 2.

Monolayer	Film Thickness (Å)	Film Thickness After Silanization (Å)
4-(12-mercaptodo-decyloxy)phenol (**1**)	23.8 $\pm$ (1.1)	52.8 $\pm$ (3.1)
3-(12-mercaptodo-decyloxy)phenol (**2**)	23.8 $\pm$ (1.5)	23.5 $\pm$ (1.8)

The film thickness for silanized SAM **1** indicates that addition of OTS took place and has more than doubled the monolayer thickness. This increase is also reflected in the RAIRS spectrum of silanized SAM **1**. The ellipsometric thickness for SAM **2** + OTS does not increase, indicating that OTS did not add to the surface. The terminal –OH could be less

accessible for reaction and the OTS is stiil in the adsorbing solution. Although the RAIRS spectra shows an increase in the signal alliphatic C-H stretching modes (2950-2840 cm^{-1}), the ellipsometric thicknesses do not reflect this increase. This may be due to a small increase in the amount of OTS chains added to the monolayer and is not detectable by ellipsometry. It appears that a decrease in the tilt angle of the alkyl chains for SAMs **1** and **2**, observed in the RAIRS spectra, is reflected in the ellipsometric thicknesses. Meta-substitution of the aromatic ring in SAM **2** seems to limit the accessibility of the terminal –OH group for reaction with OTS. This is corroborated by the water contact angle for SAM **2** which indicates that SAM **2** is largely hydrophobic and that the terminal –OH is not dictating surface energy. Also, water contact angles or silanized SAM **2** do not significantly increase corroborating the ellipsometric thickness obtained for the silanized monolayer.

5.5 Impedance Spectroscopy Results

Impedance measurements were performed on SAMs **1** and **2** and the results of the fitting of the experimental data the equivalent circuit model in Figure 27 are shown in Table 20. Figure 54 shows the complex impedance plot for SAMs **1** and **2**. Again, the mathematical fit is shown and the individual experimental data points are omitted for clarity.

Table 20. Film resistance and capacitance values determined for SAMs 1 and 2 following fitting of experimental data to the equivalent circuit model shown in Figure 27.

Monolayer	Monolayer Resistance (KΩ)	Monolayer Capacitance (μF)
4-(12-mercaptododecyloxy)-phenol (**1**)	1.80 $\pm$ 0.04	0.37 $\pm$ (0.09)
3-(12-mercaptododecyloxy)-phenol (**2**)	2.25 $\pm$ 0.31	0.31 $\pm$ (0.03)

The other terms in the equivalent circuit model such as: solution resistance, resistance due to charge transfer (double layer resistance), and capacitance due to charge transfer (double layer capacitance) are not included in the above table for clarity. Suffice it to say the values are similar to the values obtained for SAMs **3**, **4**, **5**, and **6** and do not significantly change for SAMs **1** and **2**.

Introduction of meta or para substitution does not seem to affect the monolayer resistance to electron transfer in SAMs **1** and **2**. The film resistance values are similar, within experimental error, to the values obtained for SAMs **4** ad **5**, indicating that inclusion of an ether linkage along with substitution of the aromatic ring decreases the resistive properties of SAMs **1** and **2**. SAM **6** also includes an ether linkage into it's structure but the aromatic ring is not substituted. It appears that a combination of ring substitution and an ether linkage leads to less resistive monolayers. The ~ 4Å thickness difference between SAMs **3**, **4**, **5**, and **6** and SAMs **1** and **2** do not seem to be a major factor affecting the resistance values in SAMs **1** and **2**. It is thought the alkyl chains are more perpendicular in SAMs **1** and **2** which may lead to less permeable layers with disordered alkyl chains which can provide channels for easier ion and electron transfer to the substrate surface.

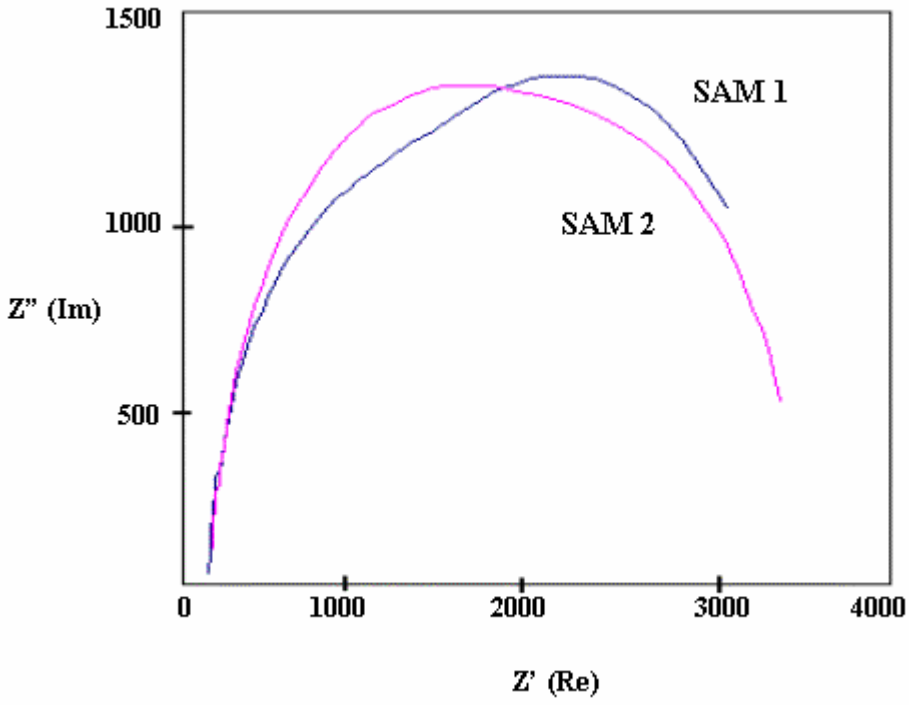

Figure 54. Complex impedance plots for SAMs 1 and 2

Figure 54 shows the complex impedance plots for SAMs **1** and **2**. Visual inspection reveals no significant differences between SAMs **1** and **2**. It is clear from comparison of the results summarized in Tables 12 and 20 that inclusion of an ether linkage and increased aromatic ring tilt combine to lower the resistive properties of resulting monolayers as evidenced by the impedance results for SAMs **1**, **2**, **4**, and **5**.

5.6 Chapter Conclusions

From the RAIRS spectra of SAMs 1 and 2 it can be seen that meta-substitution of the aromatic ring forces the phenyl ring into a more planar arrangement with respect to the substrate surface as is the case for SAM **4**. The change in orientation of the terminal aromatic moiety results in a decrease in the stability of the monolayer reflected by the more positive desorption potential obtained for SAM **2** relative to SAM **1**. Meta-subtitution also has the effect of lowering the surface free energy and, more importantly, increasing the dispersive contribution to the surface free energy. It appears that the face of the aromatic ring in SAM **2** is exposed more than in SAM **1** and, consequently, decreases the contribution that the terminal –OH group has on surface energy. Ellipsometric measurements suggest that the terminal –OH is less accessible for reaction in SAM **4**, reflected in the lower ellipsometric thicknesses found for SAM **4** following reaction with OTS. Impedance measurements suggest that inclusion of an ether linkage along with –OH substitution of the aromatic ring, combines to lower the resistance properties of SAMs **1** and **2** relative to SAMs **3** and **6**. These results again, seem to suggest that the orientation of the terminal aromatic moiety and the inclusion of an ether linkage have a significant effect on the properties of these monolayer surfaces.

Chapter 6 Surface Characterization Results: SAMs 7 and 8

Introduction

The last pair of monolayer surfaces, which were characterized, are also within a homologous series with respect to alkyl chain length. SAM **7** and **8** both have six units in the alkyl chain. SAM **8** has an ether linkage and SAM **7** has a methylene linkage to the aromatic ring. Both are para-substituted with a terminal –OH group. By decreasing the alkyl chain length, less stabilization due to van der Waals interactions is expected and may be reflected by a decrease in desorption potentials for each SAM. Shorter chain lengths may also result in a decrease in resistive properties of the monolayer. Also, shorter chains may result in an increase in the disorder of the alkyl chains within the monolayer and a decrease in the measured ellipsometric thicknesses.

6.1 IR and RAIRS spectra of compounds 7 and 8

6.1.1 Transmission and RAIRS spectra of 4-(6-mercapto-hexyl)phenol(**7**). The transmission infrared spectrum of thiol **7** is shown in Figure 55 and the RAIRS spectrum of SAM **7** is shown in Figure 56. Vibrational frequency assignments are summarized in Table 21. There are vibrational features at ~ 2400 cm^{-1} in the RAIRS spectrum attributable to gaseous CO_2 present in the reflection chamber of the IR spectrometer.

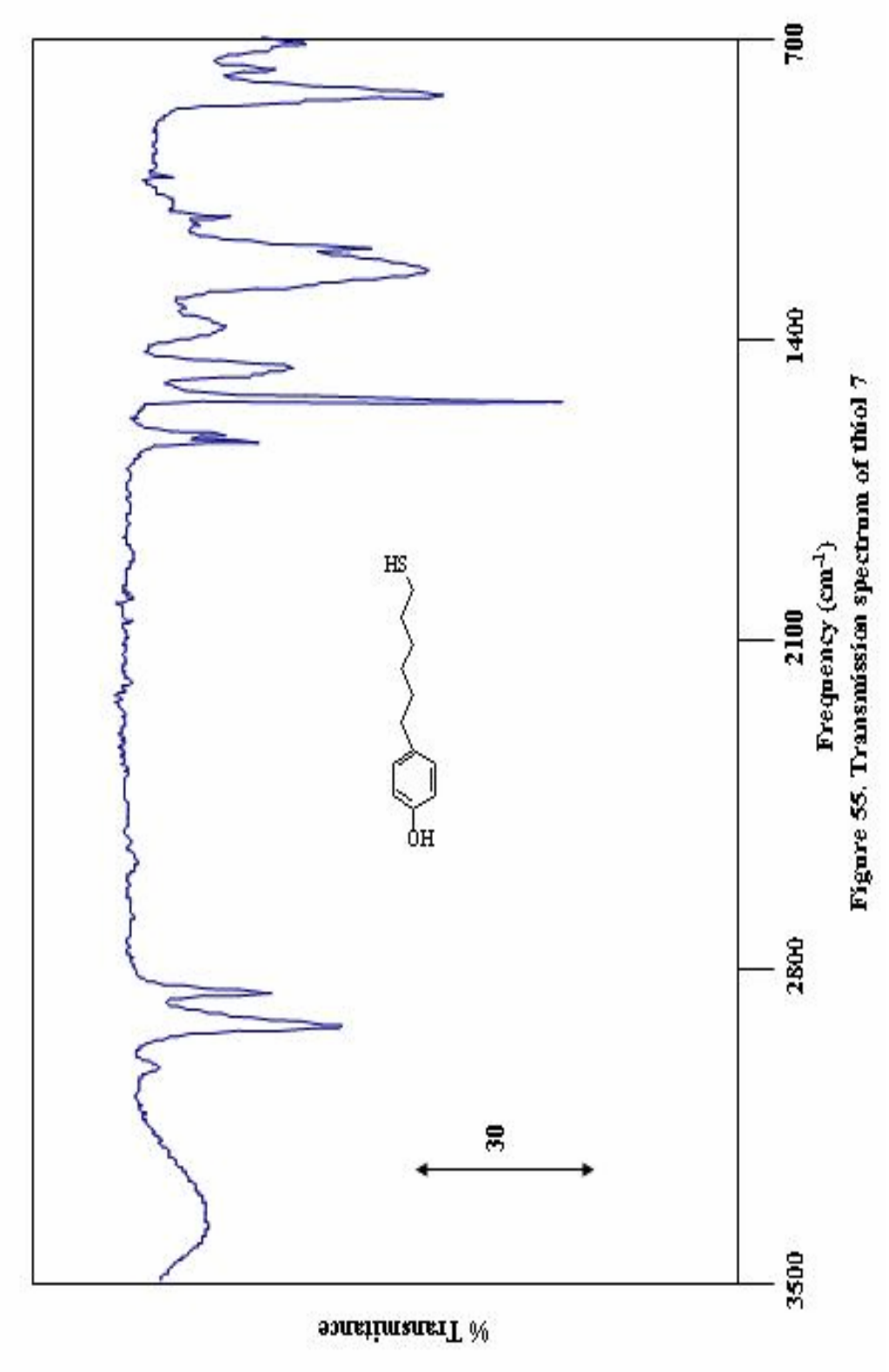

Figure 55. Transmission spectrum of thiol 7

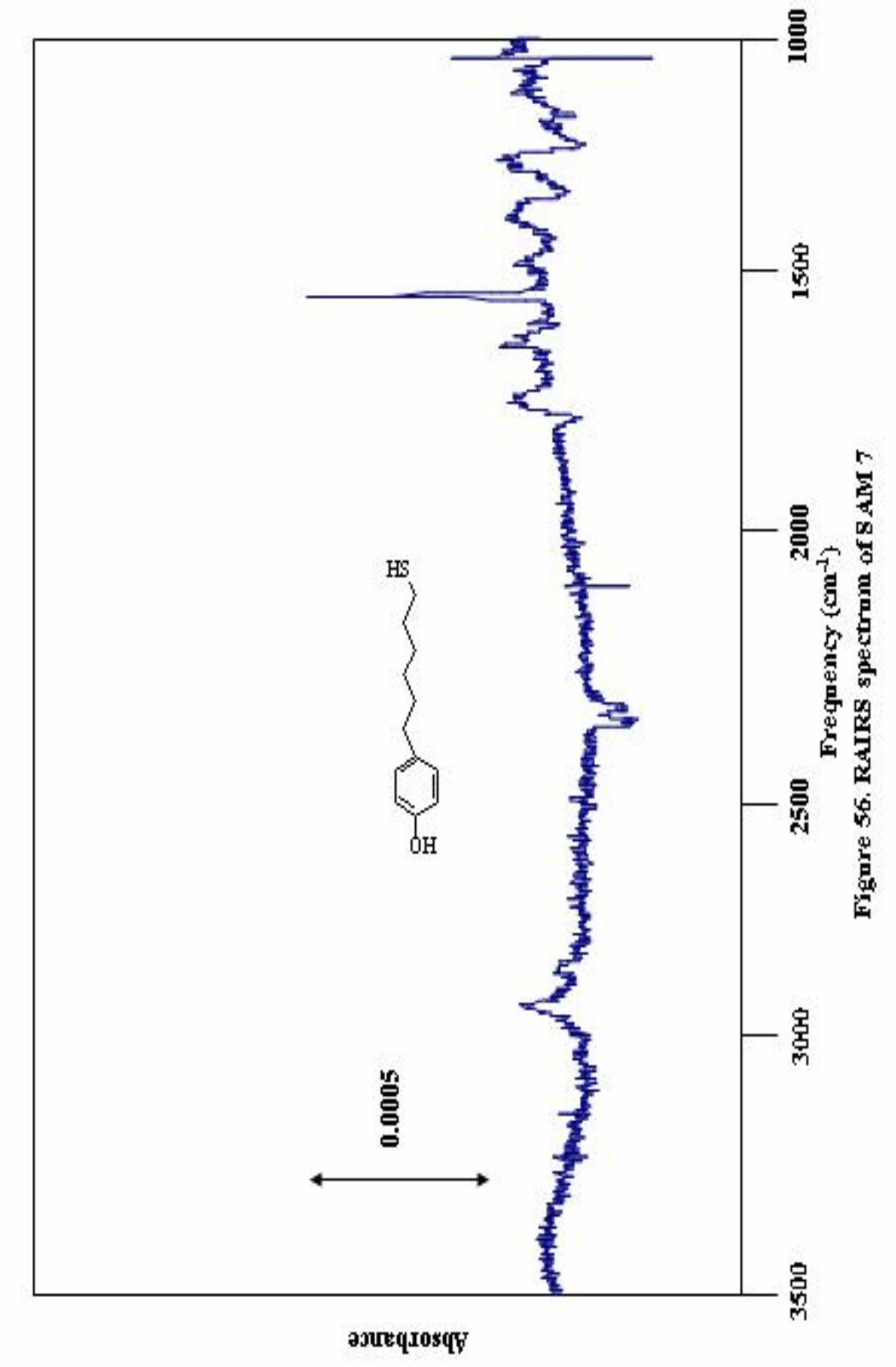

Figure 56. RAIRS spectrum of SAM 7

Table 21. Assignment of the transmission IR spectrum of thiol (7) (Figure 55) and the RAIRS spectrum of thiol (7) on gold (Figure 56).

Transmission (cm-1)	RAIRS (cm^{-1})	Assignment	Wilson Notation
3386(br)	----	OH stretch	----
3039(w)	----	νC-H (ring)	----
2927(s)	2929(w)	ν_{as}-$(CH_2)_n$-	----
2854(s)	2858(w)	ν_s-$(CH_2)_n$-	----
1608(m)	1620(w)	νC-C(ring stretch)	8a
1512(s)	1516(s)	νC-C(ring stretch)	19a
1226(s)	----	νC-O	----

There is good correspondence between the vibrational frequencies in the transmission IR of thiol **7** and the RAIRS spectrum of SAM **7**. Like SAM **1**, the transmission spectrum has a feature due to an aromatic C-H stretching mode that is absent from the RAIRS spectrum, indicating no stabilization due to face-to-edge interactions of the terminal moiety. Vibration 19b is not observed in the transmission or in the RAIRS spectrum indicating there is no canting of the phenyl ring along the C2-C3 or C5-C6 edges. The intensities of the alkyl C-H stretching modes are small in both the transmission and RAIRS spectrum as is expected with a shorter alkyl chain. Vibration 19a and 8a are present indicating the plane of the phenyl ring is largely perpendicular to the substrate surface as was the case for SAM **3**. The orientation of the aromatic ring is believed to be the same as in SAM **3** based on the intensities of the observed vibrations in the RAIRS spectrum of SAM **7** relative to the observed vibrational features in the RAIRS spectrum of SAM **3**. It appears from the RAIRS spectra that no significant orientation differences result from a decrease in the chain length.

6.1.2 Transmission and RAIRS spectra of 4-(6-mercapto-pentyloxy)phenol(**8**) The transmission spectrum of thiol **8** is shown in Figure 57 and the RAIRS spectrum of SAM **8** is shown in Figure 58. The vibrational frequency assignments are summarized in Table 22. There are vibrational features at ~ 2400 cm^{-1} in the RAIRS spectrum attributable to gaseous CO_2 present in the reflection chamber of the IR spectrometer.

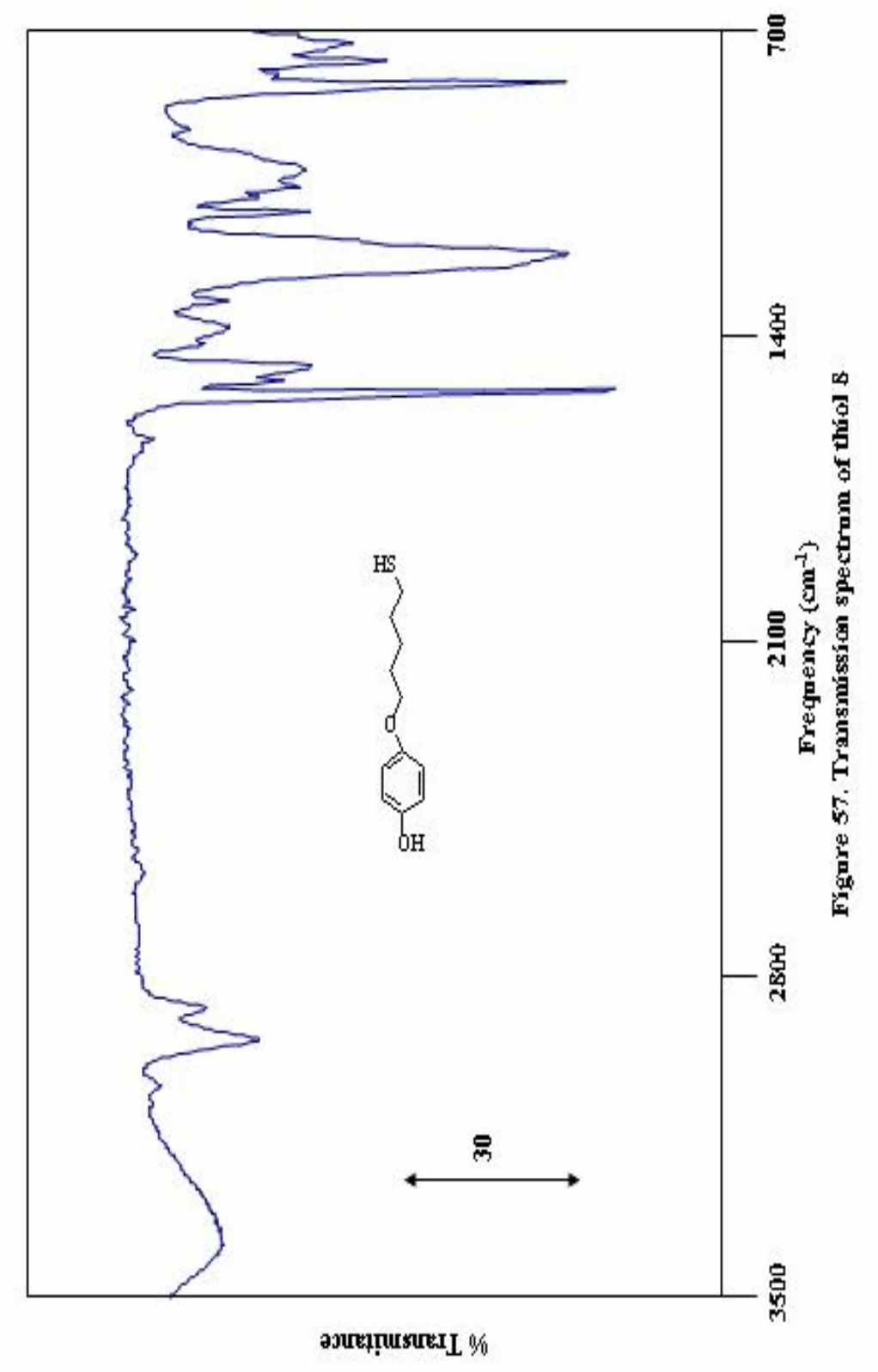

Figure 57. Transmission spectrum of thiol 8

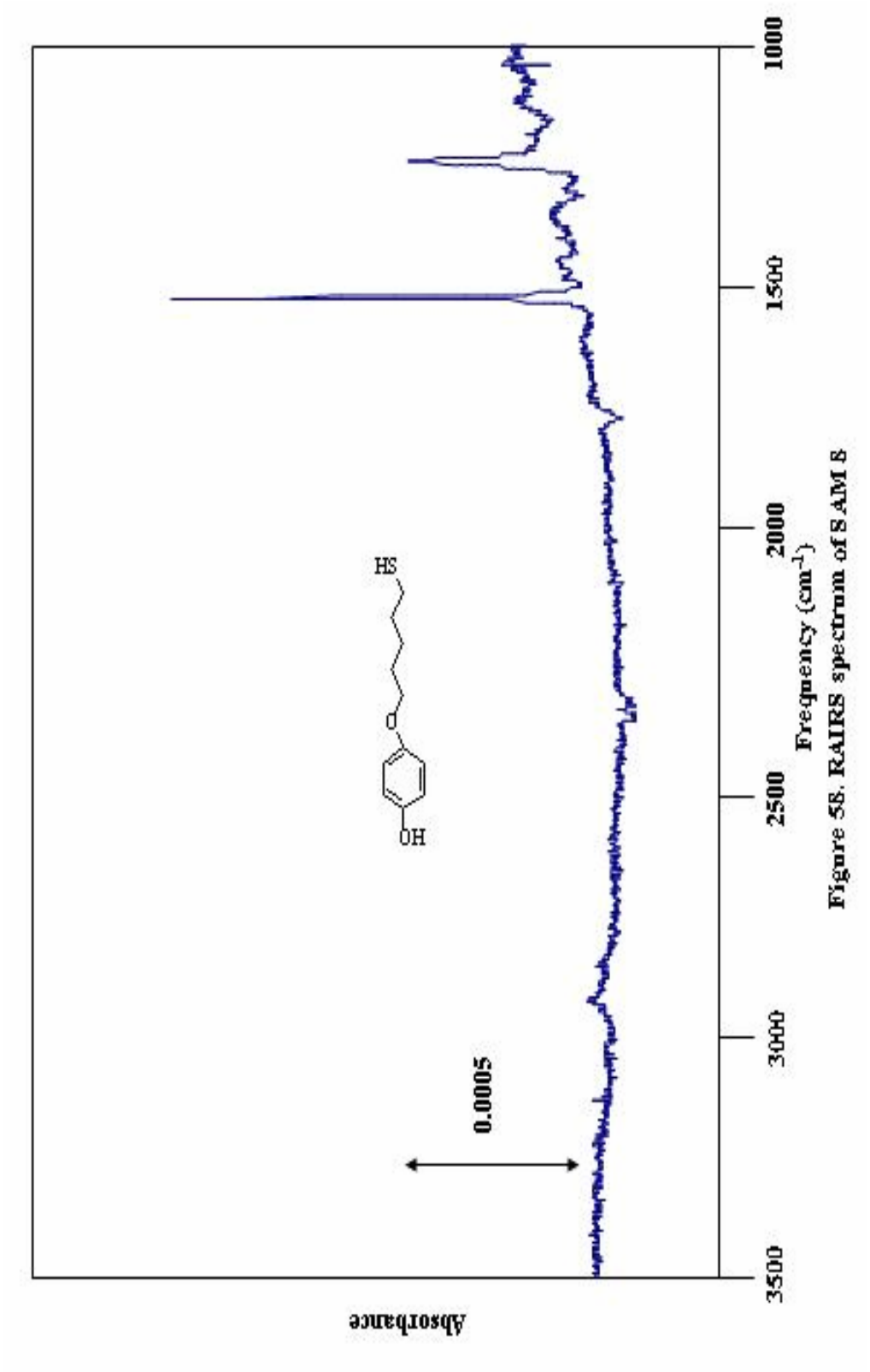

Figure 58. RAIRS spectrum of SAM 8

Table 22. Assignment of the transmission IR spectrum of thiol (8) (Figure 57) and the RAIRS spectrum of thiol (8) on gold (Figure 58).

Transmission (cm-1)	RAIRS (cm^{-1})	Assignment	Wilson Notation
3394(br)	----	OH stretch	----
2930(m) 2860(m)	2939(w) 2860(w)	ν_{as}-$(CH_2)_n$- ν_s-$(CH_2)_n$-	---- ----
1620(w)	----	νC-C(ring stretch)	8a
1508(s)	1520(s)	νC-C(ring stretch)	19a
1480(m)	----	νC-C(ring stretch)	19b
1208(s)	----	νC-O	----

There is good agreement between the vibrational frequencies in the transmission spectrum of thiol **8** and the RAIRS spectrum of SAM **8**. Vibration 19b is observed in the transmission IR but is absent in the RAIRS spectrum indicating there is no canting of the phenyl ring in the monolayer. The intensity of vibration 19b in para-substitutted benzenes is similar to the intensity of vibrations 8a and 19a, so the absence of 19b suggests there is no ring canting. The intensity of the alkyl C-H stretching modes are small just as were observed for SAM **1**. This is a result of a decrease in the number of methylene units in the chain but also a result of the tilt angle of the alkyl chain. Comparing the RAIRS spectra of SAM **1** and SAM **8** it is clear, from the relative intensities of the vibrational features observed, that both monolayers are similar, suggesting the orientation of the alkyl chain and the tilt of the phenyl ring are largely the same. The intensity of vibration 19a is also uncharacteristically large suggesting the plane of the phenyl ring is largely perpendicular to the substrate surface. It appears that the alkyl chain length does not seem to alter the structure of the monolayer as is also observed for SAMs **7** and **3**.

6.1.3 RAIRs spectra of silanized SAMs (**7**) and (**8**) SAMs **7** and **8** were also reacted with OTS and RAIRS spectra were obtained for the silanized surfaces. Figure 59 shows the RAIRS spectrum of SAM **7** and SAM **7** following silanization. A large increase in the intensity of the alkyl C-H vibrations (2930-2860 cm-1) is observed as would be expected from addition of alkyl groups to the monolayer structure from OTS. The

features assigned to vibrations 8a and 19b are not observed following silanization. The intensity of vibration 19a diminishes significantly and indicates the plane of the aromatic ring becomes largely parallel to the substrate surface following addition of OTS. This planarization of the aromatic ring is also observed in SAM **3,** which is the longer chain analog of SAM **7**. As with SAM **3**, the terminal hydroxyl group is accessible for reaction at the monolayer/air interface.

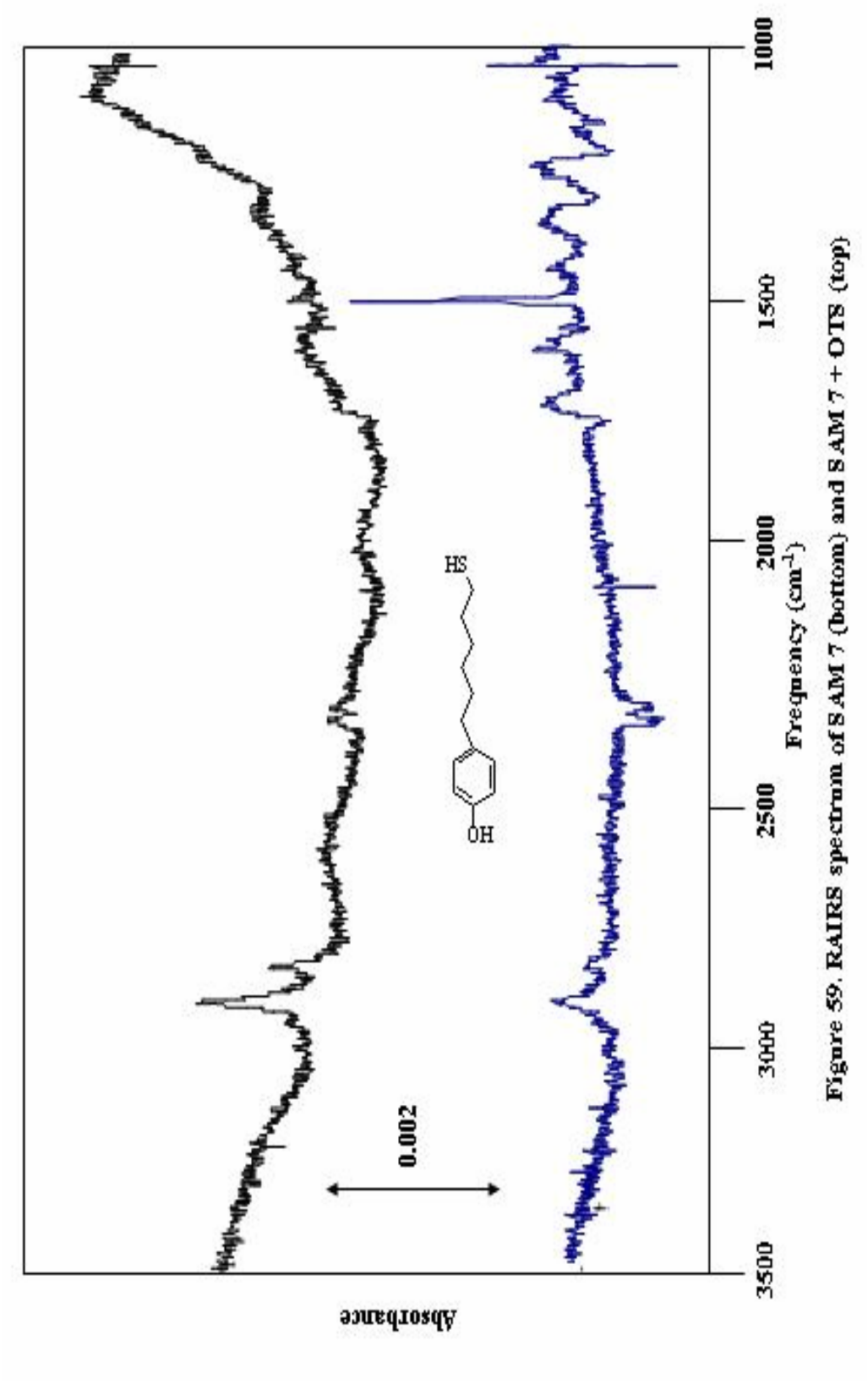

Figure 59. RAIRS spectra of SAM 7 and SAM 7+OTS

Figure 60 shows the RAIRS spectrum of SAM **8** and SAM **8** following reaction with OTS. The features due to C-H stretching vibrations of the alkyl chain increase following silanization as is expected. Vibration 19a significantly diminishes following silanization. Unlike in the case of SAM **1**, silanization of SAM **8** forces the plane of the aromatic ring to be largely parallel to the substrate surface. This planarization is likely due to the decreased order in the packing of the alkyl chains in SAM **8** as a result of a decrease in the number of methylene units present. It appears that even though an ether linkage is included, SAM **8** is not as well ordered as SAM **1** and the structure of the underlying monolayer is disrupted following addition of OTS. The alkyl chains in SAM **8** are less crystalline and likely allow deformations to impose a new orientation on the terminal phenol.

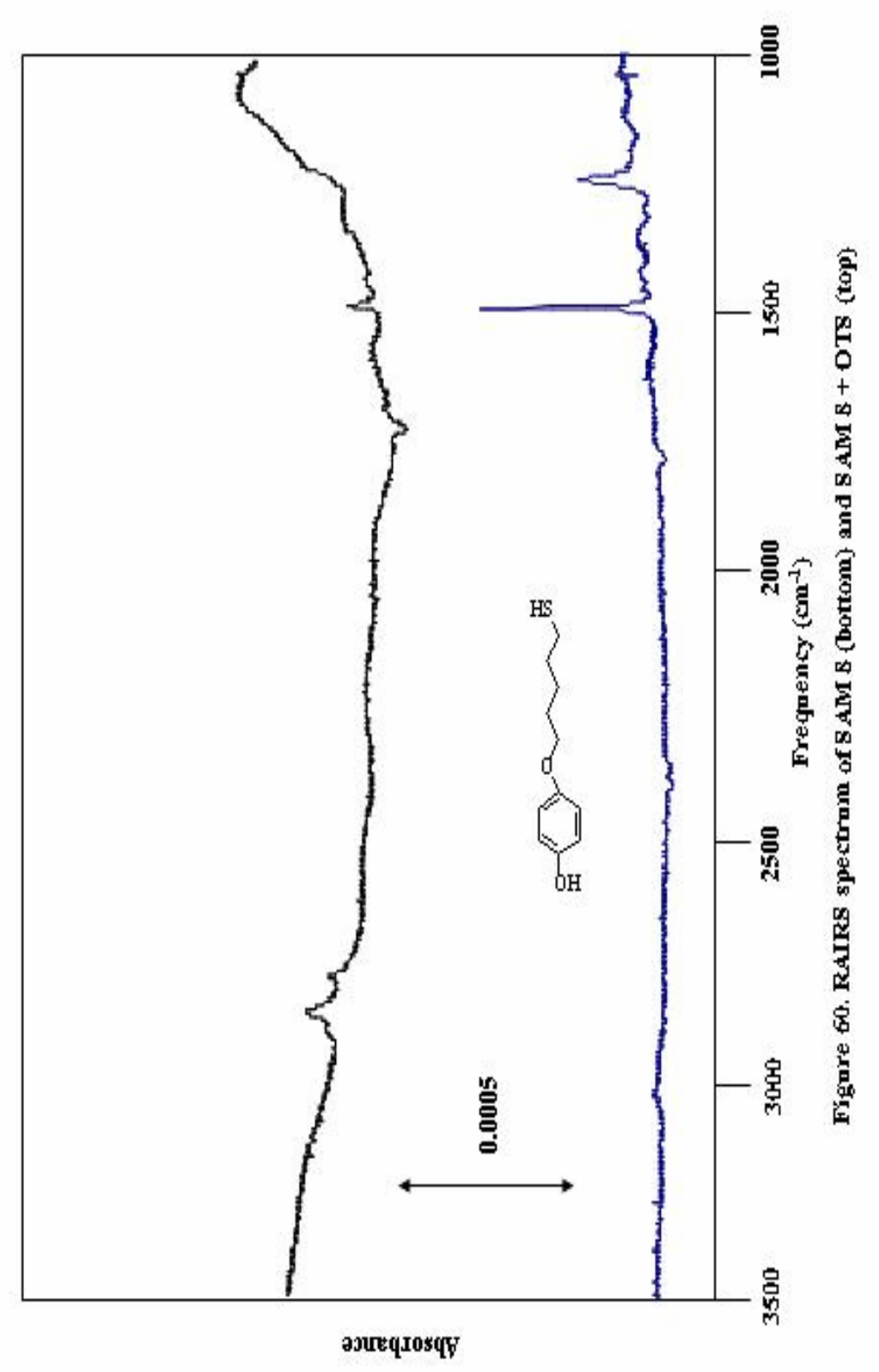

Figure 60. RAIRS spectra of SAM 8 and SAM8+OTS

6.1.4 Discussion of IR spectra From the RAIRS spectra of SAMs **7** and **8** it appears that the decrease of the alkyl chain length has does not have a serious impact upon the orientational structure of the monolayer. In the long chain analogs, SAMs **1** and **3**, the vibrational frequencies for the alkyl C-H stretching modes are smaller indicating the chains are more ordered and crystalline which likely imposes a more rigid orientation to the terminal aromatic ring. For SAMs **7** and **8**, the vibrational frequencies corresponding to the alkyl C-H stretching modes are much larger than in the long chain analogs, SAM **1** and **3**, reflecting increased disorder and a less crystalline ordering environment of the alkyl chains. This may contribute to the increased tilt of the aromatic rings with respect to the surface normal following silanization with OTS. Figure 61 shows the orientation SAMs **7** and **8** are believed to adopt.

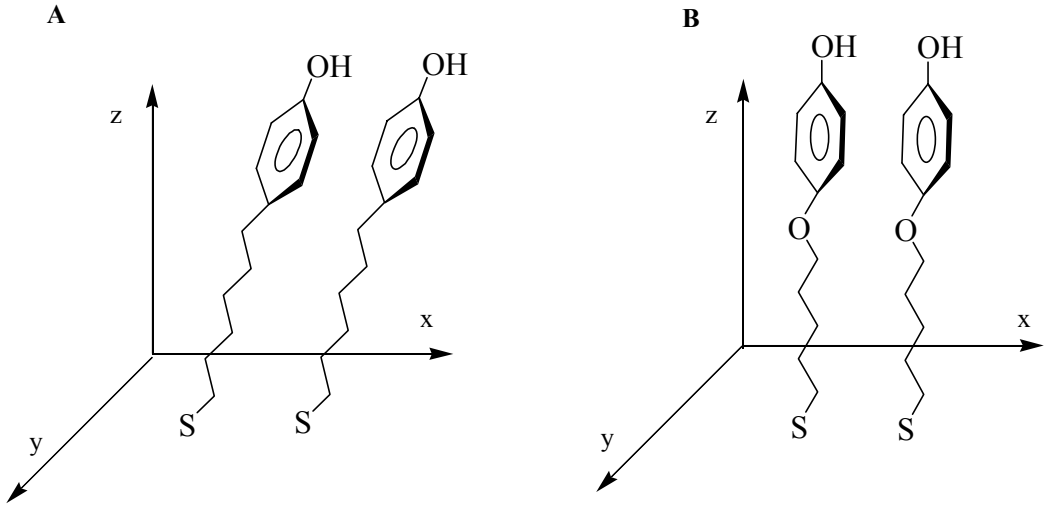

Figure 61. a) Orientation of SAM 7, b) Orientation of SAM 8

The decrease in intensity of the alkyl C-H stretching modes for SAMs **7** and **8** may in part be due to less methylene units in the alkyl chain but is also due to the tilt angle of the chains. This conclusion is supported by comparison of the RAIRS spectra between SAMs **1** and **8** and comparisons between the RAIRS spectra of SAMs **3** and **7** are made. The relative intensities of the vibrational features are similar and this suggests a similar structure for each pair of SAMs.

6.2 Contact Angle Results

6.2.1 Experimental details and data Contact angle measurements were performed on SAMs **7** and **8** as done with previous monolayer surfaces and are summarized in Table 23. The water contact angles for both surfaces are different although both surfaces appear to be hydrophilic.

Table 23. SAM-liquid interfacial contact angles for SAMS 7 and 8, and silanized SAMS 7 and 8.

Monolayer	Water (deg)	Ethylene Glycol (deg)	Glycerol (deg)
4-(6-mercapto-hexyl)phenol (**7**)	52(3)	31(3)	50(2)
4-(6-mercapto-pentyloxy)phenol (**8**)	40(3)	24(3)	40(3)
SAM **7** + OTS	70(3)	------	------
SAM **8** + OTS	68(3)	------	------

SAM **7** is less hydrophilic which suggests that the face of the aromatic ring is more exposed at the monolayer/air interface as is the case for SAM **3**. SAM **8** on the other hand is more hydrophilic. Comparison of water contact angles of SAM **1** and SAM **8** suggests a similar surface energy for both monolayers. Following silanization, contact angles for SAMs **7** and **8** increase dramatically indicating OTS was added to the monolayer structure.

6.2.2 Results and discussion of Zisman analyses A combined Zisman plot was prepared for SAMs **7** and **8** and is shown in Figure 62. The calculated surface energies and associated errors are summarized in Table 24.

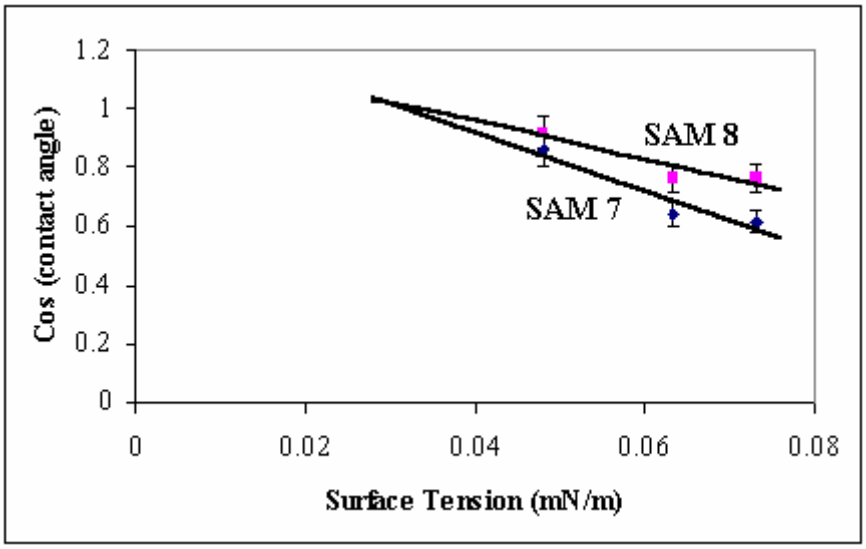

Figure 62. Zisman plot for SAMs 7 and 8.

From visual inspection of the above plot there is not a significant difference between the points at which both lines cross the value of 1 on the y-axis, indicating the surface energies from both monolayers are similar. The calculated surface free energy for SAM **7** is 33.2 mN/m $\pm$ 10.7 mN/m.

Table 24. Calculated surface free energies for SAMs 7 and 8. Slopes, intercepts, and R^2 values for each regression line shown in Figure 62 are included along with associated errors.

Monolayer	Slope	Error in Slope	Intercept	Error in intercept	R^2	Surface Energy (mN/m)
SAM **7**	-10.18	3.02	1.33	0.19	0.918	33.2 $\pm$ 10.7
SAM **8**	-6.55	2.72	1.22	0.17	0.853	33.6 $\pm$ 0.9

When compared to SAM **3,** the surface energy for SAM **7** is lower. The surface free energy for SAM **8** is 33.6 mN/m $\pm$ 0.9 mN/m. When compared to the surface energy value for SAM **1**, SAM **8** is also lower but is still considered a high energy surface. The decrease in surface energies for SAMs **7** and **8**, relative to their long chain counterparts (SAMs **3** and **1**), suggests that a shorter chain length tends to lower the surface energy, as

a result of less order in the alkyl chain, which allows the terminal functional groups to vary their orientations and allow contributions from dispersive components.

6.2.3 Results and discussion of Fowkes analyses A combined Fowkes plot for SAMs **7** and **8** was prepared and is shown in Figure 63. The dispersive contributions along with the associated errors are summarized in Table 25.

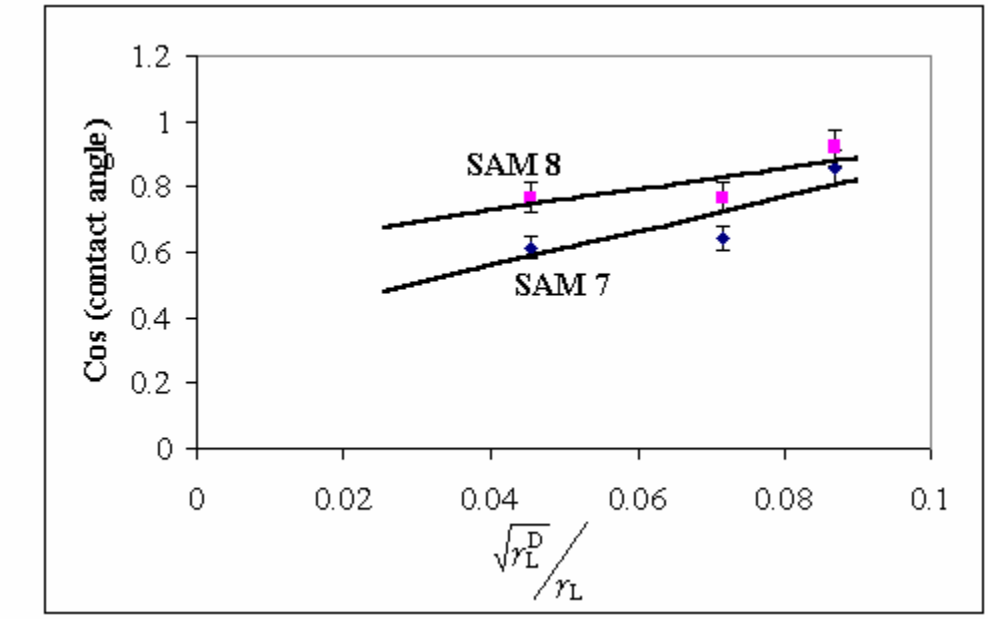

Figure 63. Fowkes plot for SAMs 7 and 8

From visual inspection of the above plot it is clear the slopes of the lines for SAM **7** and **8** are different indicating the dispersive contributions to their surface free energies are different. The calculated dispersive contribution for SAM **7** is 7.2 mN/m $\pm$ 5.4 mN/m. Most of the surface free energy in SAM **7** is due to the polar contributions from the terminal –OH group. The calculated dispersive contribution for SAM **8** is 2.8 mN/m $\pm$ 2.0 mN/m.

Table 25. Calculated dispersive components for SAMs 7 and 8. Slopes, intercepts, and R^2 values for each regression line shown in Figure 63 are included along with associated errors.

Monolayer	Slope	Error in Slope	Intercept	Error in intercept	R^2	Dispersive Component (mN/m)
SAM **7**	5.36	3.43	0.34	----	0.710	7.2 ± 5.4
SAM **8**	3.36	2.67	0.59	----	0.613	2.8 ± 2.0

Only 22 % of the surface free energy of SAM **7** is due to dispersive contributions and is only 8.4% for SAM **8**. The surface free energy is largely polar as is expected if the terminal –OH moiety is projected towards the solid/air interface. The dispersive contribution of SAM **7** is larger than the dispersive contribution calculated for SAM **3** indicating shorter alkyl chains allow to the phenyl moiety to tilt over more exposing more of the aromatic ring plane at the interface. It appears that the ether linkage does not allow the tilt angle of the aromatic ring to increase as much as inclusion of a methylene linkage allows. From the contact angle analysis the structural picture which emerges agrees with the proposed orientation model in Figure 61.

6.2.4 Discussion of contact angle results From the Zisman analysis for SAMs **7** and **8**, large differences in surface energy were not observed as would be expected if the terminal –OH is projected differently at the monolayer/air interface. Both monolayers are hydrophilic, high energy surfaces. From the Fowkes analysis small differences in the dispersive contributions to the surface free energy are seen. SAM **8** is more polar at the interface than is SAM **7**. Inclusion of the methylene unit is believed to increase the tilt angle of the plane aromatic ring with respect to the surface normal. The tilt angle increase is reflected in an increased dispersive contribution determined for SAM **8**. Both SAM surfaces react with OTS as is reflected by the water contact angle increase observed for the silanized surfaces.

6.3 Reductive Desorption Results

Desorption data obtained for SAMs **7** and **8** is summarized in Table 26. The measured desorption potentials for both monolayers are similar but are significantly more positive than the desorption potentials determined for the previously discussed SAMs.

Table 26. Desoprtion potentials and calculated coverage densities for SAMs 7 and 8.

Monolayer	**Desorption Potential (V)**	**Coverage (Γ) (10^{-10} mol/cm^2)**
4-(6-mercaptohexyl)phenol (**7**)	-1.031 $\pm$ (0.005)	5.3 $\pm$ (0.4)
4-(6-mercaptopentyloxy)-phenol (**8**)	-1.006 $\pm$ (0.007)	4.5 $\pm$ (0.4)

The calculated monolayer coverage densities are similar to calculated coverage densities obtained for the previously discussed monolayer surfaces. Chain length does not seem to have a measurable effect on the monolayer packing density but does have a significant effect on desorption potential. A decrease in chain length should decrease the amount of lateral Van der Waals interactions among the methylene units of alkyl chains within a monolayer and consequently the monolayer should be less stable towards desorption from the surface. A lower desorption potential than SAMs **1** and **3**, is observed for SAMs **7** and **8** indicating that the decrease in lateral Van der Waals interactions destabilizes the monolayer structure. Comparison of reported desorption potentials for docanethiol to the desorption potentials of hexadecanthiol thiol indicate that, a significant decrease in the desorption potential occurs as a result of reduced Van der Waals interactions in dodecanthiol.[105] The decrease in the desorption potential in SAMs **7** and **8** is attributed to the decrease in the number of methylene units in the alkyl chain and not to a decrease in possible interactions of the terminal functionalities. It is also known in the literature that as alkyl chain length decreases in linear alkanethiol monolayers, the stability of the monolayer decreases as well as the ordering of the chains within the monolayer.[49]

6.4 Ellipsometry Results

Monolayer thicknesses obtained for SAMs **7**, **8**, and their silanized analogs are summarized in Table 27.

Table 27. Monolayer thicknesses obtained for SAMs 7 and 8 as well as for silanized SAMs 7 and 8.

Monolayer	Film Thickness (Å)
4-(6-mercaptohexyl)phenol (**7**)	13.5*
4-(6-mercaptopentyloxy)-phenol (**8**)	13.1 $\pm$ (0.5)
SAM **7** + OTS	30.7 $\pm$ (3.3)
SAM **8** + OTS	11.3 $\pm$ (2.4)

* One measurement

There are no measurable differences between SAMs **7** and **8**. The monolayer thicknesses are lower than SAMs **1**-**6**, since the alkyl chain is six or seven methylenes shorter than the previously discussed surfaces. Following addition of OTS the ellipsometric thicknesses increase for SAM **7** indicating addition of OTS occurred. The determined thickness for SAM **8** + OTS is less than the thickness determined prior to silanization. Measurements were repeated on three different freshly prepared monolayers and only one thickness measurement was obtained for SAM **7**. The RAIRS spectra and contact angle data for SAM **8** confirm addition of OTS yet ellipsometric data does not indicate addition of OTS occurred. Reaction of OTS with SAM **7** indicates the terminal –OH group is accessible at the monolayer/air interface. This conclusion agrees with the results obtained for SAM **3** and further support the proposed structure model shown in Figure 61.

6.5 Impedance Spectroscopy Results

Impedance measurements were obtained for SAMs **7** and **8** and the results from fitting of the experimental to the circuit model shown in Figure 27 are summarized in Table 28. The complex impedance plot for SAMs **7** and **8** is shown in Figure 64. Again,

the plot includes only the lines resulting from the mathematical fit of the experimental data. The experimental data points are omitted for clarity.

Table 28. Film resistance and capacitance values determined for SAMs 7 and 8 following fitting of experimental data to the equivalent circuit model shown in Figure 27.

Monolayer	Monolayer Resistance (KΩ)	Monolayer Capacitance (μF)
4-(6-mercaptohexyl)phenol (**7**)	0.742 + 0.036	0.15 $\pm$ (0.03)
4-(6-mercaptopentyloxy)-phenol (**8**)	0.409 $\pm$ 0.046	0.20 $\pm$ (0.05)

The other terms in the equivalent circuit model such as: solution resistance, resistance due to charge transfer (double layer resistance), and capacitance due to charge transfer (double layer capacitance) are not included in the above table for clarity. Suffice it to say the values are similar to the values obtained for SAMs **1**, **2**, **3**, **4**, **5**, and **6** and do not significantly change for SAMs **7** and **8**.

The determined resistance and capacitance values indicate that a decrease in chain length also significantly decreases the resistance and capacitance of the monolayer. The resistance values for SAM **7** and **8** are significantly lower than the resistance values obtained for the previously discussed SAMs. This decrease is believed to be due to a decrease in the alkyl chain length. Porter *et al*.[49] also reports that for linear alkanethiol monolayers, a decrease in chain length decreases the monolayers ability to resist electron transfer.[49] Porter also reports that shorter chain alkanethiols have more pinhole defects in their monolayer structure, weaking the ability of the monolayer to protect the underlying substrate.[49] It is believed these conclusions are also applicable to SAMs **7** and **8**. As was the case for SAM **3** and SAM **1**, inclusion of the ether linkage lowers the resistance barrier to electron transfer for SAM **8** relative to SAM **7**. It appears that even for the short chain analogs of SAMS **1** and **3** the same structural features govern the resistive properties of the monolayer.

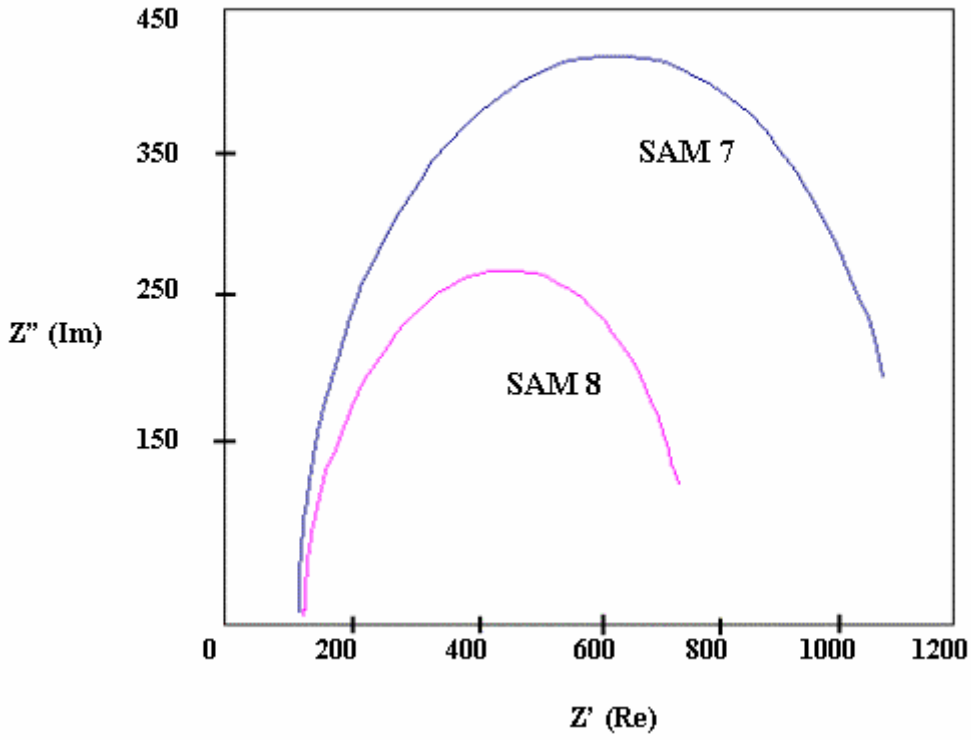

Figure 64. Complex impedance plots for SAMs 7 and 8

Visual inspection of the stacked complex impedance plot shown above, reveals a difference between SAMs **7** and **8**, also evidenced by the obtained resistance values for each monolayer. It is clear that structure differences, in the molecules comprising a monolayer, have a significant impact upon the resistive properties of the monolayer. The impedance results for SAMs **7** and **8** further support the idea that chain length has a significant impact upon the stability and structure of the resulting interface.

6.6 Chapter Conclusions

From the large vibrational stretching frequencies for the alkyl C-H stretching modes in the RAIRS spectra for SAMs **7** and **8**, it can be concluded that the shorter alkyl chains are not as organized as in SAMs **1-6** and that this leads to less ordered monolayers which reductively desorb from gold substrates at significantly more positive potentials. This

disorder is also evidenced in the greater dispersive contribution to the surface free energy and also in the lower surface free energy values for SAMs **7** and **8** compared to their longer chain analogs (SAM **1** and **3**). Impedance measurements also confirm that shortening the alkyl chain decreases the resistance properties of SAMs **7** and **8** relative to their longer chain analogs. It seems shorter alkyl chains in these phenoxy and phenyloxy-terminated SAMs limits monolayer ordering resulting in structurally less rigid and stable interfaces.

Chapter 7 Conclusions And Future Work

7.1 Conclusions

The data presented for all eight SAM surfaces seems to demonstrate that there is a definite relationship between molecular structure and resultant interfacial properties. RAIRS spectra reveal that the presence of an ether linkage forces the plane of the aromatic ring into a normal arrangement with respect to the substrate surface, as reflected in the intensities of vibrations 8a and 19a for SAMs **1**, **2**, **6**, and **8**. Inclusion of the ether linkage seems to decrease the tilt angle of the plane of the phenyl ring with respect to the substrate surface. This may be a result of a difference in a C-O-C bond angle versus a C-C-C bond angle.

RAIRS also reveals that meta-substitution imposes a packing arrangement in which the plane aromatic ring is more parallel to the surface. This is evidenced by the increase in the tilt angle of the plane of the aromaic ring in SAMs **2** and **4**. The intensity of vibrations 19a and 8a decrease significantly. This increase in tilt angle is also reflected in the Zisman and Fowkes analyses which reveal that monolayers **2** and **4** are lower energy surfaces with a large dispersive contribution to the surface free energy resulting from increased exposure of the face of the aromatic ring at the monolayer/air inerface. Vibrational frequency values for the alkyl C-H stretching modes in SAMs **7** and **8** reveal that they are less ordered than SAMs **1**-**6**. This, I believe, is a consequence of a smaller chain length, which leads to less Van der Waals interactions. The electrochemical data presented also supports this conclusion since a lower desorption potential was observed for SAMs **7** and **8** in accordance to other published findings which support our conclusions. Furthermore, RAIRS spectra also reveals that SAM **5** is better ordered than all other investigated surfaces and this increased ordering may be due to edge to face π- π interactions of the terminal phenyl ring leading to the appearance of aromatic C-H vibrational features at 3060 cm^{-1}. It is also believed that this increased stabilization is reflected in a more negative desorption potential for SAM **5** equivalent to 6.7 kJ/mole (1.6 kcla/mole), which is on the order of benzene-benzene interactions (2.0 kcal/mole).[117]

These edge-to-face interactions seem to be absent from all other investigated SAMs and are believed to be absent as a result of substitution of the aromatic ring or as a result of inclusion of an ether linkage.

Desorption data reveal that SAM **1** is much more stable than any of the other SAMs investigated. It is believed that the more negative desorption potential for this monolayer is due to increased Van der Waals interactions. A decrease in the tilt angle of the alkyl chains and a decrease in the tilt angle of the phenyl ring, resulting from the inclusion of an ether linkage, seem to increase the stability of SAM **1** relative to the rest of the discussed surfaces. Meta-substitution (SAM **2**) disrupts the packing, resulting in a lower desorption potential. The desorption data also indicates that monolayer packing densities are largely dictated by the steric bulk of the terminal aromatic ring. Linear alkanethiols have average coverage densities on the order of 7.5-8.0 x 10^{-10} moles/cm^2.[49] Average coverage densities for SAMs **1**-**8** are ~35% lower.

Contact angle analysis of each SAM, and consequent calculation of surface free energy and dispersive contributions to the total surface free from Zisman and Fowkes plots, indicate that the proposed orientation models agree with a variance in tilt angle of the aromatic terminus as a result of changes in substitution regiochemistry. Monolayers which are believed to project the terminal –OH group directly into the solid/air interface (SAMs **1**, **3**, **7**, **8**), have a larger surface energy and a lower dispersive contribution to the total surface free energy. Their surface energy is largely dictated by polar contributions. There are large errors associated with the surface free energy determinations and with the dispersive contribution analyses, yet the calculated values still reveal a direct relationship between surface free energy and ring substitution regiochemistry. Inclusion of an ether linkage also seems to vary the surface free energy as evidenced by the differences in the dispersive contributions calculated for SAMs **7** and **8**.

Ellipsometric measurements reveal that monolayers form and that reaction with OTS occurs to form multilayer structures on SAMs **1**, **3**, **4**, **7**, and **8**. Differences resulting from substitution regiochemsitry as also evidenced for SAM 4. The increased tilt angle of the aromatic ring in SAM **4** is reflected in a lower film thickness. Variance in the tilt angle of the alkyl chain is also detected in the ellipsometric thicknesses. The lower tilt angle of the alkyl chain in SAMs **1** and **2** is corroborated by an increase in the measured

monolayer thicknesses. Problems were encountered in measuring the film thickness of SAMs **7** and **8** and also of SAM **8** + OTS. It is known that ellipsometric thickness determinations in very thin film systems are problematic and can result in erroneous values.[50]

Impedance spectroscopic results also indicate a relationship between structure and interfacial properties. It appears from the presented resistance and capacitance values that there is a relationship between alkyl chain tilt and aromatic ring tilt and monolayer resistance. As the aromatic ring tilts further from the surface normal, a decrease in resistance of the monolayer to electron transfer is found. There is also a relationship between alkyl chain tilt angle and resistance as evidenced by the low resistance values obtained for SAMs **1** and **2**. Inclusion of an ether linkage in SAM **8** lowers the monoalyer resistance relative to SAM **7**. Resistance is also a function of the length of the alkyl chain. The smaller the length of the chain the lower the resistance as is seen in SAMs **7** and **8**. This decrease in resistance to electron transfer for SAMs **7** and **8** is more a function of the ordering of the underlying alkyl chains. As the alkyl chains become shorter, disorder increases causing more pinhole defects in the monolayer structure and consequently lowering the monolayers ability to protect the substrate surface.[49]

From the spectroscopic, electrochemical, and physical evidenced obtained for SAMs **1**-**8** the structural picture which emerges is a relatively simple one, and is shown in Figure 65.

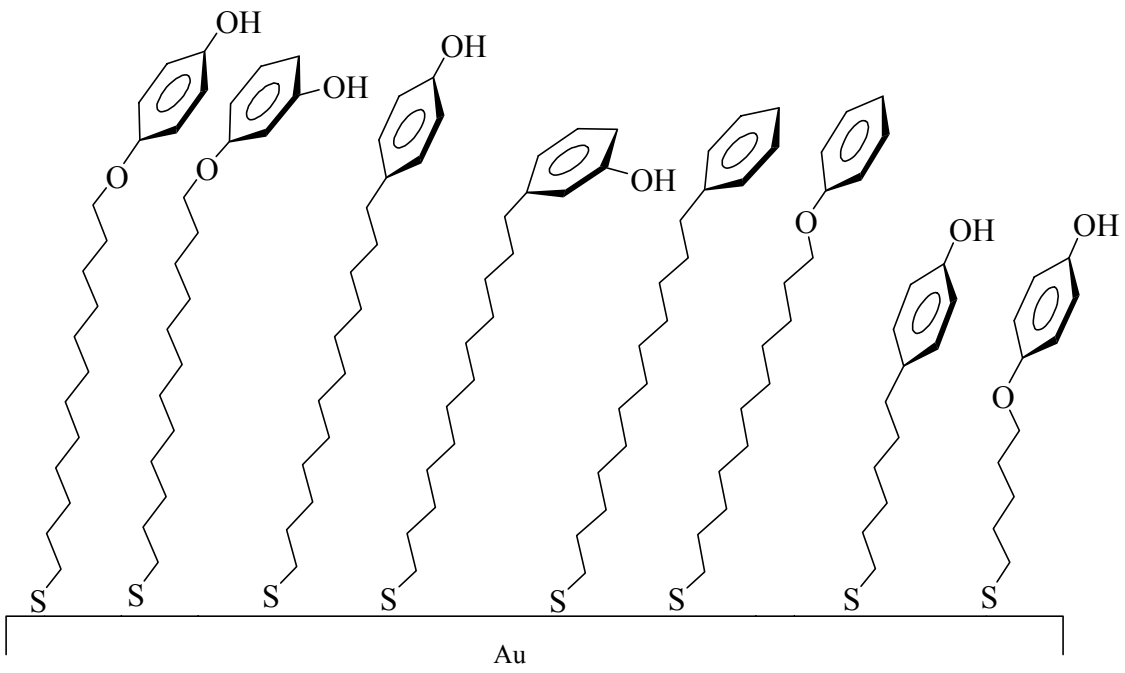

Figure 65. Proposed structure model for SAMs 1-8

As seen above, it is possible to obtain changes in surface energy and changes in the projection of terminal functional groups by changing the substitution regiochemistry and the linkage atom in these phenyl, phenoxy and phenyloxy-terminated alkanethiols. There seems to be a direct relationship between structure and interfacial macroscopic properties as evidenced by the previously presented experimental results.

7.2 Future Work

In order to further determine the structure of these phenyl terminated alkanethiol monolayers, additional techniques may be employed to contribute more spectroscopic or imaging evidence that can further assist in establishing the structure of these types of monolayer surfaces. Examples of these techniques are: Surface Enhanced Raman spectroscopy (SERS) and Atomic Force Microscopy (AFM). SERS can provide additional vibrational information, which can be used to further establish the structure of these monolayers. AFM can be used to determine whether differences in monolayer structure can be observed by imaging techniques.

From a synthetic standpoint it also possible to incorporate structural features, which can function as spectroscopic handles for further structural analysis. Incorporation of fluorine can facilitate further RAIRS and SERS characterization. Compounds, such as the ones shown in Figure 66, are synthetically accessible and should not significantly alter the structure of the resultant monolayer.

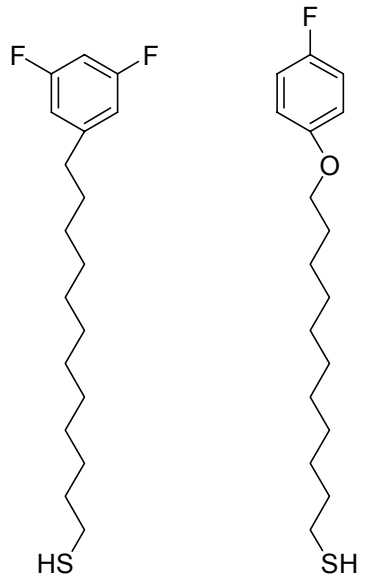

Figure 66. Proposed fluorinated targets

Fluorine's covalent radius resembles that of hydrogen and therefore the steric bulk of the terminal group should not change following incorporation of fluorine. More importantly C-F vibrational features are intense and are in a range (1250-1100 cm^{-1}), which should not interfere with other vibrational features. Ongoing work in our lab is directed at obtaining the compounds illustrated in Figure 66.

The ultimate goal of this type of research, is to establish a firm and direct relationship between structural changes to molecules comprising a monolayer and resulting interfacial macroscopic properties. These types of studies involving the use of various analytical techniques can ultimately contribute to the understanding of SAM structure and chemistry and aid in the systematic design of surfaces with predictable interfacial properties

Bibliography

(1) Swalen, J. D.; Allara, D. L.; Andrade, J. D.; Chandross, E. A.; Garoff, S.; Israelachvili, J.; McCarthy, T. J.; Murray, R.; Pease, R. F.; Rabolt, J. F.; Wynne, K. J.; Yu, H. *Langmuir* **1987**, *3*, 932.

(2) Ulman, A. *Introduction to Ultrathin Organic Films*; Academic: Boston, MA, 1991.

(3) Ulman, A. *Chemical Reviews* **1996**, *96*, 1533.

(4) Schierbaum, K. D.; Weiss, T.; Thoden van Welzen, J. F. J.; Reinhoudt, D. N.; Goepel, W. *Science* **1994**, *265*, 1413.

(5) Duan, C. M.; Meyerhoff, M. E. *Analytical Chemistry* **1994**, *66*, 1369.

(6) Hickman, J. J.; Ofer, D.; Laibinis, P. E.; Whitesides, G. M.; Wrighton, M. S. *Science* **1991**, *252*, 688.

(7) Kumar, A.; Abbott, N. L.; Kim, E.; Biebuyck, H. A.; Whitesides, G. M. *Accounts of Chemical Research* **1995**, *28*, 219.

(8) Schomburg, K. C.; McCarley, R. L. *Langmuir* **2001**, *17*, 1983.

(9) Itoh, M.; Nishihara, H.; Aramaki, K. *Journal of the Electrochemical Society* **1994**, *141*, 2018.

(10) Zamborini, F. P.; Crooks, R. M. *Langmuir* **1998**, *14*, 3279.

(11) Tremont, R.; Cabrera, C. R. *Journal of Applied Electrochemistry* **2002**, *32*, 783.

(12) Yamamoto, Y.; Nishihara, H.; Aramaki, K. *Journal of the Electrochemical Society* **1993**, *140*, 436.

(13) Haneda, R.; Aramaki, K. *Journal of the Electrochemical Society* **1998**, *145*, 1856.

(14) Laibinis, P. E.; Whitesides, G. M. *Journal of the American Chemical Society* **1992**, *114*, 9022.

(15) Novotny, V. J. *Journal of Chemical Physics* **1990**, 3189.

(16) Kim, H.; Jang, J. *Polymer* **2000**, *41*, 6553.

(17) Inagaki, N.; Tasaka, S.; Onodera, A. J. *Journal of Applied Polymer Science* **1999**, *73*, 1645.

(18) Gonon, L.; Chadert, B.; Bernard, A.; Van Hoyweghen, D.; Gerard, J. F. *Journal of Adhesion* **1997**, *61*, 271.

(19) Li, D. Q.; Ratner, M. A.; Marks, T. J.; Zhang, C. H.; Yang, J.; Wong, G. K. J. *Journal of the American Chemical Society* **1990**, *112*, 7389.

(20) Ogawa, K.; Mino, N.; Tamura, H.; Hatada, M. *Langmuir* **1990**, *6*, 1807.

(21) Roscoe, S. B.; Yitzchaik, S.; Kakkar, A. K.; Marks, T. J.; Lin, W. L.; Wong, G. K. *Langmuir* **1994**, *10*, 1337.

(22) Siewierski, L. M.; Brittain, W. J.; Petrash, S.; Foster, M. D. *Langmuir* **1996**, *12*, 5838.

(23) Li, Q.; Marthur, G.; Homsi, M.; Surthi, S.; Misra, V.; Malinovskii, V.; Schweikart, K.-H.; Yu, L.; Lindsey, J. S.; Liu, Z.; Dabke, R. B.; Yasseri, A.; Bocian, D. F.; Kuhr, W. G. *Applied Physics Letters* **2002**, *81*, 1494.

(24) Eckhardt, A. E. Electrochemical detection of single nucleotide polymorphisms using capture probe immobilized on self-assembled monolayer; Xanthon, Inc: US, 2002.

(25) Buriak, J. M.; Stewart, M. P.; Robins, E. Functionalized silicon surfaces for electronic device fabrication; Purdue Research Foundation:, 2002.
(26) Fukushima, H.; Miyashita, S.; Ishida, M.; Holmes, A. Fabrication of Self-Assembled monolayers USA, 2002.
(27) Bamdad, C. C.; Sigal, G. B.; Strominger, J. L.; Whitesides, G. M. Molecular recognition at surfaces derivatized with self-assembled monolayers; President and fellows of Harvard College: USA, 2002.
(28) Iwayama, M.; Tanaka, M. Method for forming pattern by electroplating using self-assembled monolayers; Star Mfg Co.: Japan, 2002.
(29) Ramanath, G.; Krishnamoorthy, A.; Chanda, K.; Murarka, S. P. Diffusion barriers comprising a self-assembled monolayer for integrated circuits USA, 2002.
(30) Lee, R. T.; Colorado, R. Dithiocarboxylic acid self-assembled monolayers and methods for their use in microcontact printing USA, 2002.
(31) Laibinis, P. E.; Whitesides, G. M.; Allara, D. L.; Tao, Y. T.; Parikh, A. N.; Nuzzo, R. G. *Journal of the American Chemical Society* **1991**, *113*, 7152.
(32) Nuzzo, R. G.; Fusco, F. A.; Allara, D. L. *Journal of the American Chemical Society* **1987**, *109*, 2358.
(33) Nuzzo, R. G.; Dubois, L. H.; Allara, D. L. *Journal of the American Chemical Society* **1990**, *112*, 558.
(34) Whitesides, G. M.; Laibinis, P. E. *Langmuir* **1990**, *6*, 87.
(35) Nuzzo, R. G.; Korenic, E. M.; Dubois, L. H. *Journal of Physical Chemistry* **1990**, *93*, 767.
(36) Lee, S.; Puck, A.; Graupe, M.; Colorado, R.; Shon, Y. S.; Lee, T. R.; Perry, S. S. *Langmuir* **2001**, *17*, 7364.
(37) Bain, C. D.; Whitesides, G. M. *Science* **1988**, *240*, 62.
(38) Azzam, W.; Wehner, B. I.; Fischer, R. A.; Terfort, A.; Woll, C. *Langmuir* **2002**, *18*, 7766.
(39) Bain, C. D.; Whitesides, G. M. *Angewandte Chemie. International Edition in English* **1989**, *28*, 506.
(40) Clegg, R. S.; Reed, S. M.; Huthchinson, J. E. *Journal of the American Chemical Society* **1998**, *120*, 2486.
(41) Clegg, R. S.; Reed, S. M.; Smith, R. K.; Barron, B. L.; Rear, J. A.; Huthchinson, J. E. *Langmuir* **1999**, *15*, 8876.
(42) Clegg, R. S.; Huthchinson, J. E. *Journal of the American Chemical Society* **1999**, *121*, 5319.
(43) Miura, Y. F.; Takenaga, M.; Koini, T.; Graupe, M.; Garg, N.; Graham, R. L.; Lee, R. T. *Langmuir* **1998**, *14*, 5821.
(44) Tsuji, N.; Nozawa, K.; Aramaki, K. *Corrosion Science* **2000**, *42*, 1523.
(45) Bain, C. D.; Whitesides, G. M. *Journal of the American Chemical Society* **1988**, *110*, 6560.
(46) Naselli, J. F.; Rabolt, J. F.; Swalen, J. D. *Journal of Chemical Physics* **1985**, *82*, 2136.
(47) Bigelow, W. C.; Pickett, D. L.; Zisman, W. A. *Journal of Colloid Interface Science* **1946**, *1*, 513.
(48) Nuzzo, R. G.; Allara, D. L. *Journal of the American Chemical Society* **1983**, *105*, 4481.

(49) Porter, M. D.; Bright, T. B.; Allara, D. L.; Chidsey, C. E. D. *Journal of the American Chemical Society* **1987**, *109*, 3559.
(50) Bain, C. D.; Whitesides, G. M. *Journal of the American Chemical Society* **1988**, *110*, 5897.
(51) Dubois, L. H.; Zegarski, B. R.; Nuzzo, R. G. *Journal of the American Chemical Society* **1990**, *112*, 570.
(52) Harris, J.; Rice, S. A. *Journal of Chemical Physics* **1988**, *88*, 1298.
(53) Bain, C. D.; Troughton, E. B.; Tao, Y. T.; Evall, J.; Whitesides, G. M.; Nuzzo, R. G. *Journal of the American Chemical Society* **1989**, *111*, 321.
(54) Bain, C. D.; Whitesides, G. M. *Journal of the American Chemical Society* **1989**, *111*, 7164.
(55) Bain, C. D.; Evall, J.; Whitesides, G. M. *Journal of the American Chemical Society* **1989**, *111*, 7155.
(56) Tao, Y. T. *Journal of the American Chemical Society* **1993**, *115*, 4350.
(57) Wong, S. S.; Takano, H.; Porter, M. D. *Analytical Chemistry* **1998**, *70*.
(58) Colorado, R.; Villazana, R. J.; Lee, T. R. *Langmuir* **1998**, *14*, 6337.
(59) Lee, R. T.; Carey, R. I.; Biebuyck, H. A.; Whitesides, G. M. *Langmuir* **1994**, *10*, 741.
(60) Chidsey, C. E. D.; Loiacono, D. N. *Langmuir* **1990**, *6*, 682.
(61) Cooper, E.; Leggett, G. J. *Langmuir* **1999**, *15*, 1024.
(62) Sun, L.; Kepley, L. J.; Crooks, R. M. *Langmuir* **1992**, *8*, 2101.
(63) Hutt, D. A.; Leggett, G. J. *Langmuir* **1997**, *13*, 2740.
(64) Tam-Chang, S. W.; Biebuyck, H. A.; Whitesides, G. M.; Jeon, N.; Nuzzo, R. G. *Langmuir* **1995**, *11*, 4371.
(65) Chirakul, P.; Perez-Luna, V. H.; Owen, H.; Lopez, G. P.; Hampton, P. D. *Langmuir* **2002**, *18*, 4324.
(66) Duevel, R. V.; Corn, R. M. *Analytical Chemistry* **1992**, *64*, 337.
(67) Naud, C.; Calas, P.; Commeyras, A. *Langmuir* **2001**, *17*, 4851.
(68) Liu, G. Y.; Genter, P.; Chidsey, C. E. D.; Olgletree, D. F.; Eisenberger, P.; Salmeron, M. *Journal of Chemical Physics* **1994**, *101*, 4301.
(69) Alves, C. A.; Porter, M. D. *Langmuir* **1993**, *9*, 3507.
(70) Motomatsu, M.; Mizutani, W.; Nie, H. Y.; Tokumoto, H. *Thin Solid Films* **1996**, *281-282*, 548.
(71) Fukushima, H.; Seki, S.; Nishikawa, T.; Takiguchi, H.; Tamada, K.; Abe, K.; Colorado, R.; Graupe, M.; Shmakova, O. E.; Lee, T. R. *Journal of physical Chemistry B* **2000**, *104*, 7417.
(72) Miller, C.; Cuendet, P.; Gratzel, M. J. *Journal of Physical Chemistry* **1991**, *95*, 877.
(73) Cheng, J.; Saghi-Szabo, G.; Tossell, J. A.; Miller, C. J. *Journal of the American Chemical Society* **1996**, *118*, 680.
(74) Sabapathy, R. C.; Crooks, R. M. *Langmuir* **2000**, *16*, 1777.
(75) Kang, J. F.; Ulman, A.; Liao, S.; Jordan, R.; Yang, G.; Liu, G. *Langmuir* **2001**, *17*, 95.
(76) Liao, S.; Shnidman, Y.; Ulman, A. *Journal of the American Chemical Society* **2000**, *122*, 3688.
(77) Sabatani, E.; Boulakia, C.; Bruening, M.; Rubinstein, I. *Langmuir* **1993**, *9*, 2974.

(78) Creager, S. E.; Steiger, C. M. *Langmuir* **1995**, *11*, 1852.
(79) Tao, Y. T.; Wu, C. C.; Eu, J. Y.; Lin, W. L.; Wu, K. C.; Chen, C. H. *Langmuir* **1997**, *13*, 4018.
(80) Whelan, C. M.; Smyth, M. R.; Barnes, C. J. *Langmuir* **1999**, *15*, 116.
(81) Kang, J. F.; Jordan, R.; Ulman, A. *Langmuir* **1998**, *14*, 3983.
(82) Kang, J. F.; Liao, S.; Jordan, R.; Ulman, A. *Journal of the American Chemical Society* **1998**, *120*, 9662.
(83) Laibinis, P. E.; Fox, M. A.; Folkers, J. P.; Whitesides, G. M. *Langmuir* **1991**, *7*, 3167.
(84) Laibinis, P. E.; Whitesides, G. M. *Journal of the American Chemical Society* **1992**, *114*, 1990.
(85) Walczak, M. M.; Chung, C.; Stole, S. M.; Widrig, C. A.; Porter, M. D. *Journal of the American Chemical Society* **1991**, *113*, 2370.
(86) Maoz, R.; Sagiv, J. *Langmuir* **1987**, *3*, 1045.
(87) Wasserman, S. R.; Tao, Y. T.; Whitesides, G. M. *Langmuir* **1989**, *5*, 1074.
(88) Allara, D. L.; Parikh, A. L.; Rondelez. *Langmuir* **1995**, *11*, 2357.
(89) Abdelghani, A.; Hleli, S.; Cherif, K. *Materials Letters* **2002**, *56*, 1064.
(90) Baptiste, A.; Gibaud, A.; Bardeau, J. F.; Wen, K.; Maoz, R.; Sagiv, J.; Ocko, B. M. *Langmuir* **2002**, *18*, 3916.
(91) Bierbaum, K.; Kinzler, M.; Woll, C.; Grunze, M.; Hahner, G.; Heid, S.; Effecberger, F. *Langmuir* **1995**, *11*, 512.
(92) Taylor, C. D.; Anderson, M. R. *Langmuir* **2002**, *18*, 120.
(93) Pangborn, A. B.; Giardello, M. A.; Grubbs, R. H.; Rosen, R. K.; Timmers, F. J. *Organometallics* **1996**, *15*, 1518.
(94) Greenler, R. G. *Journal of Chemical Physics* **1966**, *44*, 310.
(95) Greenler, R. G. *Journal of Chemical Physics* **1969**, *50*, 1963.
(96) Pemble, M. E. *Surface Analysis: The principal techniques*; John Wiley & Sons: West Sussex, 1997.
(97) Adamson, A. W. *Physical Chemistry of Surfaces*, 5th ed.; John Wiley and Sons: New York, 1990.
(98) Zisman, W. A. *Ind. Eng. Chem.* **1963**, *55*, 18.
(99) Fowkes, F. M. *Ind. Eng. Chem.* **1964**, *56*, 40.
(100) Tyndall, G. W.; Leezenberg, P. B.; Waltman, R. J.; Castaneda, J. *Tribology Letters* **1998**, *4*, 103.
(101) Wu, J.; Mate, M. C. *Langmuir* **1998**, *14*, 4929.
(102) Bard, A. J.; Faulkner, R. L. *Electrochemical methods: fundamentals and application*, 2nd ed.; Wiley: New York, 2001.
(103) Tompkins, H. G. *A User's guide to ellipsometry*; Academic Press: Boston, 1993.
(104) Walczak, M. M.; Popenoe, D. D.; Deinhammer, R. S.; Lamp, B. D.; Chung, C. K.; Porter, M. D. *Langmuir* **1991**, *7*, 2687.
(105) Imabayashi, S.; Iida, M.; Hobara, D.; Feng, Z. Q.; Niki, K.; Kakiuchi, T. J. *Journal of Electroanalytical Chemistry* **1997**, *428*, 33.
(106) Taylor, C. D., Virginia Polytechnic Institute and State University, 2001.
(107) Itoh, M.; Nishihara, H.; Aramaki, K. *Journal of the Electrochemical Society* **1995**, *142*, 3696.

(108) Jennings, G. K.; Munro, J. C.; Yong, T.-H.; Laibinis, P. E. *Langmuir* **1998**, *14*, 6130.
(109) Protsailo, L. V.; Fawcett, W. R. *Langmuir* **2002**, *18*, 8933.
(110) Boubour, E.; Lennox, R. B. *Langmuir* **2000**, *16*, 4222.
(111) Janek, R. P.; Fawcett, W. R.; Ulman, A. *Langmuir* **1998**, *14*, 3011.
(112) Dai, J.; Sullivan, D. M.; Bruening, M. L. *Industrial Engeneering and Chemical Research* **2000**, *39*, 3528.
(113) Diao, P.; Guo, M.; Tong, R. *Journal of Electroanalytical Chemistry* **2001**, *495*, 98.
(114) Varsanyi, G. *Vibrational Spectra of Benzene Derivatives*; Academic Press: New York, 1969.
(115) Wilson, E. B.; Decius, J. C.; Cross, P. C. *Molecular Vibrations*; McGraw-Hill: New York, 1955.
(116) Duan, L.; Garrett, S. J. *Langmuir* **2001**, *17*, 2986.

(117) Slejko, F. L.; Drago, R. S.; Brown, D. G. *Journal of the American Chemical Society* **1972**, *94*, 9210.

Vita

The author was born on April 3, 1971 in Pousada, province of Pontevedra (Spain). He grew up both in Spain and the United States. He obtained his Bachelors of Science in Chemistry from the University of North Carolina at Asheville (1994). He then worked in industry for 4 years with Roche Biomedical Corporation (RTP, NC). He enrolled in Virginia Tech in August of 1998 and obtained his Masters of Science in Chemistry from Virginia Tech in 2001. Following completion of his Ph.D in Chemistry he will reside and work in Mexico.